EFFECT OF STRUCTURAL PARAMETERS ON THE SEISMIC PERFORMANCE ON REINFORCED CONCRETE WALL BUILDINGS AND DEVELOPMENT OF A PRACTITIONER FRIENDLY STRUCTURAL ANALYSIS PLATFORM

AUTHOR:

Frank Daniel Vidales Herrera

C.C. 1036961293

ADVISOR:

Ricardo León Bonett Díaz

CO-ADVISOR:

Orlando Daniel Arroyo Amell

UNIVERSIDAD DE MEDELLÍN

MAESTRÍA EN INGENIERÍA CIVIL MIXTA

2024

Abstract

Effect of structural parameters on the seismic performance on reinforced concrete wall buildings and development of a practitioner friendly structural analysis platform

By

Frank Daniel Vidales Herrera

Master's degree in

Mixed Civil Engineering

Universidad de Medellín, Medellín, Colombia

Professor Ricardo León Bonett Diaz, Advisor

Professor Orlando Daniel Arroyo Amell, Co-Advisor

This thesis examines the influence of structural parameters on the seismic performance of reinforced concrete wall buildings and develops a user-friendly structural analysis platform. The research highlights the relationships between geometric and mechanical parameters, which are essential for understanding the seismic performance of thin-walled structures.

Utilizing the OpenSeesPy framework, nonlinear planar models were created to conduct pushover and nonlinear time-history analyses. These analyses provided critical insights into the seismic response of the buildings, revealing performance limitations and opportunities for improvement. To streamline the process, algorithms were developed in Python and C# to automate model creation, optimize data processing, and facilitate result visualization, ensuring alignment with the architectural and structural characteristics of the studied buildings.

Key outputs of the platform include detailed summaries of building attributes, pushover curves, and comprehensive analysis results, which are valuable for engineers and researchers seeking to understand the interplay between structural parameters and seismic performance. This research also establishes a foundation for future investigations aimed at improving reinforced concrete wall structures.

Additionally, all developed algorithms, user manuals, and the platform installer are publicly accessible via a GitHub repository, fostering collaboration and further exploration within the academic community.

To my mother and my brother,

For their unwavering support and trust in my abilities.

ACKNOWLEDGMENTS

Life gives us the invaluable opportunity to recognize and express gratitude to all those who have contributed to the realization of our dreams. Their support and trust are the driving forces that propel us to achieve our goals and complete this challenging journey.

I would like to express my sincere gratitude to all those who have supported me throughout my master's journey.

I would like to express my heartfelt gratitude to my mother, Gloria, and my brother, Kevin, for their unwavering support and companionship throughout my academic journey. Their presence has been a constant source of encouragement.

I owe a profound debt of gratitude to my advisor, Professor Ricardo Bonett. His unwavering belief in my potential has been a guiding light, opening the door to the world of research and enabling me to embark on and successfully complete my studies. Throughout my academic journey, from my undergraduate studies to my master's program, Professor Bonett has been a constant source of support and guidance. His mentorship has shaped not only my academic pursuits but also my professional character as an engineer and researcher. He has been instrumental in my growth at every stage, providing invaluable insights and encouragement that have empowered me to overcome challenges and reach my goals. For all these reasons and more, I am deeply thankful for his guidance and for the opportunities he has provided me along this journey.

I also wish to thank my co-advisor, Professor Orlando Arroyo, who guided me in various aspects beyond technical knowledge. His faith in my abilities and his direction throughout this journey have greatly contributed greatly to my professional and personal growth.

My sincere appreciation goes to my study and research colleagues, Juan José Ocampo and Dirsa Feliciano. Their support was crucial in the development of our analysis and evaluation algorithms. They generously shared their expertise and accompanied me throughout all the processes.

I’m grateful to EstrucMed Ingeniería Especializada for their invaluable support throughout my student years. Their flexibility, knowledge, and innovative ideas have profoundly shaped my approach in the field of structural consulting. Over the past five years, they have been instrumental in forging my identity as a structural engineer, providing me with essential experience and guidance that were crucial for obtaining the results of this study.

I would also like to acknowledge the doctors from the Colombian Network for Earthquake Engineering Research (CEER). Their contributions to my education over the years have been instrumental. Additionally, their support enabled me to generate a significant portion of the buildings included in the studied database.

Lastly, this research would not have been possible without the financial support provided by the National Model of Seismic Engineering of Colombia (MNRS). The knowledge gained from all the professors and fellow students involved in this project was essential for developing the analysis algorithms and achieving meaningful results.

TABLE OF CONTENTS

LIST OF FIGURES

LIST OF TABLES

1. EXECUTIVE SUMMARY

In Colombia, the use of industrialized thin reinforced concrete (RC) walls has become increasingly popular, especially in regions with moderate to high seismic hazard. This construction system is chosen for its efficiency in cost reduction and faster project completion, making it an attractive alternative to traditional systems. However, the lateral force-resisting capabilities of these structures depend on thin walls with minimal reinforcement, often utilizing cold-drawn wire of limited ductility instead of more ductile steel. This research aims to evaluate the displacement capacity and seismic vulnerability of thin RC wall structures, particularly in Colombian high-risk seismic zones where their implementation remains limited..

This thesis presents a methodology grounded in nonlinear dynamic analysis to assess the seismic performance of these buildings, identifying engineering demand parameters (EDPs) that indicate potential failure thresholds. A detailed case study focuses on buildings that reflect the Colombian typology, featuring specific geometric characteristics and reinforcement configurations common in the country. The analysis encompasses both local (elemental) and global (overall structure) response capacities under seismic loading, offering a robust evaluation framework. Through the chapters of this document, the methodology is explored in depth alongside the findings from the case study, highlighting the implications of seismic fragility for thin RC wall structures in Colombia.

The following is a summary of the main topics addressed in the main chapters of this research.

Chapter 6 – To analyze the behavior of reinforced concrete wall buildings (RCWB), a database was created, encompassing 259 buildings located in various cities across Colombia, covering low, intermediate, and high seismic hazard zones as defined by NSR-10. This database was developed based on CEER Report No. 002-2018 and expanded with additional data obtained through collaboration with consulting and construction firms. The buildings are categorized into three groups based on height: low-rise (up to 8 stories), mid-rise (9 to 15 stories), and high-rise (over 16 stories). Additionally, the seismic hazard zones in Colombia were analyzed, classified according to peak horizontal acceleration (Aa) and effective peak horizontal velocity (Av), defining high, intermediate, and low seismic risk areas.

The NSR-10 establishes three levels of seismic detailing for walls, based on energy dissipation capacity: Special (DES), Moderate (DMO), and Minimum (DMI). These levels determine specific design requirements and height limitations according to the seismic hazard zone and response modification factor (Ro). Buildings in high seismic hazard zones must meet DES requirements, while those in intermediate and low zones may use DMO or DMI detailing, depending on height and location.

Chapter 7 – Examined the relationship between key structural parameters and the seismic performance of reinforced concrete wall buildings in Colombia. Essential design attributes, such as Wall Index (WI), slenderness (S), aspect ratio (Ar), stiffness ratio (H/Tcr), and axial load ratio (ALR), were evaluated to understand their influence on building behavior under seismic and gravitational loads.

Using ETABS 17® models, the structural periods of buildings were calculated, allowing an in-depth analysis of cracked wall stiffness and dynamic response in low-, mid-, and high-rise structures. Findings showed that buildings with reinforced concrete walls exhibit stable behavior and adapt well to local seismic demands. Notable variations were observed in reinforcement detailing, especially in taller buildings, where increased compressive strength in lower levels is crucial for structural performance.

Analyzing representative archetypes along specific directions provided a clearer characterization of these systems' behavior in residential and commercial buildings, laying a valuable foundation for optimized design in high-seismicity areas. The conclusions of Chapter 5 offer recommendations to enhance future designs, ensuring greater stability and durability of reinforced concrete structures in the Colombian context.

Chapter 8 – Presents the numerical modeling methodology used to analyze reinforced concrete wall buildings (RCW) for seismic performance. The chapter begins by explaining the modeling approach, detailing how walls are represented and the selection of elements based on dynamic properties. Representative archetypes of buildings were modeled in two directions—longitudinal and transverse—using OpenSees software, with wall selections based on their contribution to seismic base shear. Nonlinear pushover and time-history analyses were conducted to evaluate the structures' performance points and assess their seismic fragility using country-specific earthquake records.

Macroscopic models, particularly the MVLEM (Multiple Vertical Line Element Model), were chosen over finite element models due to their computational efficiency and stability. Although SFI-MVLEM elements were initially considered, numerical convergence challenges necessitated the use of MVLEM for more robust results. The MVLEM elements allowed for simplified and effective analysis, dividing the walls into macrofibers that simulate axial and flexural responses while capturing shear behavior through horizontal springs.

The chapter further details the configuration of the MVLEM macrofibers, illustrating the material properties and reinforcement types within each section. Special wall configurations common in Colombia, such as T-, L-, H-, and C-shaped walls, required specific adaptations to the MVLEM approach to capture their out-of-plane boundary elements. For instance, flange and web elements were adjusted to ensure accurate representation while maintaining computational efficiency.

Material properties were defined using OpenSees material libraries, specifically with Concrete01 and Hysteretic models. Concrete01 was applied to simulate nonlinear compressive behavior with zero tensile strength, while Hysteretic was used to represent reinforcing steel, capturing essential cyclic degradation characteristics. This modeling strategy provided a practical and accurate means to analyze RCW buildings' inelastic behavior and laid the groundwork for future structural improvements in seismic performance design.

Chapter 9 – This chapter provides a detailed analysis of the structural response of reinforced concrete wall buildings under seismic demands, employing two primary approaches: the capacity curve and nonlinear time-history analysis. The capacity curve, derived through Pushover analysis, allows for the assessment of the buildings' overall behavior under lateral loads, determining their ultimate capacity and identifying potential failure mechanisms. Conversely, the nonlinear time-history analysis offers an accurate view of the dynamic response under actual seismic loads, capturing the inelastic behavior of materials and cumulative vibration effects. Together, these approaches provide a comprehensive understanding of seismic performance, including ductility, energy dissipation capacity, and potential modes of structural collapse.

Chapter 10 - This chapter analyzes the results of structural assessments for buildings, focusing on the development of simplified expressions that facilitate preliminary seismic performance evaluations. Key findings include the examination of the vibration periods of the TRC wall building system, revealing lower periods than code estimations for low-rise structures, indicating increased rigidity. The overstrength factor, derived from pushover analysis, suggests that reinforced concrete wall buildings should maintain an overstrength value of at least 2.5.

Additionally, the chapter presents simplified equations for estimating lateral displacements, emphasizing the significance of curvature and story drift in assessing structural behavior. Relationships between damage states and roof displacements are established, while idealized pushover curves are developed to represent critical capacity points effectively. The proposed expressions and relationships enhance seismic design methodologies, improving the resilience of reinforced concrete buildings against seismic events..

Chapter 11 – This chapter outlines the methodology for developing fragility curves for thin reinforced concrete wall buildings, drawing from the National Seismic Risk Model's vulnerability group and detailed by Ocampo et al. (2024). The process begins with building characterization, assessing aspects such as story count, dimensions, and occupancy types. It then identifies key walls to define archetypes for numerical modeling using OpenSeesPy, ensuring computational efficiency through multi-vertical-line-element models (MVLEM). The methodology incorporates the selection of ground motions consistent with site-specific seismic hazards and performs dynamic analyses to evaluate structural responses, ultimately establishing collapse thresholds and computing fragility functions.

Additionally, the chapter delves into ground motion selection and scaling, leveraging Conditional Scenario Spectra (CSS) to create hazard-consistent records for various Colombian cities. Nonlinear dynamic analyses yield crucial data on inter-story drifts and roof displacements, which are utilized to define collapse thresholds based on median roof drift ratios. The fragility curves, fitted to a lognormal distribution, highlight the probability of collapse under varying seismic demands, emphasizing significant differences among archetypes of the same height. These findings contribute to performance-based design methodologies aimed at enhancing seismic resilience in the construction of TLRCW buildings throughout Colombia.

Chapter 12 – This chapter focuses on the seismic performance assessment of reinforced concrete wall (RCW) buildings in Colombia, particularly their collapse potential during Maximum Considered Earthquake (MCE) scenarios. The study specifically targets TRCW buildings, which are commonly employed in low- and mid-rise structures up to 14 stories. By examining structural characteristics and reinforcement detailing, the chapter emphasizes the significance of these buildings in mitigating seismic risks and highlights the need for further research on taller structures that require thicker shear walls.

The assessment employs advanced modeling techniques to analyze key performance metrics such as inter-story drift ratios, roof drift ratios, and base shear. It categorizes buildings based on stiffness index and detailing level, directly linked to the seismic hazard levels defined in Colombian regulations. The fragility analysis estimates the probability of collapse under MCE conditions, with an acceptable threshold set at 20%. The findings provide insights into design methodologies that enhance safety and economic efficiency in seismic design, particularly for low- and mid-rise buildings in seismically active regions.

Chapter 13 - This chapter provides an in-depth overview of the structural configuration analysis platform developed in this study, specifically designed to facilitate the nonlinear modeling, analysis, and interpretation of reinforced concrete wall buildings under seismic loading. The platform consists of two main components: Python-based algorithms for modeling and analysis, and a C#-based platform for visualization and detailed examination of critical variables. The algorithms automate various tasks in the analysis workflow, including the generation of nonlinear planar models, pushover analysis, nonlinear time-history analysis, and post-processing of results, all aimed at improving efficiency and accuracy.

The chapter details the functionalities of each algorithm, highlighting their contributions to the modeling process and the generation of valuable insights into the behavior of reinforced concrete structures. Visualizations produced by the platform illustrate key performance indicators such as maximum lateral load capacity, inter-story drift, and time-dependent structural behavior. These tools not only aid in the comprehensive assessment of seismic performance but also support informed decision-making in design and retrofitting efforts. The platform’s integration of Python for computational modeling and C# for result

visualization establishes a robust framework for exploring the seismic resilience of reinforced concrete wall systems, laying the groundwork for future research in the field.

2. INTRODUCTION

Reinforced concrete wall systems represent an efficient design alternative that allows for the industrialization of building construction with numerous and repetitive housing units at a cost that is highly competitive compared to traditional market offerings. This system serves as load-bearing walls for both gravity and seismic loads. The superstructure mainly consists of two elements: the walls and the floor slabs that directly rest on these walls. The widespread adoption of this system in Colombia began primarily due to the need to address the low-cost housing deficit and the lessons learned from the damages caused by the earthquake in the Coffee Axis region. This adoption coincided with the implementation of the regulations set forth by the Colombian Seismic Design and Construction Standards of 1998, NSR-98. Gradually, during the 1990s, it became widely used for low-income housing construction and has since become the second most used construction system in Colombia for housing, according to the Colombian Chamber of Construction, CAMACOL (CAMACOL, 2019). The popularity of this system in Colombia is mainly attributed to its high stiffness which allows for better control of displacements induced by strong ground accelerations compared to traditional systems such as reinforced concrete frames or masonry structures.

However, current market trends demand designs that maximize the usable space of the building, industrialize construction and reduce the amount of material used. In practice, this trend has led to the use of thinner and significantly slender walls (typically 100 mm thick), with an aspect ratio, defined as the ratio between the interstory height and its thickness, greater than 16 ($h_s/t_w > 16$). Experimental observations on the seismic performance of slender walls (Hube et al., 2014; De Almeida et al., 2014; Blandón et al., 2015) and of buildings impacted by recent earthquakes, such as the Maule earthquake in Chile (2010) and the Christchurch earthquake in New Zealand (2011) demonstrate the poor performance of slender walls under seismic loads (Wallace et al., 2012; Sritharan et al., 2014). Both field and laboratory observations showed that the failures were predominantly brittle, occurring over a relatively short segment of the wall length. The evidence indicated buckling of the longitudinal rebar at the edges and, in some instances, lateral instability of the wall's web section. The estimated drifts associated with these failures are low (close to 1%), which is related to scenarios of frequent seismic demand.

The use of this structural system is mainly concentrated in housing and is used for building construction ranging from 4 to 30 floors. The increase in height is mainly observed in the country's large urban centers, due to the limitations due to land scarcity that drive vertical growth. There are some areas in Colombia, such as the Coffee Axis region, where this system is efficiently used for the construction of two or three-story houses (Carrillo et al., 2012); however, this is not the national trend.

Architectural and structural demands have led to a wide range of geometric shapes, ranging from typical rectangular T, C, or L-shaped sections to unconventional and more complex geometries. The length of these walls varies between 1.0 m and 10 m, with an average close to 4.5 m, leading to significant variations in the aspect ratio (total height/length); a parameter directly related to the element's inelastic rotation capacity. The reinforcement of these walls is generally arranged in one layer, or in some cases, two layers distributed along the web. Some walls may have concentrated steel at the ends, which may or may not be confined, depending on the compression stress level or the level of strain. Welded Wire Mesh (WWM) is widely used as shear and flexural reinforcement in the web. In some cases, edge elements are included, but given the reduced thickness, the increase in resistance and deformation capacity in these areas is highly questionable.

The aforementioned characteristics have raised questions about the seismic performance of this type of building (Pérez, 2014; Gonzales and López-Almansa, 2012). Studies have focused on evaluating the inelastic deformation capacity, lateral stability, and the different failure mechanisms that may occur. In Colombia, a gap has been identified in the current Colombian Seismic Resistant Construction Regulations, NSR-10 (AIS, 2010), as this regulation does not explicitly distinguish between the design requirements of buildings with thick and thin walls (CEER Report No. 001-2021). This work focuses on evaluating the impact of the main structural attributes of the industrialized wall system on its seismic performance and fragility. Configurations that may increase system fragility are identified, and structural recommendations are provided to ensure adequate seismic performance. The evaluation of seismic fragility has been carried out through a nonlinear analysis methodology developed within the project "Development of the National Seismic Risk Model for Colombia" led by the Colombian Geological Service and the Association of Engineering Faculties, ACOFI. This evaluation process is conducted through the development of an efficient computational platform that allows generating warnings about the structural configuration and enables designers to make changes to achieve the desired performance. It is expected that this platform can be used by consulting firms and the entities responsible for supervising structural designs, such as planning offices and oversight bodies.

3. OBJECTIVES

3.1. GENERAL OBJECTIVES

To analyze the impact of the structural configuration of buildings with industrialized walls on their seismic performance and fragility, encompassing various levels of seismic hazard. This analysis will be carried out through the development of an efficient platform designed to provide guidance in decision-making during the initial conception phase of projects.

3.2. SPECIFIC OBJECTIVES

- Develop a comprehensive database of reinforced concrete wall buildings that compiles key structural parameters relevant to their seismic performance assessment and evaluates the impact of these main parameters on the seismic performance of the wall system.
- Evaluate the variability of key structural parameters in the buildings within the database and determine their influence on seismic performance, using results obtained from pushover and nonlinear time-history analyses.
- Propose simplified expressions that relate the main structural attributes to different damage indicator parameters as a useful tool for structural pre-sizing.
- Develop a platform that allows for the efficient evaluation of the behavior within the inelastic range of industrialized wall buildings and enables decision-making within the same structural conception of a project.

4. METHODOLOGY

➢ **Objective 1**: Develop a comprehensive database of reinforced concrete wall buildings that compiles key structural parameters relevant to their seismic performance assessment and evaluates the impact of these main parameters on the seismic performance of the wall system.

1. A robust database will be compiled primarily from the Colombian Earthquake Engineering Research Network (CEER). This database contains detailed information about existing reinforced concrete wall buildings and will serve as the foundation for the analysis. In addition to the CEER database, supplementary data will be gathered through outreach to structural design offices, construction companies, and local regulatory offices.
2. Next, the buildings will be classified based on typical structural configurations according to their height:
   - Low-rise buildings (fewer than 9 stories)
   - Mid-rise buildings (between 9 and 16 stories)
   - High-rise buildings (more than 16 stories)

   This classification will facilitate the identification of patterns in seismic response within each group of selected buildings.
3. For each building in the database, the following key structural parameters will be calculated and classified:
   - Length of primary walls
   - Thickness of primary walls
   - Interstory height
   - Total height of primary walls
   - Percentage of openings in slabs
   - Maximum load levels on primary walls
   - Compressive strength of primary walls
   - Reinforcement detailing of primary walls
   - Energy dissipation capacity of the building
   - Seismic hazard level of the building
4. Finally, statistical techniques will be applied using programming languages “Python” to determine the relative significance of geometric and mechanical parameters in the seismic response of the buildings. This analysis will help identify which parameters have the most substantial influence on the seismic performance of the structures.

➢ **Objective 2**: Evaluate the variability of key structural parameters in the buildings within the database and determine their influence on seismic performance, using results obtained from pushover and nonlinear time-history analyses.

1. Identify primary wall sections likely to govern seismic response and model them in 2D within OpenSeesPy for efficient pushover and nonlinear time-history analyses.
2. Conduct pushover analyses to generate capacity curves, documenting key performance points, and use time-history analyses for selected cases to capture dynamic response under earthquake loads.
3. Apply statistical methods to evaluate relationships between structural parameters and seismic performance metrics, comparing linear and nonlinear approaches to identify critical disparities.
4. Highlight structural parameters with significant impact on seismic behavior, forming the basis for recommendations to enhance seismic resilience in building design.

➢ **Objective 3**: Propose simplified expressions that relate the main structural attributes to different damage indicator parameters as a useful tool for structural pre-sizing.

1. Review the database to select primary structural attributes (e.g., wall height-to-thickness ratio, wall index, stiffness) and define relevant damage indicators based on analysis results.
2. Use Python for regression analysis to establish relationships between structural attributes and damage indicators, testing multiple models to ensure predictive accuracy.
3. Calibrate the expressions with analysis data, applying them to a subset of buildings to validate their effectiveness in structural pre-sizing and assess accuracy for common Colombian configurations.
4. Refine the expressions as needed, documenting their application scope, limitations, and recommendations for use in early design stages.

➢ **Objective 4**: Develop a platform that allows for the efficient evaluation of the behavior within the inelastic range of industrialized wall buildings and enables decision-making within the same structural conception of a project.

1. Implement a Python module using OpenSeesPy to conduct pushover and nonlinear time-history analyses by creating scripts for 2D building models that incorporate reinforcement and material properties, defining loading conditions and constraints for the analyses, and developing procedures for executing simulations and collecting structural response data.
2. Compare results from the nonlinear analyses with empirical data and previous case studies to ensure the accuracy and reliability of the modeling module.
3. Develop an intuitive user interface in C# for result interaction, which includes an input panel for entering modeling parameters and selecting analysis types, as well as interactive graphics for visualizing capacity curves, maximum displacements, and other seismic performance indicators.

4. Perform usability tests with potential users to ensure the interface is intuitive and data visualization is clear. Collect feedback for necessary improvements.
5. Create comprehensive documentation detailing platform functionality, including user manuals, installation guides, and technical support resources.
6. Release the platform for public use on GitHub.

5. LITERATURE REVIEW

The seismic performance of reinforced concrete (RC) shear wall buildings during seismic events, notably observed during the 2010 Chile earthquake, has highlighted specific damage patterns across Latin America. Identified damages include concrete crushing, buckling of vertical reinforcement, and the opening of horizontal reinforcements. These damages are triggered by high axial loads, inadequate concrete confinement, and poor detailing of horizontal reinforcement (Alarcon et al., 2014) as well as vertical irregularities (Jünemann et al., 2016). Such damage leads to a rapid degradation in strength and stiffness, offering limited ductility (Jünemann, 2016). The failure mechanisms of these walls are characterized by a strong interaction between lateral and vertical deformations (Jünemann, 2016), with damage potentially onset at the boundaries due to high compression and propagating into the wall web (Westenenk et al., 2012). These findings suggest that the damage in the buildings during seismic events may be due to a combination of factors, including the design and construction of the buildings, as well as the specific characteristics of the seismic events. In these aspects, some researchers have made efforts in analyzing the effects of such factors in the performance of the buildings. In an extensive study analyzing the 2010 Chile earthquake's impact, (Alarcon et al., 2015) delved into the geometric and design parameters of RC walls in five critically damaged buildings. Among the critical damaged walls, it was found that the average thickness of these walls was 190 mm—deemed small by Chilean standards. The limited wall thickness was a significant factor in the out-of-plane buckling post-earthquake. Further analysis revealed an average wall aspect ratio of 2.02, which implies that the wall flexural behavior was relevant and dominated the behavior. The ALRs, derived from finite element models, showed high average values for gravitational loads and design seismic loads of 0.18 and 0.30, respectively. The study also highlighted an average vertical boundary reinforcement ratio, uniformly distributed vertical reinforcement ratio, and horizontal reinforcement ratio of 0.43%, 1.08%, and 0.45%, respectively. Despite some walls having a large amount of vertical reinforcement for strength, the lack of adequate transverse reinforcement compromised their ductility. The s/d_b ratio averaged at 8.3, exceeding the ACI 318-08 (2008) maximum limit of 6 for controlling vertical reinforcement buckling at plastic hinge locations, with ratios larger than 10 observed in 26% of studied walls and the most critical ratio found to be 16.7. The authors suggested that for walls with significant vertical reinforcement, detailing should include closed stirrups at the boundary and transverse hooks along the web to enhance concrete confinement and limit bar buckling. The findings advocate for adhering to the ACI 318-08 limit of $s/d_b = 6$ in critical wall boundary elements to mitigate the risk of buckling and enhance overall structural integrity in seismic events.

A series of studies have highlighted the inadequacy of current minimum vertical reinforcement requirements for RC walls. Lu & Henry, (2018) analyzed the seismic behavior of lightly RC walls with minimum vertical reinforcement in accordance with different concrete design standards. The drift capacities of walls without end reinforcement were all less than 1%. However, for walls with a higher end region vertical reinforcement ratio, the drift capacity was significantly larger, ranging from 1.63% to 2.45%. The drift capacity increased from 0.05% to 2.1% while the edge reinforcement ratio increased from 0.15% to 0.64%. Nonetheless, when the reinforcement ratio was higher, the trend was not as apparent, as an optimum number of secondary cracks had formed, and thus the drift capacity could not increase further. RC walls modeled with a uniform distributed minimum steel reinforcement ratio of 0.25% or less could not generate many distributed cracks in the wall's plastic hinge, resulting in premature reinforcement fracture and low drift capacities of approximately 0.50%. The response of RC walls modeled with a reinforcement ratio of 1.00% concentrated at wall edges and 0.25% distributed along the wall web were significantly better compared with the other ones. However, concentrating too much reinforcement at the ends of the wall can leave the web region vulnerable to the formation of discrete wide cracks, causing premature web reinforcement fracture and large shear deformations. A good uniform drift distribution of the walls was found when the relation between end and web reinforcement ratios are of 0.50 which corresponds to ends reinforcement between 0.64% and 0.78% with web reinforcements varying 0.32% to 0.39%. The researchers also evaluated the effects of the concrete shear strength and yield strength reinforcements. Remarkably, it was determined that for walls with uniform yield strength, increasing concrete strength detracted from their performance. This was evidenced through a reduction in both cracking capacity and drift potential. Additionally, the study underscored the critical role of reinforcement yield strength; a lower yield strength was associated with diminished drift capacity of the walls.

The same authors also analyzed the size effects when considering the failure of lightly reinforced concrete walls (Lu & Henry, 2017) who concluded that when keeping the reinforcement ratio and shear span ratio constant, the lateral drift capacity decreased significantly as the wall length increased.

Building on the theme of structural performance, Cando et al. (2020) examined the influence of stiffness on the seismic performance of residential shear wall buildings designed according to Chilean regulations. Their study found that increased stiffness not only reduces the likelihood of exceeding Life Safety (LS) and collapse limit states but also enhances the overall resilience of these structures. Interestingly, while lower stiffness improves displacement ductility, higher stiffness unexpectedly raises the probability of collapse. This complex interplay highlights the need for careful consideration of stiffness in the design of structures exposed to seismic hazards.

In a complementary analysis, Miao et al. (2022) explored the size effect on reinforced concrete (RC) shear walls using a two-dimensional meso-scale simulation method. They confirmed that as the shear span ratio increases, the failure mode transitions from shear failure to bending failure, leading to reduced shear capacity and increased ductility. Their findings indicate that the vertical reinforcement ratio has a minimal impact on shear capacity and ductility. Notably, they propose a new size effect law that quantifies the influence of shear span ratio, further contributing to the understanding of RC shear wall behavior in structural engineering contexts.

6. DATABASE DESCRIPTION

For the development of this study and to evaluate the behavior of the reinforced concrete wall buildings (RCWB), A database of 256 buildings with this structural system was constructed. The purpose was to obtain a diverse sample of buildings using this structural system in various locations across the country. Additionally, the aim is to cover the three seismic hazard levels previously defined for the Colombian territory; low, intermediate, and high, in accordance with the guidelines established in the Colombian Seismic Design Code, NSR-10 for its acronym in Spanish.

In this regard, the original database developed by the Colombian Earthquake Engineering Research Network, CEER, documented in CEER Report No. 002-2018, was used as a starting point. This database includes detailed information on 207 buildings constructed between 1998 and 2020.

Additionally, as part of this research, this database was expanded to a total of 52 additional buildings. These new buildings were obtained through collaborative interaction with various consulting companies and construction firms located in different cities across the country, bringing the total to 259 buildings.

The Figure 1 describes the different sources used to build the database.

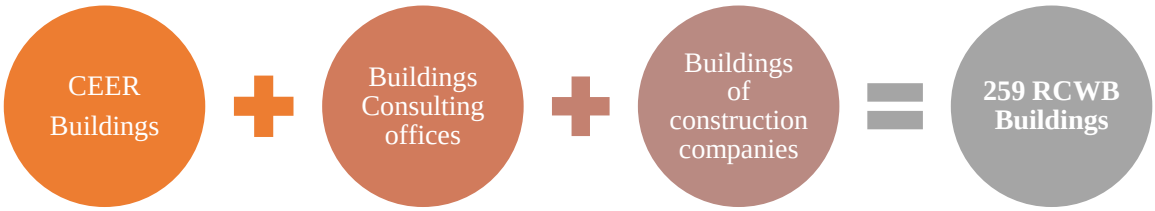

Figure 1. Sources for the construction of the database of RCWB in Colombia.

The following is a description and analysis of the main attributes that highlight the distribution of the buildings contained in the database.

6.1. LOCATION

The study database features a geographical distribution of the buildings across a total of 14 cities throughout Colombia. Figure 2 illustrates this distribution, showing both the percentage of buildings located in each city and their spatial concentration across the country.

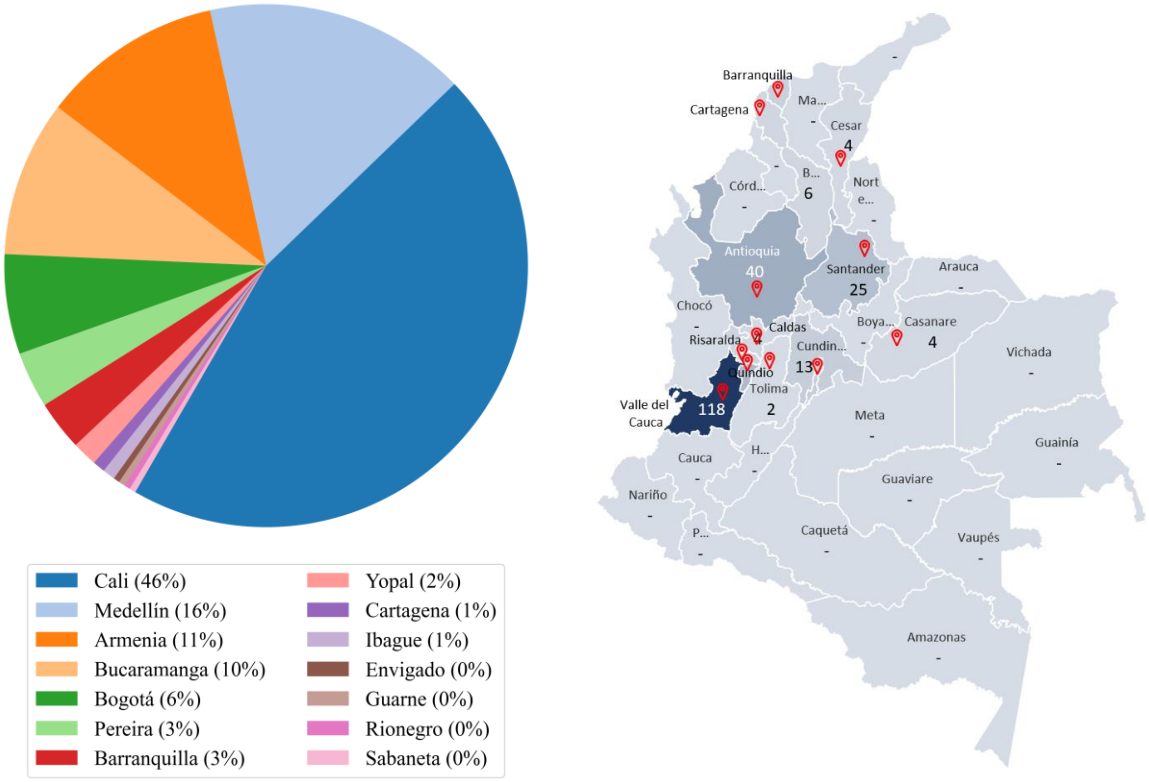

Figure 2. Distribution of RCWB by city.

6.2. HEIGHT DISTRIBUTION

The database analyzed contains information on buildings of varying heights, ranging from 4 to 30 stories. For a clearer interpretation, the buildings were divided into it has been decided to split them into three (3) subgroups based on their height: Low-rise buildings are defined as structures with a height of 8 floors or fewer; mid-rise buildings have a height ranging from 9 to 15 floors; and high-rise buildings exceed 16 floors in height. Figure 3 shows the distribution of these buildings in relation to their quantity.

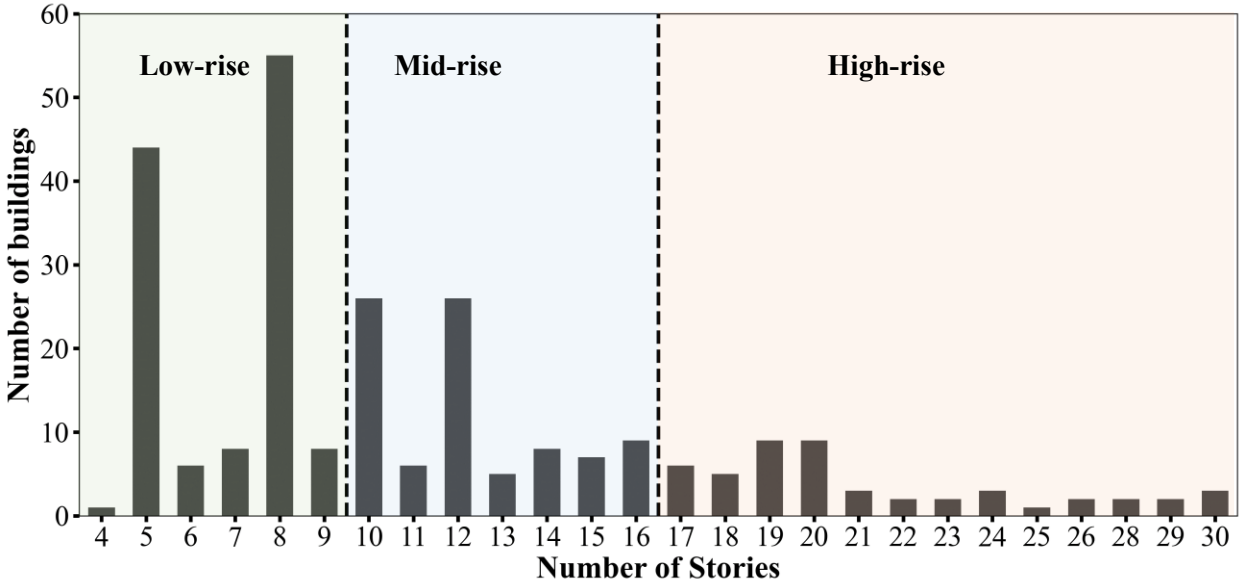

Figure 3. Distribution of RCWB by its number of stories and height categories.

6.3. SEISMIC HAZARD ZONE

In Colombia, three different seismic hazard zones are identified, defined as High Seismic Hazard Zone (HSHZ), Intermediate Seismic Hazard Zone (ISHZ), and Low Seismic Hazard Zone (LSHZ). The high seismic hazard zone indicates areas with a higher probability of experiencing high-magnitude earthquakes and, therefore, a greater seismic risk. The intermediate seismic hazard zones present a moderate risk, while the low seismic hazard zones have a relatively lower probability of suffering significant magnitude earthquakes.

The seismic hazard level in Colombia is determined by the peak horizontal acceleration (Aa) and effective peak horizontal velocity (Av) coefficients. Zones with values of 0.25 or above are categorized as high seismic hazard areas. Intermediate seismic hazard zones are indicated by values ranging from 0.15 to 0.20. Zones with values of 0.10 or below are classified as low seismic hazard areas.

Figure 4 shows the distribution of RCWB database in these seismic hazard zones. This graphical representation illustrates the location of the buildings in relation to the different seismic hazard zones throughout the country.

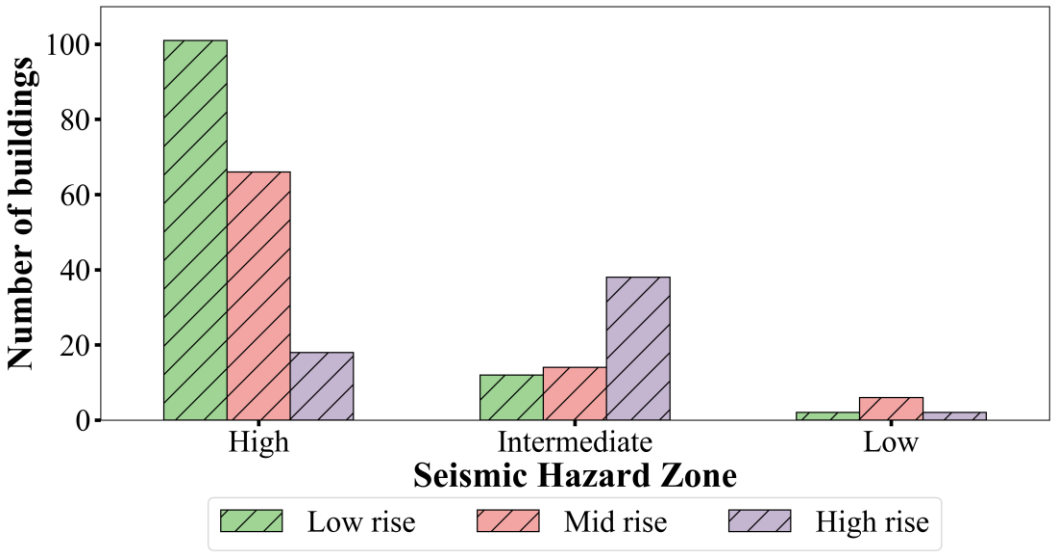

Figure 4. Distribution of buildings in the three seismic hazard zones.

6.3.1. Elastic design acceleration

To determine the seismic design parameters, the general requirements mentioned in chapters A.2 and A.3 of the NSR-10 were followed. For each project in the database, the elastic acceleration design spectrum was estimated, considering the seismic hazard zone, soil profile, and building use group. Figure 5 displays the elastic acceleration spectrum and the design elastic Sa for a 5-story building located in a high seismic hazard zone with a soil profile type D. The estimation of the elastic acceleration demand is based on the fundamental vibration period of the structure in the two principal directions (Tx, Ty).

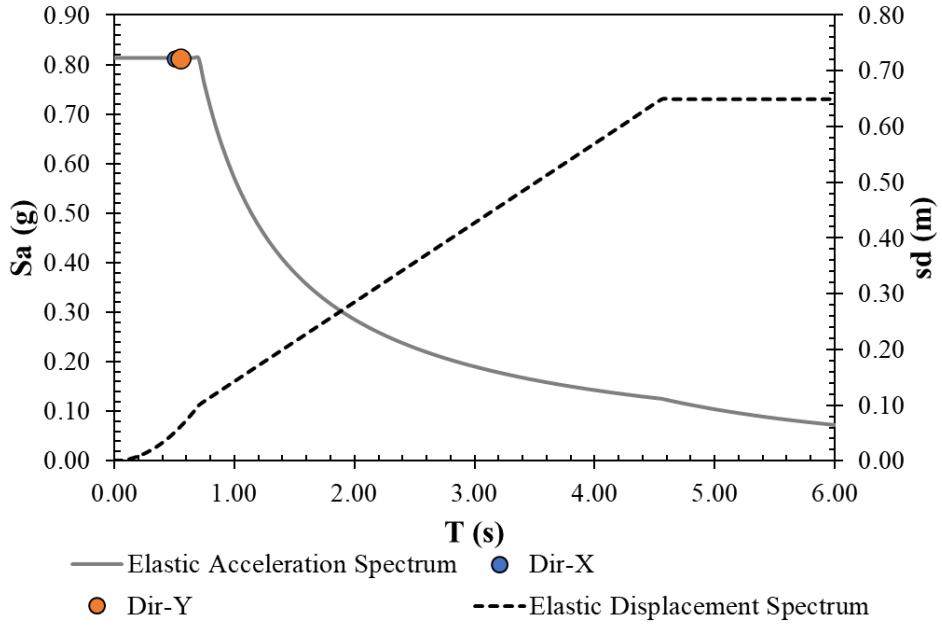

Figure 5. Elastic spectrum of accelerations for a high seismic hazard zone and a type D soil profile.

Taking into account this design elastic acceleration and the weight of the structure, the design elastic shear (Ve) is determined.

$$Ve = W * Sa \quad (1)$$

Where W is the weight of the structure and Sa is the design elastic acceleration corresponding to the fundamental vibration period.

6.4. SEISMIC DETAILING LEVEL

The Colombian code for earthquake-resistant construction (NSR-10) categorizes wall detailing into three levels based on their target energy dissipation capacity: Special (DES), Intermediate (DMO), and Minimum Energy Dissipation (DMI). For concrete structures, the design provisions in the NSR-10 are similar to those of the ACI 318-08 (Arroyo et al, 2018). The seismic hazard level in Colombia is determined by the peak ground horizontal acceleration (Aa) and effective peak horizontal velocity (Av) coefficients. Zones with values of 0.25 or above are categorized as high seismic hazard areas. Intermediate seismic hazard zones are characterized by values ranging from 0.15 to 0.20. Zones with values of 0.10 or below are classified as low seismic hazard areas. Based on this classification, the NSR-10 code prescribes a minimum detailing requirements for buildings (Table 1). Each detailing level has an associated basic response modification factor (Ro), ranging from 2.5 to 5.0, while the overstrength factor (Ωo) remains constant at 2.5. Buildings with RC walls can meet DES requirements in high, intermediate, and low seismic zones. However, buildings

with DMO or DMI detailing are not permitted in high seismic areas. Furthermore, RC wall buildings with DMO capacity are also limited in intermediate hazard zones. Building height limitations depend on the detailing level and seismic risk as shown in Table 1. For buildings with fewer than 20 stories, where the total height is less than 50 m, the detailing level is directly related to the seismic hazard area. Thus, DMI detailing is associated to low seismic hazard zones while DMO and DES detailing correspond to intermediate and high seismic hazard zones, respectively. However, for buildings located in an intermediate seismic zone exceeding 50 m, their detailing should be DES.

Table 1. Seismic design parameters according to the target energy dissipation capacity – Detailing requirement.

Detailing requirement	**Ro**	**Overstrength Ω_0**	**Seismic Hazard level**					
			High		**Intermediate**		**Low**	
			Allowed?	**H_{max} (m)**	**Allowed?**	**H_{max} (m)**	**Allowed?**	**H_{max} (m)**
DES	5.0	2.5	Yes	50	Yes	No limit	Yes	No limit.
DMO	4.0	2.5	No		Yes	50	Yes	No limit.
DMI	2.5	2.5	No		No		Yes	50

The NSR-10 code includes two approaches for determining whether boundary elements are necessary in RC walls, as shown in Table 2. The first approach depends on compressive stress at wall ends (*Lim. σ*), while the second one uses a critical section rotation limit (*Lim. c*) related to top-level displacements, *δu*. Boundary element requirements differ depending on the level of detailing, while confinement (*Ash*) and transverse reinforcement spacing (*s0*) varying accordingly (Table 2). The code provides these requirements for each seismic hazard level. In high hazard zones, only DES is allowed, whereas both DES and DMO are permitted in intermediate areas. However, for buildings with fewer than 20 stories structural designers always use DMO detailing in intermediate seismic hazard zones. Buildings in low seismic hazard regions have no restrictions for selecting energy dissipation levels and can conform to DMI, DMO, or DES requirements. However, most buildings in these zones follow the DMI design provisions.

Table 2. Minimum requirements for seismic-resistant design according to the target energy dissipation capacity – Detailing requirement.

Detailing requirement	**Minimum requirements according to NSR-10**			
	Lim. σ	**Lim. c**	**A_{sh}**	**S_0**
DES	$0.20 \cdot f'c$	$c \geq \frac{l_w}{600 * \left(\delta_u / h_w\right)} \therefore \delta_u / h_w \geq 0.007$	$A_{sh} = 0.09 \cdot \frac{s \cdot b_c \cdot f'c}{f_{yt}}$	$So_1 = min(L_{EB}, tw)/3$ $So_2 = 6 \cdot d_{bmin}$
DMO	*0.30*f'c*	$c \geq \frac{l_w}{600 * (\delta_u / h_w)} \therefore \delta_u / h_w \geq 0.0035$	$A_{sh} = 0.06 \cdot \frac{s \cdot b_c \cdot f'c}{f_{yt}}$	$So_1 = min(L_{EB}, tw)/2$ $So_2 = 8 \cdot d_{bmin}$
DMI	N.A	N.A	N.A	N.A

N.A. stands for "Not Applicable" or indicates that there are no requirements specified in the design code.

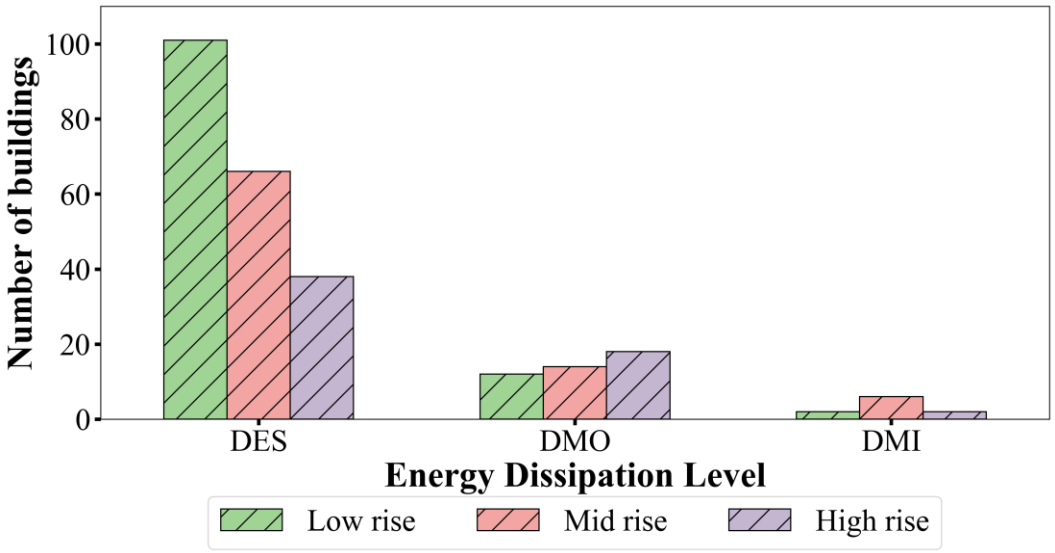

Figure 6. Distribution of buildings in the three-energy dissipation level.

7. CHARACTERIZATION OF THE INDUSTRIALIZED REINFORCED CONCRETE WALL SYSTEM IN COLOMBIA

In this section, a comprehensive characterization of the RCW system in Colombia is presented. Its configuration in plan and elevation is examined. To evaluate its structural performance, key parameters have been identified: Wall Index (*WI*), Slenderness (*S*), Aspect Ratio (*Ar*), Stiffness Index (*H/Tcr*), and Axial Load Ratio (*ALR*). These parameters are classified into two groups:

- Global Attributes: These parameters reflect general characteristics of the structural response.
- Local Attributes: These parameters offer insights into the individual geometry and characteristics of the buildings' walls.

The distributions of these parameters for the buildings in the database are detailed below.

7.1. GRAVITY AND LATERAL FORCE RESISTANCE SYSTEM

The structural system designed to resist vertical and seismic loads consists of reinforced concrete walls, which exhibit varying compressive strength (*f'c*) depending on the building's height. The structural configuration of these buildings typically features predominantly rectangular floor plans, with wall distributions that may be either symmetrical (see Figure 7) or asymmetrical (see Figure 8), depending on architectural requirements. The number of residential units per floor generally varies based on the floor area of the project and the economic stratum, typically ranging between 4 and 8 units per floor.

The industrialized wall system used in Colombia employs two main types of wall cross-sections: 1) rectangular sections (Figure 9a) and 2) non-rectangular sections. For the first type, distributed reinforcement within the web of the wall is used, consisting of one or two layers of reinforcement, which may include either ductile steel bars or electro welded wire mesh (non-ductile steel). Non-rectangular sections include typical L-, T-, or C-shaped sections (Figure 9b), as well as irregular sections, as shown in Figure 9c. In mid- to high-rise buildings, ductile steel bars are generally concentrated at the ends, which may or may not include confinement provided by closed stirrups and supplementary hooks. Figure 9d illustrates the three most representative cases of boundary elements.

Figure 7. Typical Distributions of RCWB with Symmetrical Floor Plans.

Source: Adapted from information collected from a 26-story building located in Medellín, Antioquia.

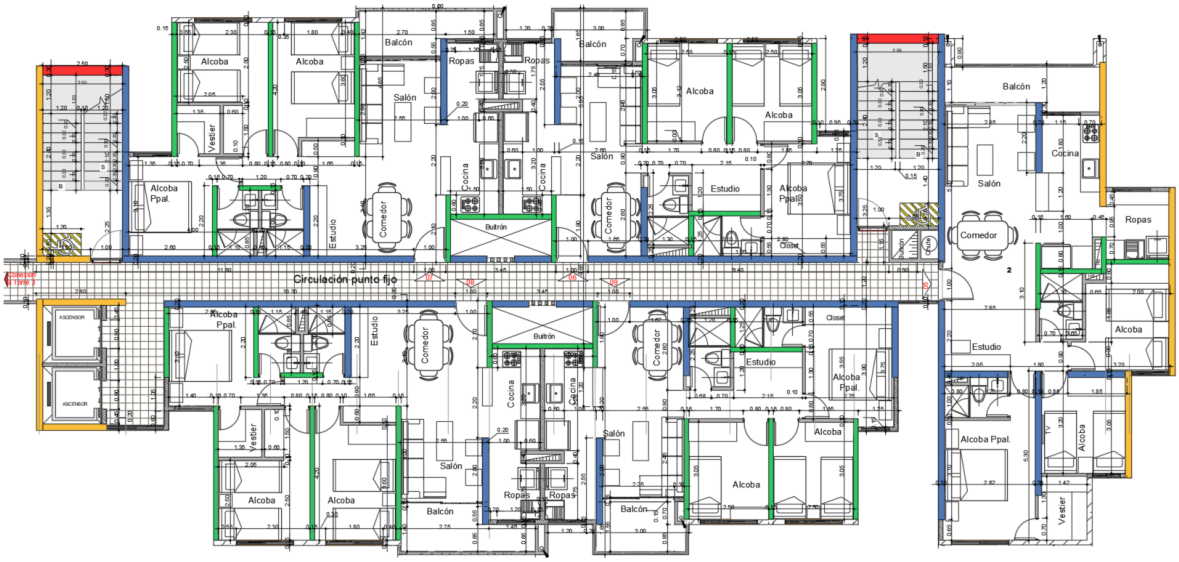

Figure 8. Typical Distributions of RCWB with Asymmetrical Floor Plans.

Source: Adapted from information collected from a 26-story building in the database 0315-MCR-SAB-26P.

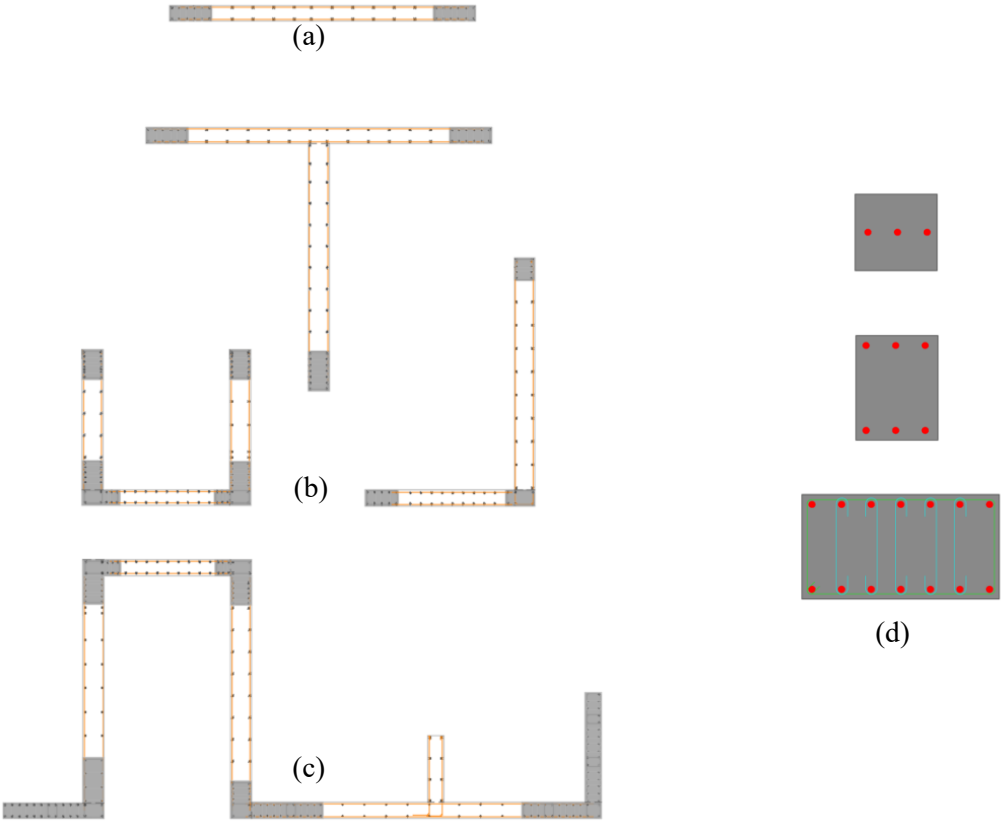

Figure 9. Typical Reinforcement Detail in Reinforced Concrete Walls.

For low-rise buildings, the compressive strength of these elements ranges from 21 MPa to 28 MPa. Mid-rise buildings exhibit compressive strengths varying from 21 MPa to 35 MPa, with a notable variation in strength with height. In high-rise buildings, the compressive strength at the base of the building ranges from 35 MPa to 49 MPa, while the upper floors have reduced strengths between 21 MPa and 28 MPa.

In terms of reinforcement detailing, the web typically incorporates one or two layers of electro WWM, with a minimum reinforcement ratio of $\rho l,v = 0.0025$. Some elements exhibit a higher concentration of reinforcement at their ends, which depends on factors such as energy dissipation level, height, and the specific conditions of the structure.

7.2. FOUNDATION SYSTEM

Based on the information gathered from the structural plans of the buildings in the database, deep foundation systems were identified for all projects, consisting of either piles or drilled shafts. The load transfer from the structural walls to the foundation is achieved through a system of interconnected foundation beams, whose dimensions vary according to the structural demands. The database includes foundation beams

ranging from 0.30 × 0.60 m to 0.60 × 1.50 m, depending on the specific requirements of each building. The following sections provide a detailed description of the identified foundation types.

7.2.1. Pile Foundations

These are reinforced concrete elements cast in situ with a cross-sectional diameter greater than 1.00 m. These piles transmit loads from the superstructure to the subsoil, ensuring the stability of the structure.

The depth of these elements depends on the soil strata upon which the structure is to be founded. For representative building types, depths range from 10.0 m to 20.0 m for mid- and high-rise buildings, while low-rise buildings typically have depths varying from 7.0 m to 12.0 m. Figure 10 shows a detail of this type of foundation.

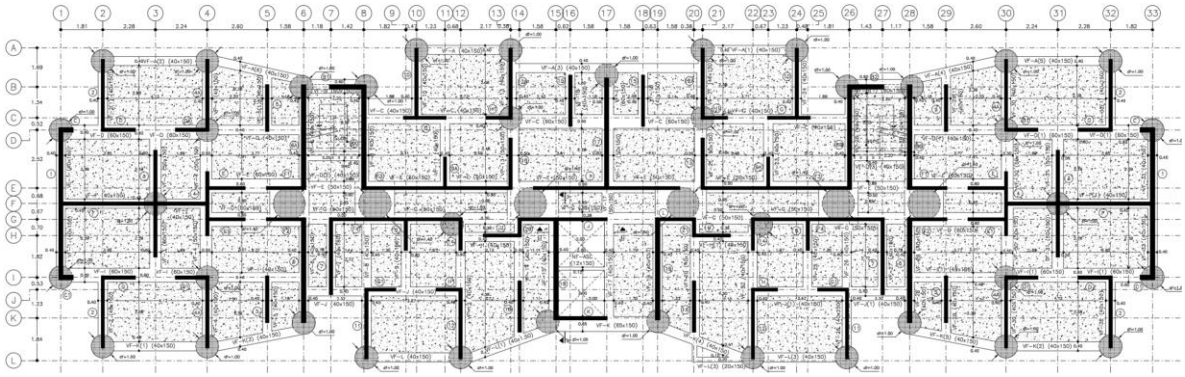

Figure 10. Detail of Pile Foundation.

Source: Adapted from information collected from a 26-story building in the database located in the city of Medellín, Antioquia.

7.2.2. Pier Foundations

Among the typologies are the drilled shafts, which, unlike piles, have a smaller cross-sectional diameter ranging from 0.35 m to 1.00 m. The depth of these elements varies from 5.0 m to 15.0 m. Figure 11 shows a detail of this type of foundation.

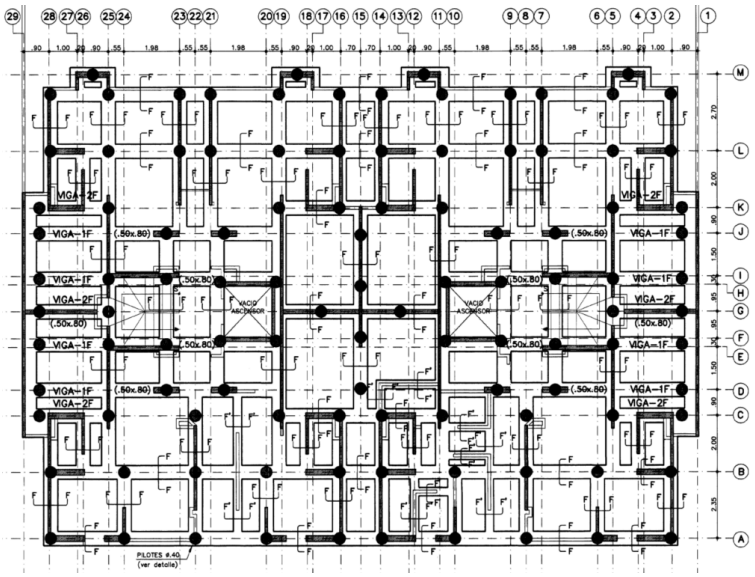

Figure 11. Details of pier foundations.

Source: Adapted from information collected from a 17-story building in the database located in Medellín, Antioquia.

7.3. FLOOR SLAB SYSTEM

The construction typologies in the database feature a floor slab system that is generally a solid slab with a thickness ranging from 0.07 m to 0.12 m. Figure 12 shows a detail of this type of slab. Additionally, some typologies present a ribbed slab system in one direction, with element heights ranging from 0.10 m to 0.15 m. In this case, for some long-span edges, heights approach 0.20 m, and above this, a solid slab with a thickness ranging from 0.05 m to 0.08 m is provided. Figure 13 shows a detail of this type of slab.

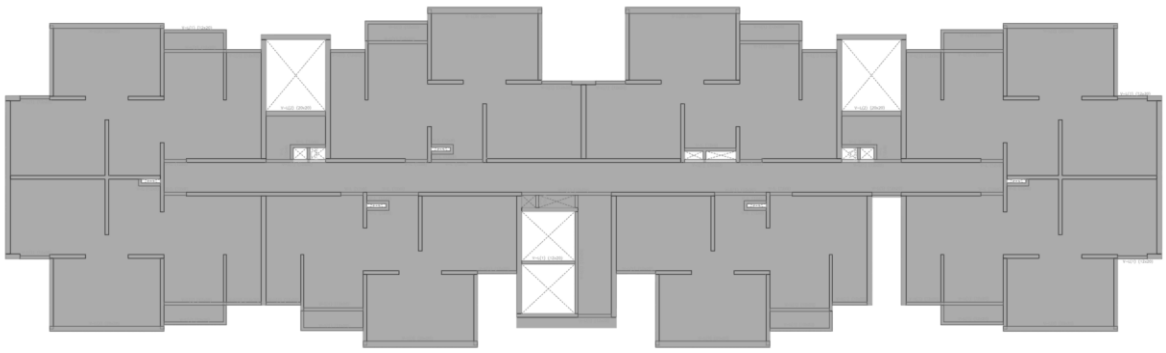

Figure 12. Solid Floor Slab System.

Source: Adapted from information collected from a 26-story building in the database located in Medellín, Antioquia.

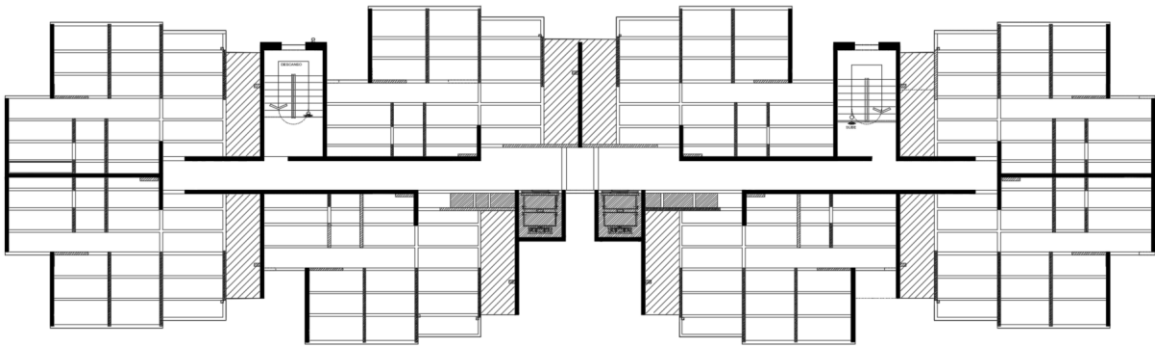

Figure 13. Ribbed Floor Slab System.

Source: Adapted from information collected from a 21-story building in the database located in Medellín, Antioquia.

Additionally, both floor systems include elements known as "lintels," which are used to improve load transfer between vertical elements. The thickness of these elements is equal to that of the main slab system. These floor slab systems are made of reinforced concrete (RC), with variations in compressive strength (f'c) ranging between 21 MPa and 28 MPa. The types of loads present include suspended steel channel ceilings with gypsum boards, ceramic tile finishes, and loads generated by partition walls.

7.4. ROOF SYSTEM

Given that the construction typologies under study are predominantly residential, the roof slabs and floor slabs share the same structural system. In this roofing system, only slight differences in dead loads are observed, as it includes a leveling mortar and a waterproofing layer due to exposure to external environmental conditions.

Additionally, in some cases, a lightweight roofing system is evident, utilizing materials not intended for pedestrian traffic or material storage. The primary materials found in this type of roofing include steel and wood, covered with clay or steel tiles.

7.5. MATERIAL PROPERTIES

7.5.1. Concrete

The concrete in the buildings of the database has a *f'c* ranging between 21 MPa and 49 MPa. Figure 14 and Figure 15 present the distribution of f'c for the walls and floor slabs, respectively, as collected in the database.

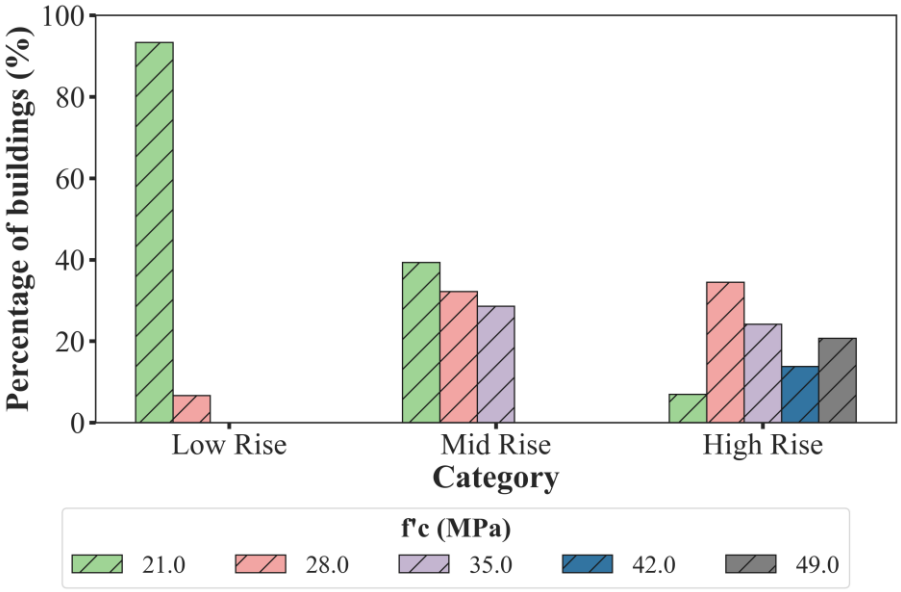

Figure 14. Distribution of the compressive strength of walls in the database.

Based on the Figure 14, the distribution of the sample within height categories and f'c values is as follows:

- Low Rise: Buildings with *f'c* of 21 MPa constitute 28 out of 30 buildings (93.3%), while those with f'c of 28 MPa make up the remaining 2 buildings (6.67%).
- Mid Rise: For buildings categorized as Mid Rise, those with f'c of 21 MPa account for 11 out of 28 buildings (39.3%), f'c of 28 MPa accounts for 9 buildings (32.1%), and f'c of 35 MPa represents 8 buildings (28.6%).
- High Rise: In the High-Rise category, buildings with f'c of 21 MPa comprise 2 out of 29 buildings (6.90%), f'c of 28 MPa make up 10 buildings (34.48%), f'c of 35 MPa represent 7 buildings (24.14%), f'c of 42.0 MPa account for 4 buildings (13.79%), and f'c of 49 MPa represent 6 buildings (20.69%).

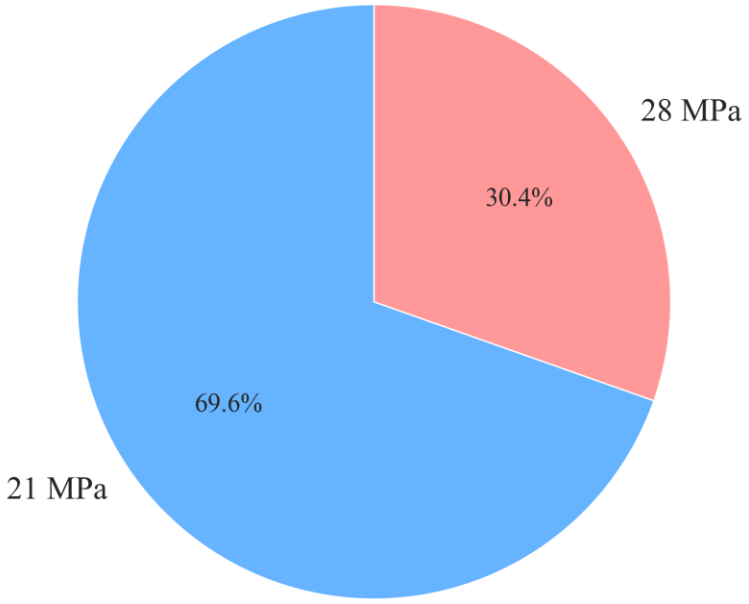

Figure 15. Distribution of compressive strength of slabs in the database.

According to the data distribution shown in Figure 15, building slabs show variations in *f'c* ranging from 21 MPa to 28 MPa. Specifically, 69.6% of the buildings feature slabs with a compressive strength of 21 MPa, while the remaining 30.4% have slabs rated at 28 MPa.

7.5.2. Reinforcing Steel

The reinforced concrete wall system in Colombia employs two types of steel reinforcement: 1) deformed steel bars, known as ductile steel (RB), typically utilized with a yield strength of *fy*=420 MPa, and 2) electro welded wire mesh (WWM), referred to in this context as non-ductile reinforcement. In design, the WWM is considered with a yield strength of *fy*=510 MPa. Additionally, this material has a modulus of elasticity (*E*) of 200,000 MPa.

7.6. DEFINITION OF REPRESENTATIVE ARCHETYPES

The foundational construction typology corresponds to the RCW buildings ranging from 4 to 30 levels. ETABS 17® software was employed for structural analysis and dynamic characterization of representative buildings. This software is widely used in Colombia for structural analysis. Other programs, such as R/C Building and Midas Design, are also available. For each selected building, a three-dimensional model was developed to represent dynamic behavior and obtain elastic behavior parameters.

In ETABS 17®, lintels and ribs were modeled as "Frame" elements, walls as "Shell" elements, and slabs as "Membrane" elements. Each model included gravitational loads on the slab, and horizontal loads were applied using the Equivalent Lateral Force method (ELF) method. For ELF, the design acceleration spectrum value for the structure's vibration period in each principal direction was used. Figure 16 presents a representation of the structural model for a building in each height category: low-, mid- and high-rise RCW buildings.

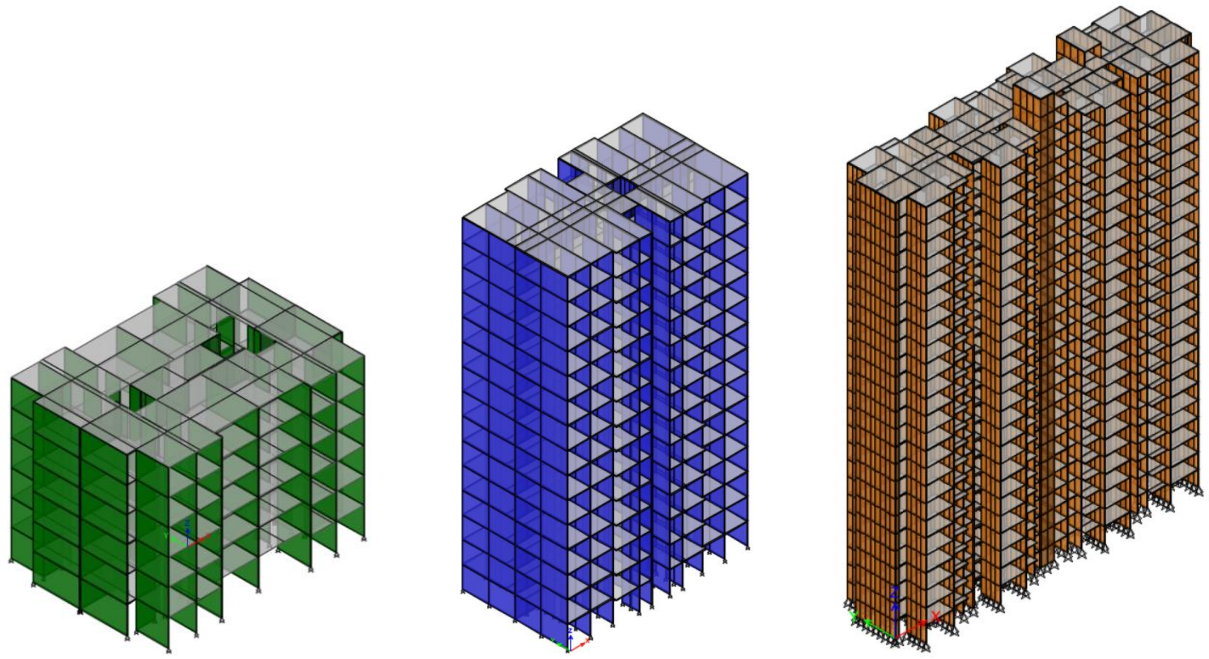

(a) (b) (c)

Figure 16. Structural model for a) low-, b) mid-, and c) high-rise RCWB.

Based on the results obtained, representative walls were defined in each principal direction, considering the prominence of each wall against the horizontal loads the structure faces. The percentage of shear taken by each wall (%Vbi) in each principal direction was calculated as presented in Eq. 2.

$$\%Vb_i = \frac{V_i}{\sum_{i=1}^{n}(V_i)} \qquad 2$$

Once the percentage of seismic shear carried by each wall was determined, the cumulative shear was evaluated, as shown in Figure 17. To select the walls representing the archetype for each building, only those contributing significantly to the seismic shear in the analyzed direction were considered. The inclusion of additional walls was assessed, and the point at which their addition no longer caused a meaningful change in the slope of the cumulative shear curve was identified. This threshold highlighted a notable variation in the shear distribution among the selected walls..

From this analysis, it was observed that a certain number of walls took a substantial amount of seismic shear, ranging between 40-60% of the building's seismic shear in each direction. Subsequently, a set of walls with similar characteristics each took a small portion of the remaining shear. After selecting the main walls, they are identified in the floor plan as shown in the Figure 18.

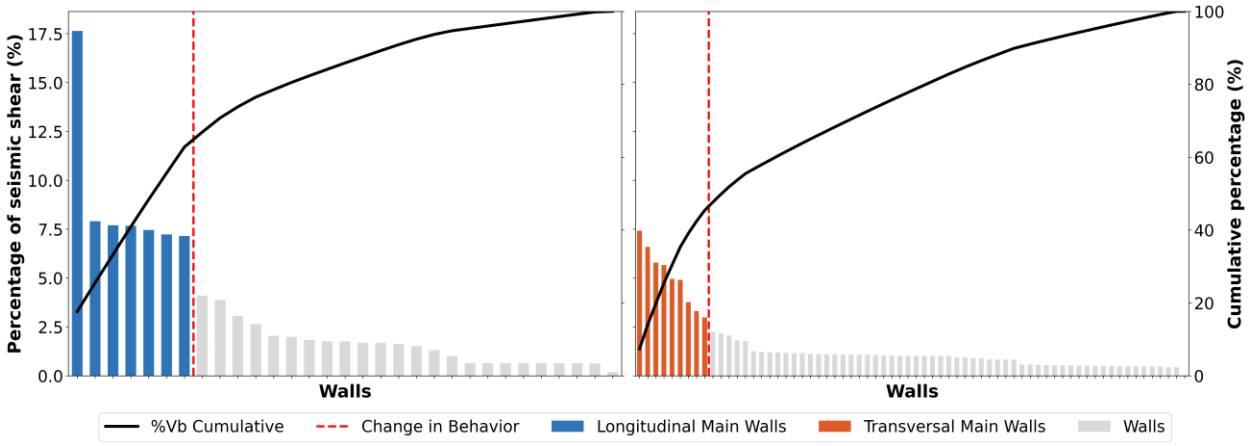

Figure 17. Example of the selection of main walls in the longitudinal and transverse directions of the building.

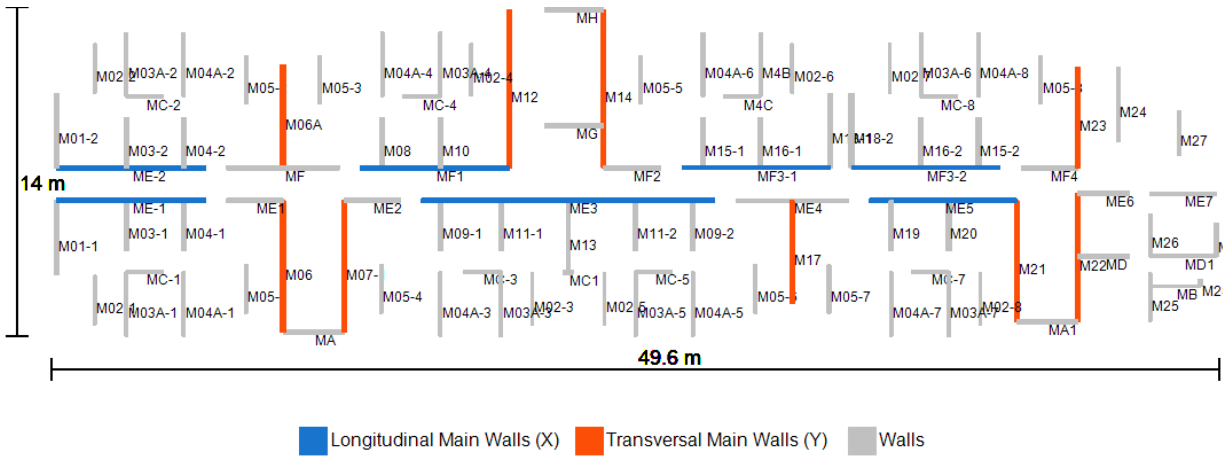

Figure 18. Localization and Nomenclature of Main Walls in the Structural Model.

Finally, a sample of 50 analyzed buildings was used to construct a total of 100 representative archetypes. This was achieved by creating one archetype for each principal direction of each building.

7.7. GLOBAL ATTRIBUTES

In this section, the parameters selected as the global attributes of the 50 buildings analyzed are presented. For each parameter, the distribution is shown based on the categories defined by the number of stories.

7.7.1. Structural period

The structural period for the buildings in the database was obtained from ETABS 17® models with gross sections. The variation of the structural period for the buildings in the database is shown in Figure 19.

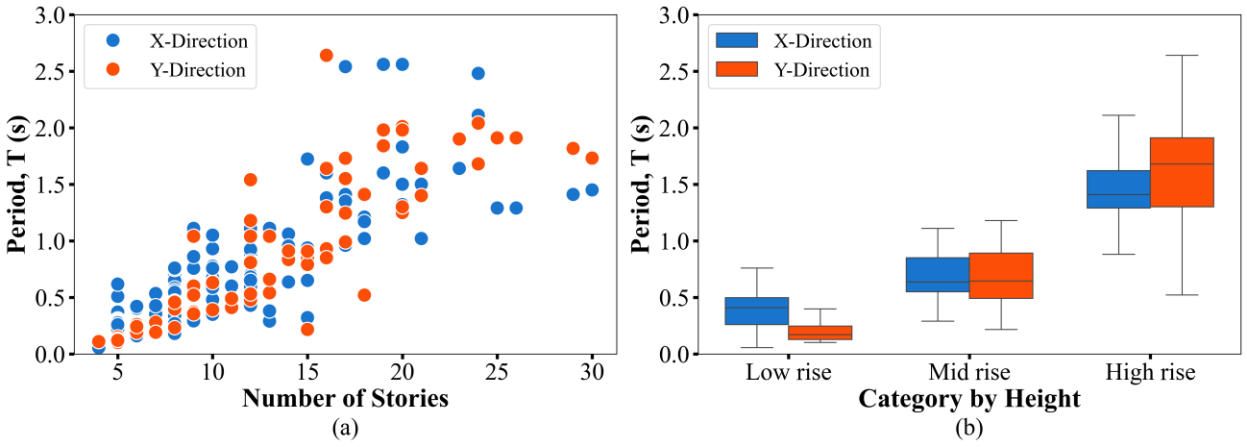

Figure 19. Variation of periods in the buildings in the database.

Based on the data dispersion in Figure 19, the lower (25th percentile) and upper (75th percentile) ends of the boxplots allow us to estimate the range where 50% of the data is concentrated. Based on this, in the longitudinal direction (major dimension), high-rise buildings have a structural period ranging from 1.29 to 1.62, mid-rise buildings range from 0.55 to 0.85, and low-rise buildings range from 0.26 to 0.50.

In the transverse direction (minor dimension), the range for high-rise buildings is between 1.30 and 1.91, for mid-rise buildings it is between 0.49 and 0.89, and for low-rise buildings, it is between 0.13 and 0.25.

Additionally, Figure 20 illustrates the variation of the cracking periods in the buildings within the database, where a reduction coefficient of 0.5 was applied to the walls to account for cracking within their principal plane.

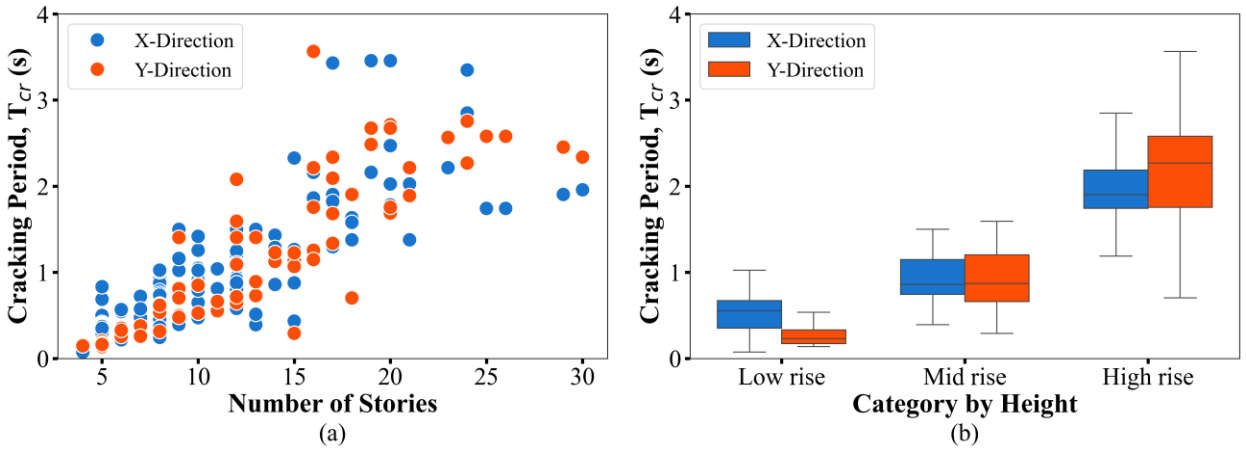

Figure 20. Variation of cracking periods in the buildings in the database.

Based on the data dispersion in Figure 20, the lower (25th percentile) and upper (75th percentile) ends of the boxplots allow us to estimate the range where 50% of the data is concentrated. Based on this, in the longitudinal direction (major dimension), high-rise buildings have a structural period ranging from 1.74 to 2.19, mid-rise buildings range from 0.74 to 1.15, and low-rise buildings range from 0.35 to 0.67.

In the transverse direction (minor dimension), the range for high-rise buildings is between 1.76 and 2.58, for mid-rise buildings it is between 0.66 and 1.20, and for low-rise buildings, it is between 0.17 and 0.33.

7.7.2. Wall Index (WI)

The Wall Index is defined as the percentage of wall area in each direction relative to the total constructed area of the building, as shown in Eq. 3:

$$WI_{ij} = \frac{\sum_{i=1}^{n}(t_{wij} \times L_{wij})}{A_{Built}} \qquad 3$$

Where:

- WI: Wall Index
- j: Analysis direction; “X” o “Y”.
- n: Number of walls in each direction
- t_W: Wall Thickness
- L_W: Wall Length
- A_{Built}: Total built-up area (The sum of the areas of all the slabs in the building)

Figure 21 displays the Wall Index (WI) for the various buildings in the database, categorized into three groups based on the number of stories. The boxplots for the two main directions of the buildings are shown on the figure; specifically, the blue color corresponds to the longitudinal direction (major dimension – "X"), and the orange color represents the transverse direction (minor dimension – "Y").

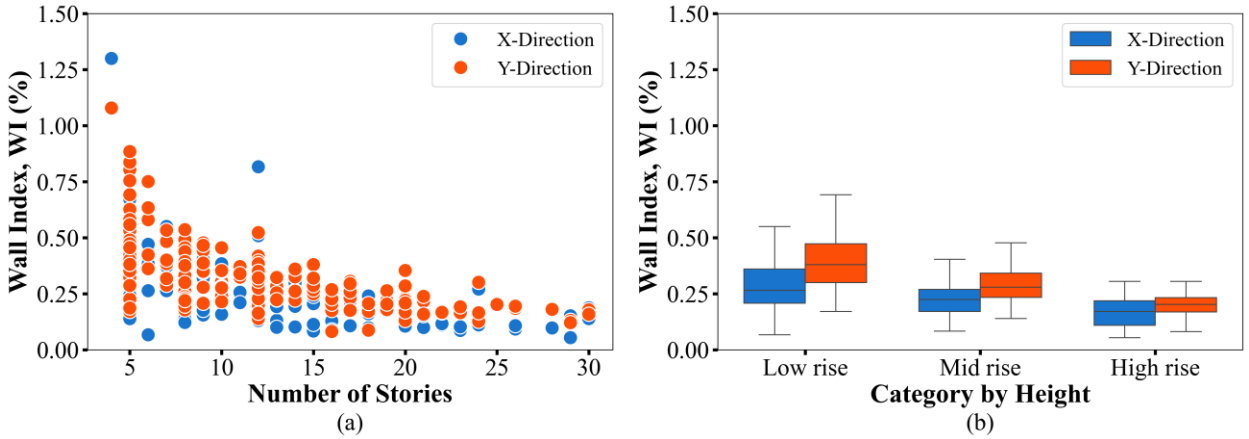

Figure 21. Distribution of Wall index by height.

Based on the data dispersion in Figure 21, the lower (25th percentile) and upper (75th percentile) ends of the boxplots allow us to estimate the range where 50% of the data is concentrated. Based on this, in the longitudinal direction (major dimension), high-rise buildings have a Wall Index ranging from 0.11 to 0.22, mid-rise buildings range from 0.17 to 0.27, and low-rise buildings range from 0.21 to 0.36.

In the transverse direction (minor dimension), it can be concluded that buildings in this direction have a slightly higher Wall Index. For high-rise buildings, the range is between 0.17 and 0.24, for mid-rise buildings it is between 0.23 and 0.34, and for low-rise buildings, it is between 0.30 and 0.48. An analysis of wall index trends indicates that the wall index decreases with increasing building height.

7.7.3. Stiffness Index (H/Tcr)

The stiffness index is defined as the ratio between the height of the building and the cracked period in each structural direction. Figure 22 displays the stiffness index for the buildings in the study database.

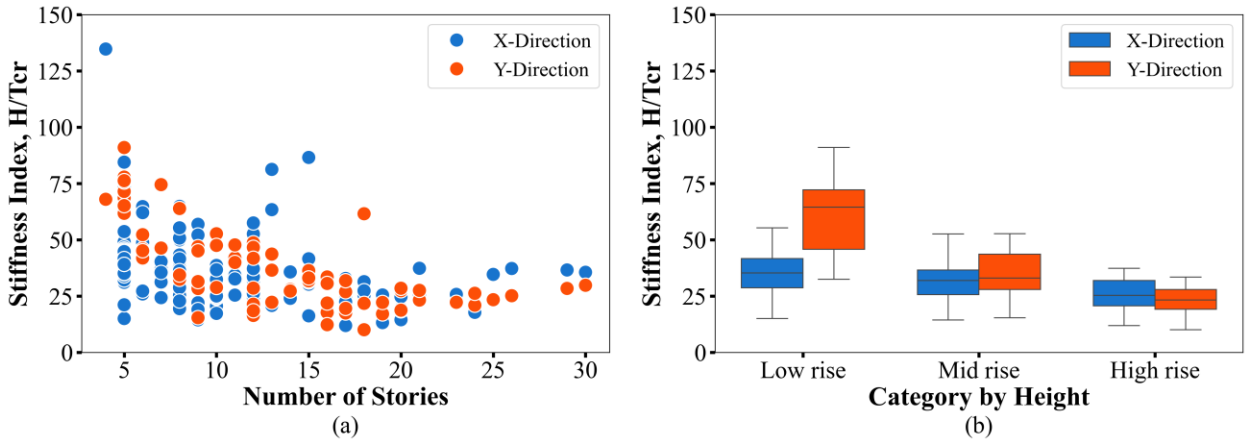

Figure 22. Stiffness index distribution by height.

Based on the data dispersion analysis represented in Figure 22, the 25th and 75th percentiles of the box and whisker plots are used to infer the variability range in which 50% of the data is concentrated. In the longitudinal direction (major dimension), tall buildings exhibit a stiffness index ranging from 21 to 32; intermediate buildings fall within an interval between 26 and 36, while low-rise buildings are between 29 and 42.

In the transverse direction (minor dimension), tall buildings are within a range of 19 and 28; intermediate buildings are in an interval between 28 and 45, and low-rise buildings are situated between 46 and 74. An analysis of the trends in the stiffness indices concludes that the index in the transverse direction is higher than in the longitudinal for low and intermediate-rise buildings, and as the building height increases, the index tends to decrease

7.8. LOCAL ATTRIBUTES

7.8.1. Aspect Ratio (Ar)

The aspect ratio is defined as the ratio between the total height of the wall from the base to the top of the building (H_W) and its length (L_W).

$$Ar = \frac{H_W}{L_W} \qquad 4$$

Figure 23 presents the aspect ratio for the walls of the buildings in the database. This variable was calculated for each principal direction; the aspect ratio in the longitudinal direction (major dimension – "X") is shown in blue, and the aspect ratio in the transverse direction (minor dimension – "Y") is shown in orange.

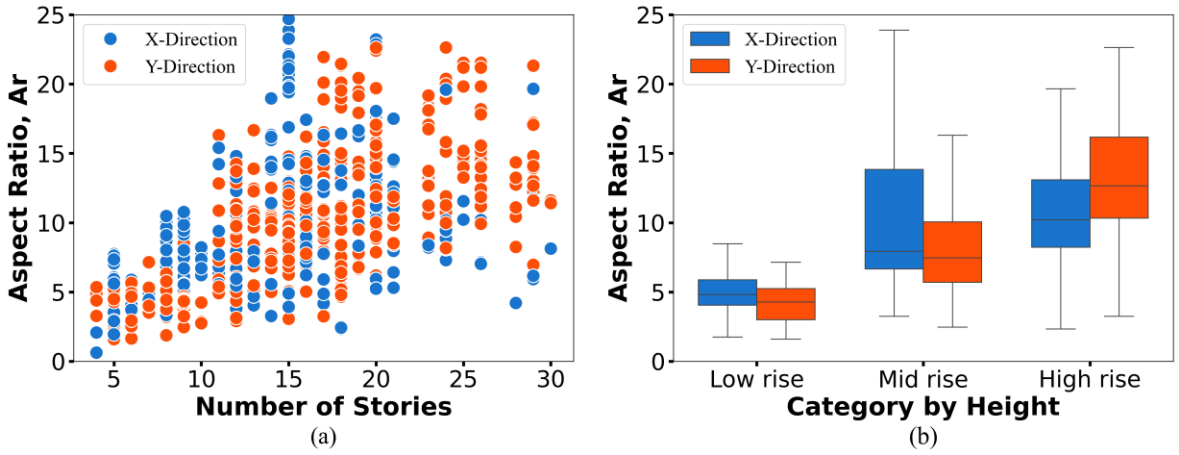

Figure 23. Distribution of the aspect ratio by height.

Based on the data dispersion in Figure 23, the lower (25th percentile) and upper (75th percentile) ends of the box and whisker plots allow us to estimate the range in which 50% of the data is concentrated. Accordingly, in the longitudinal direction, walls of tall buildings have an aspect ratio ranging from 8 to 13, walls of intermediate buildings range from 7 to 14, and walls of low-rise buildings range from 4 to 6. In the transverse direction, walls of tall buildings range from 10 to 16, in intermediate buildings, the walls range from 6 to 10, and for low-rise buildings, this parameter varies between 3 and 5. Based on the results obtained, it can be concluded that this parameter increases as the building height increases. This trend was expected since this parameter is directly related to the building height.

Based on the definition of this parameter, which represents an individual attribute of the walls that comprise the building, it was necessary to identify an attribute that could provide a general representation of the building and be characterized with this geometric information. To achieve this, two parameters were established: the mean aspect ratio (Ar_{Mean}) and the aspect ratio of the main wall ($Ar_{MainWall}$) of the building. These parameters serve as unique and representative attributes for each building under study.

7.8.1.1. Mean Aspect Ratio (Ar_{Mean})

The mean aspect ratio (Ar_{Mean}) is a key geometric parameter that reflects the overall proportions of the building`s walls. This parameter is calculated as the average aspect ratio of all walls oriented in the direction of analysis.

Figure 24 illustrates the Mean Aspect Ratio, which data grouped by building height categories. Table 3 presents the percentages distribution of each Ar_{Mean} also categorized by building height.

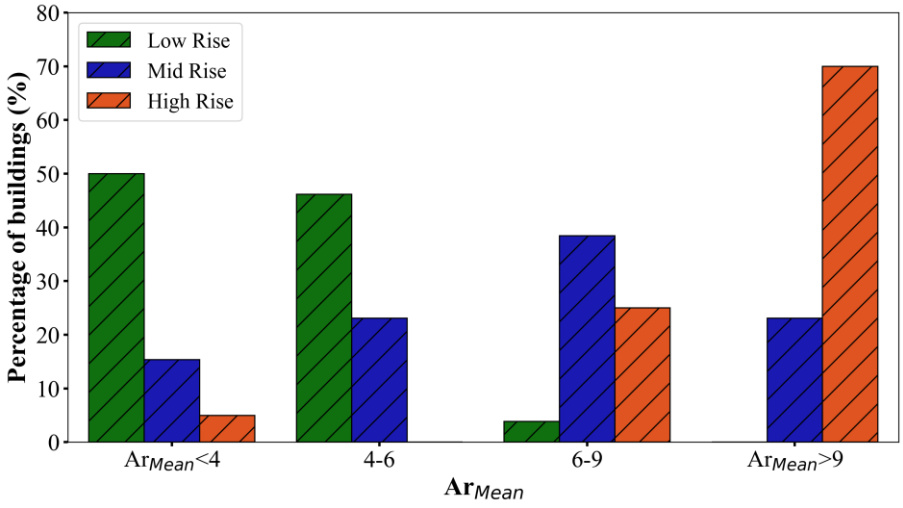

Figure 24. Ar_{Mean} distribution by height.

Table 3. Percentage buildings in each category by Ar_{Mean}.

Group of Buildings	$Ar_{Mean}<4$	4-6	6-9	$Ar_{Mean}>9$
Low-rise	50.0	46.2	3.8	0.0
Mid-rise	15.4	23.1	38.4	23.1
High-rise	5.0	0.0	25.0	70.0

Table 3 reveals that low-rise buildings predominantly exhibit a Ar_{Mean} below 4, with 50.0% falling into this category, suggesting that low-rise structures typically have broader proportions relative to their height. In mid-rise buildings, the aspect ratios distributions become more varied, 38.4% of these buildings have an Ar_{Mean} between 6 and 9, and 23.1% exceed 9. This indicates a more diverse structural configuration in mid-rise buildings.

In contrast, high-rise buildings show a notable trend, with a significant 70.0% having an Ar_{Mean} greater than 9, underscoring the tendency for taller structures to adopt narrower, taller proportions-key factors for seismic performance and overall stability. Only 5.0% of high-rise buildings have an Ar_{Mean} below 4, highlighting the distinct differences and design characteristics associated with increased building height. These findings will be further examined in the subsequent chapters, particularly regarding implications for seismic performance and structural design.

7.8.1.2. Aspect Ratio of the Main Wall ($Ar_{MainWall}$)

The aspect ratio of the main wall (ArMainWall) is a critical attribute that characterizes the primary wall of the building. Defined as the ratio of the wall's height to its width, this parameter provides a specific measure of wall geometry, servingas a unique and representative attribute for each building under in the study and facilitating a nuanced analysis of structural performance.

Figure 25 illustrate the Aspect Ratio of the Main Wall, with data grouped by building height categories. The Table 4 presents the percentages distribution of each $Ar_{MainWall}$ also categorized by building height.

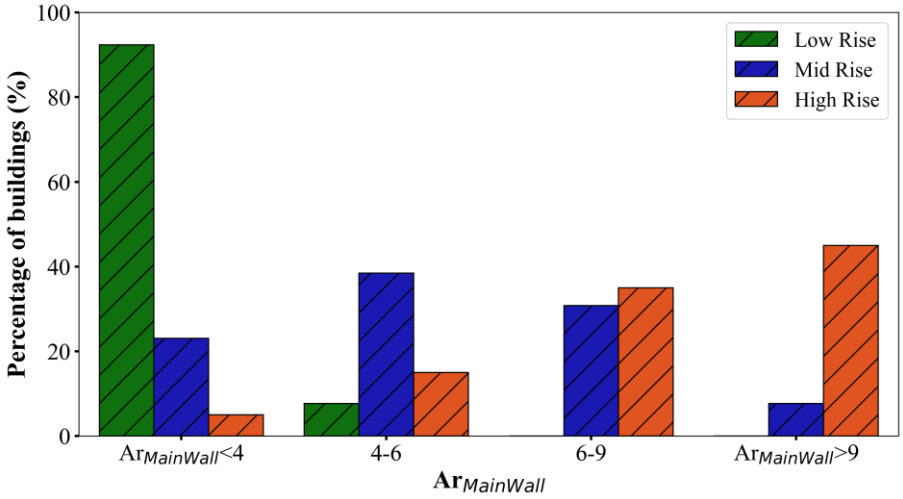

Figure 25. $Ar_{MainWall}$ distribution by height.

Table 4. Percentage of in each category by $Ar_{MainWall}$.

Group of Buildings	$Ar_{MainWall}$<4	4-6	6-9	$Ar_{MainWall}$>9
Low-rise	92.3	7.7	0.0	0.0
Mid-rise	23.0	38.5	30.8	7.7
High-rise	5.0	15.0	35.0	45.0

The data presented in Table 4 highlights significant differences in the aspect ratio of the main wall ($Ar_{MainWall}$) across various building types. For low-rise buildings, the majority (92.3%) have an ArMainWall below 4, indicating that low-rise structures generally features wider wall proportions, which may contribute to greater stability in these lower buildings.

In contrast, mid-rise buildings exhibit a more balanced distribution of $Ar_{MainWall}$ values. While 23.0% of mid-rise buildings have $Ar_{MainWall}$ below 4, 38.5% fall within the range of 4 to 6, and 30.8% between 6 and 9. This variation suggests a broader range of wall configuration in mid-rise structures, potentially reflecting diverse architectural designs and structural requirements.

High-rise buildings show a marked shift, with 45.0% having an $Ar_{MainWall}$ exceeding 9. This trend underscores the increasing prevalence of narrow, tall walls in high-rise designs, which can be critical for optimizing structural performance under seismic loading. Additionally, only 5.0% of high-rise buildings have an $Ar_{MainWall}$ below 4, reinforcing the tendency for taller structures to adopt narrower proportions.

Overall, these findings underscore the influence of building height on the main aspect ratio, with low-rise buildings favoring broader configurations and high-rise buildings trending towards narrower designs. This variation will be further analyzed in subsequent chapters, particularly in relation to its implications for the seismic resilience of different building types.

7.8.2. Axial Load Ratio (ALR)

The axial load ratio is obtained as the ratio between the actual axial load on the wall (Pu) and the nominal load-bearing capacity of the wall defined as the product of the compressive strength (f'c) and the net cross-sectional area of the wall (Ag), as shown in Eq. 5.

$$\text{ALR} = \frac{\text{Pu}}{\text{f'c} * \text{Ag}} = \frac{\text{Pu}}{\text{f'c} * (\text{L}_\text{W} * \text{t}_\text{W})} \quad 5$$

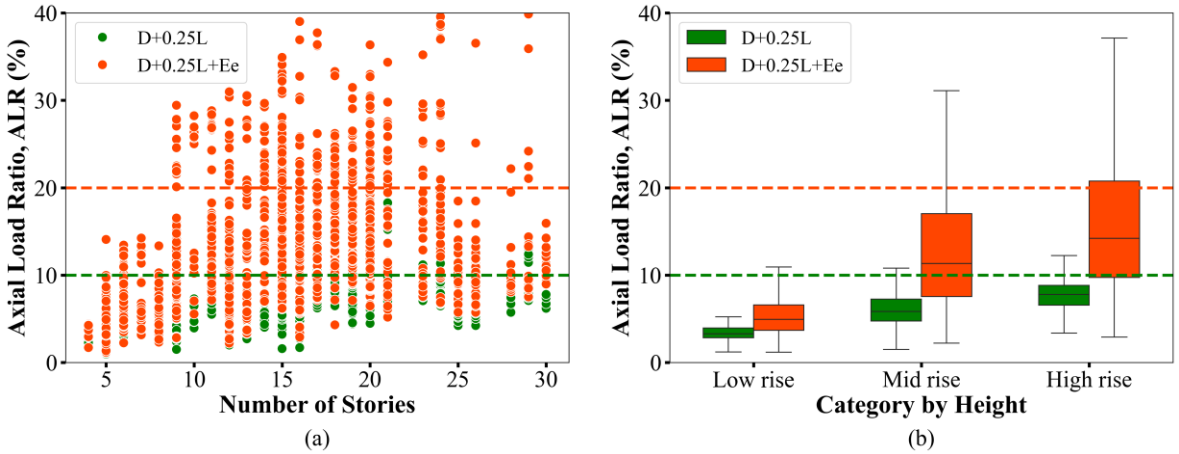

Figure 26. Distribution of axial load ratio as a function of building height.

Figure 26 shows the box and whisker plot for the three defined categories based on the building height, differentiating the two main directions. Based on this, for the case of gravitational load, which considers the entire dead load of the building plus an additional 25% of the live load (D+0.25L), the axial load ratio (ALR) for high-rise buildings ranges between 9% and 17%, for intermediate-rise buildings it is between 4% and 9%, and for low-rise buildings it is between 3% and 5%. Additionally, for the case where increments due to seismic effects are included (D+0.25L+Ee), the ALR for high-rise buildings ranges between 10% and 21%, for intermediate-rise buildings it is between 4% and 10%, and for low-rise buildings, this ratio varies between 3% and 7%. According to the results obtained, it can be concluded that this parameter increases as the building height increases. This trend was expected, as this parameter is related to the number of elevated slabs loaded in a building.

7.8.3. Slenderness (S)

Slenderness is defined as the ratio between the height of the wall interstory (Hs) and its thickness (t_W), as shown in Eq. 6:

$$\text{S} = \frac{\text{Hs}}{\text{t}_\text{W}} \quad 6$$

Figure 27 presents the slenderness for the buildings contained in the study database. For the analysis of this parameter, the categories defined for the buildings by height were considered; additionally, each of the main directions of the building analysis was discretized. Slenderness values in the longitudinal direction (major dimension – "X") are shown in blue, and in the transversal direction (minor dimension – "Y"), they are shown in orange for all buildings. The figure indicates the limit imposed by ACI-318-19, which defines a maximum slenderness of 16 for reinforced concrete walls (CR).

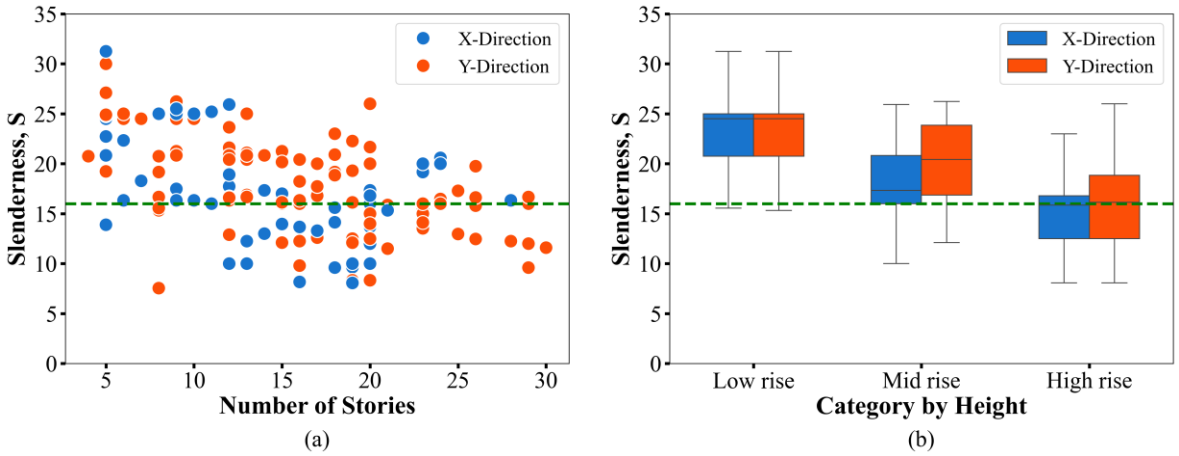

Figure 27. Slenderness distribution by height.

According to the data presented in Figure 27, the slenderness in the low-rise buildings is close to 25, indicating slender elements. For these types of structures, it was determined that walls with a thickness less than 0.12 m are present.

In the intermediate and tall buildings, the average slenderness values range between 18 and 20, indicating that the average thickness in these structures is greater than in low-rise buildings but still less than or equal to 0.15 m. In tall buildings, the slenderness value for 29% of the buildings is less than 16, with thickness close to 0.20 m.

Finally, a total of 50 buildings were analyzed from the database, all of which had complete information. The aim of this analysis was to conduct an in-depth study of the behavior and characterization of the system under study. For each of these selected buildings, the conditions of the walls composing them were processed. The results of this analysis are described in the following sections.

7.8.4. Type of Reinforcement

Figure 28 illustrates the reinforcement schematic for the studied walls, where two types of reinforcement are depicted: electro-welded wire mesh (WWM) in red and ductile steel reinforcement (RB) in blue.

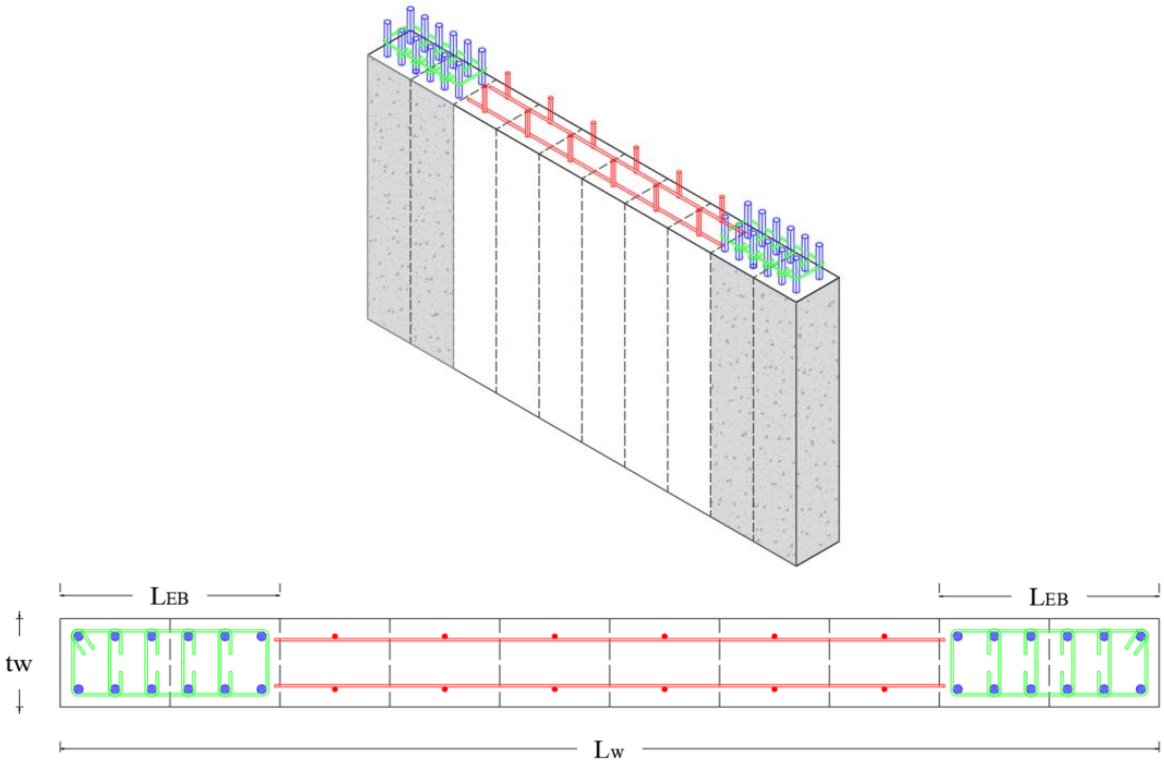

Figure 28. Types of Reinforcement for RCW.

Within the database, wall thicknesses (tw) vary from 0.08 to 0.25 m, and different reinforcement configurations are observed. Typically, walls with a thickness of 0.12 m or less are reinforced with a single central line of WWM, which may or may not include concentrated ductile reinforcement at the ends (refer to the upper wall in Figure 29). In contrast, walls with a thickness of 0.15 m or more generally require two layers of reinforcement. In these thicker walls, it is common for the end reinforcement to require some form of confinement, a characteristic that will be discussed in greater detail in subsequent chapters (see the lower wall in Figure 29).

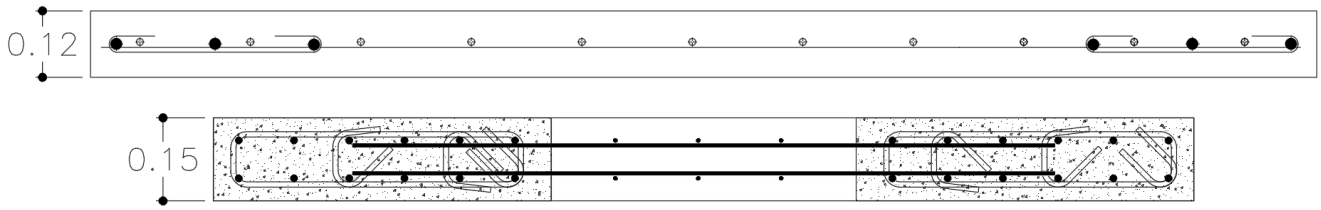

Figure 29. Reinforcement detailing of longitudinal reinforcement concentrated at the edge of walls with thickness lower than 150 mm, and confinement in boundary elements for 150 mm walls (units in m).

In Colombia, WWM has been widely used as the longitudinal reinforcement distributed in the wall web, with steel deformed bars added as concentrated longitudinal reinforcement at the ends of the walls when

necessary. The Colombian Earthquake Engineering Research Network (CEER) reported in 2019 (Carrillo et al. 2019) that WWM has very low ductility and, therefore, should not be used as the primary reinforcement in elements that are part of a building's lateral load-resisting system. Figure 30 illustrates the distribution of buildings by height and the type of reinforcement used. In low-rise buildings, WWM is used exclusively as the reinforcement in the wall web, while in mid-rise buildings, the most common configuration combines WWM in the web with deformed steel bars concentrated at the wall ends.

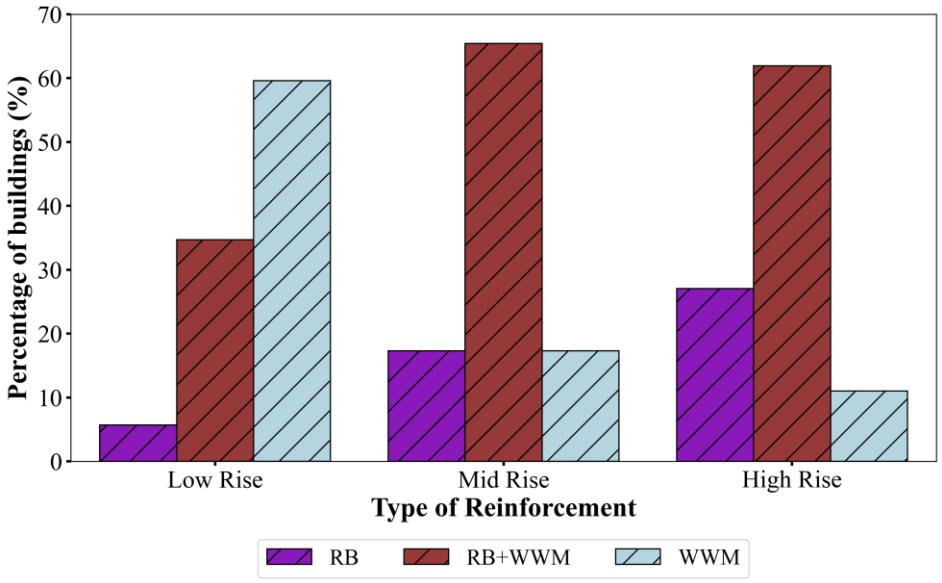

Figure 30. Type of reinforcement distribution by height.

The Table 5 presents the percentages of each reinforcement type grouped by building height categories.

Table 5. Percentage of high-rise buildings in each category by Type of Reinforcement.

Group of Buildings	RB	RB+WWM	WWM
Low-rise	5.7	34.7	59.6
Mid-rise	17.3	65.4	17.3
High-rise	27.1	61.9	11.0

Based on the findings presented in Figure 30 and Table 5, low-rise buildings generally use WWM reinforcement. In contrast, more than 60% of mid and high-rise buildings use a combination of RB in the wall edges and WWM in the web. Notably, 1 out of 6 mid-rise buildings are reinforced using WWM and roughly 3 out of 10 high-rise buildings are reinforced using only RB.

7.8.5. Type of confinement

Depending on the level of stress and wall thickness, reinforced concrete walls often require specific boundary conditions to enhance their structural performance. To achieve this, confinement reinforcement is

implemented at the wall ends, which significantly improves the ductility of the element. The configuration of this confinement reinforcement is illustrated in Figure 29.

Figure 31 examines the types of confinement used in the reinforced concrete walls. The data is presented and grouped by the building height categories. The Table 6 presents the percentages of each confinement type grouped by building height categories.

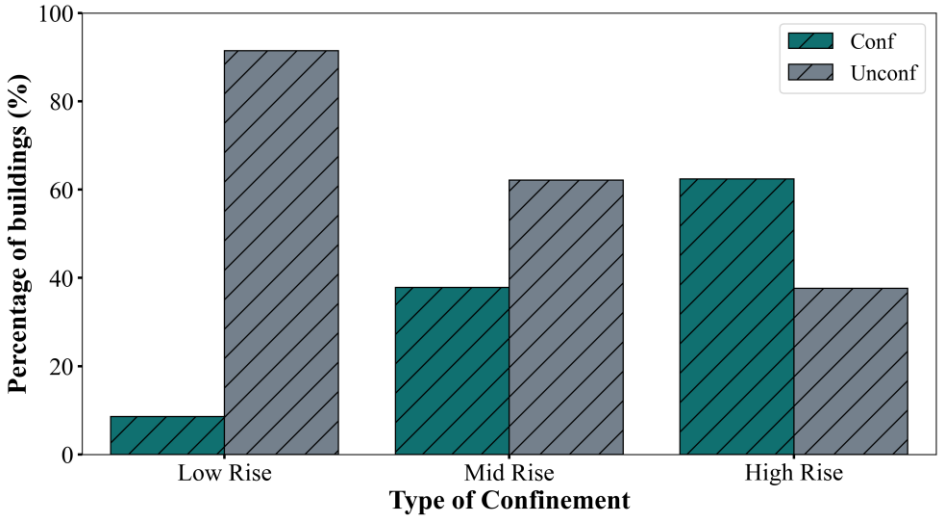

Figure 31. Type of Confinement distribution by height.

Table 6. Percentage of buildings in each category by Type of Confinement.

Group of Buildings	Confined	Unconfined
Low-rise	8.6	91.4
Mid-rise	37.8	62.2
High-rise	62.4	37.6

Based on the findings presented in Figure 31 and Table 6, It can be determined that low-rise buildings generally do not have confinement. As we move up in height, an increasing number of walls have confinement. However, it is noteworthy that a significant percentage of walls in mid-rise buildings (17.8%) and high-rise buildings (12.7%) do not have confinement. This condition is of great interest and will be further evaluated in the following chapters.

7.8.6. Edge Reinforcement Ratio, ρ_b

In this study, we differentiate between "edge reinforcement" and "boundary reinforcement."

Edge reinforcement refers specifically to the reinforcement located in the edge fibers of the wall, without considering whether it is confined or not. This means that edge reinforcement only addresses the longitudinal reinforcement present at the edges.

In contrast, when confinement is evident, the element is referred to as a boundary element. Boundary elements incorporate both edge reinforcement and additional reinforcement provided to enhance the wall's structural integrity under lateral loads.

By separating these variables in our analysis, we aim to provide a clearer understanding of their distinct roles and implications in the behavior of walls under seismic conditions.

Figure 32 analyzes the Edge reinforcement ratios of the reinforced concrete walls. The data is categorized and analyzed based on the building height groups.

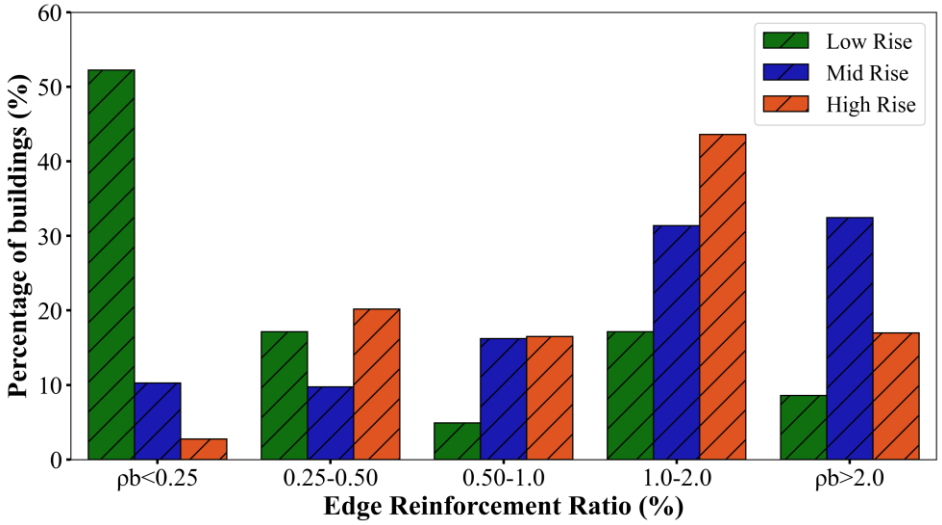

Figure 32. Distribution of Edge Reinforcement Ratio.

Table 7 presents the percentages of each group of edge reinforcement ratio grouped by building height categories.

Table 7. Percentage of high-rise buildings in each category by Edge Reinforcement Ratio.

Group of Buildings	<0.25%	0.25%-0.50%	0.50%-1.0%	1.0%-2.0%	>2.0%
Low-rise	52.3	17.1	4.9	17.1	8.6
Mid-rise	10.3	9.7	16.2	31.4	32.4
High-rise	2.7	20.2	16.5	43.6	17.0

Based on the findings presented in Figure 32 and Table 7, it can be determined that low-rise buildings generally have a reinforcement ratio of less than 0.25% at the edges. As buildings increase in height, there is an increase in the reinforcement ratio concentrated at the ends. This is consistent with their demand level, as the demand for these elements increases with building height due to flexural compression.

7.8.7. Web Reinforcement Ratio, ρ_w

According to the NSR-10 code, if the shear force Vu of the wall does not exceed 0.083*√f'c*Ag, the longitudinal reinforcement ratio of the wall can be reduced from 0.25% to 0.12%. Therefore, in many cases, low and mid-rise buildings may have a reduced longitudinal reinforcement ratio.

Figure 33 analyzes the Web reinforcement ratios of the reinforced concrete walls. The data is categorized and analyzed based on the building height groups. Table 8 presents the percentages of each group of edge reinforcement ratio grouped by building height categories.

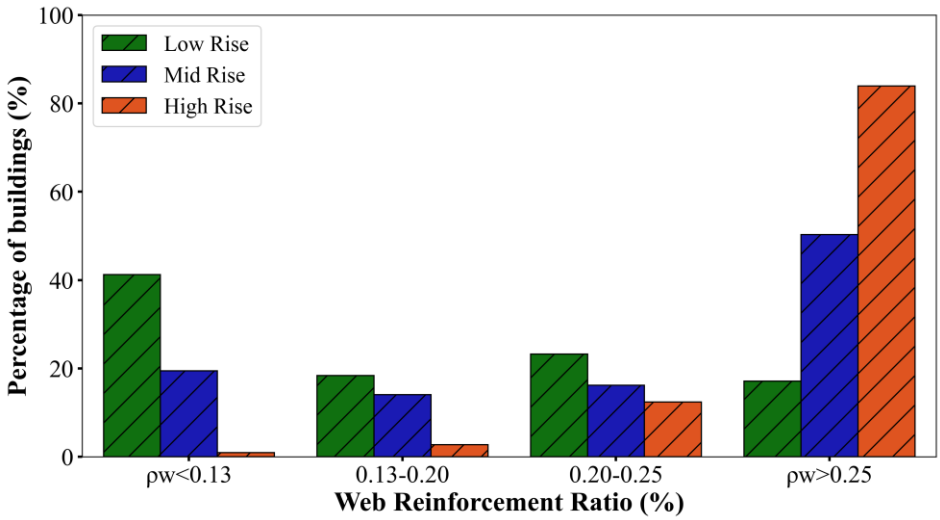

Figure 33. Distribution of Web Reinforcement Ratio.

Table 8. Percentage of high-rise buildings in each category by Web Reinforcement Ratio.

Group of Buildings	<0.13%	0.13%-0.20%	0.20%-0.25%	>0.25%
Low-rise	41.2%	18.4%	23.3%	17.1%
Mid-rise	19.4%	14.1%	16.2%	50.3%
High-rise	0.9%	2.8%	12.4%	83.9%

Based on the findings presented in Figure 33 and Table 8, low-rise buildings typically (more than 40%) have a reinforcement ratio of less than 0.13% at the web. As buildings increase in height, there is an increase in the reinforcement ratio concentrated at the web. This is consistent with their demand level, as the demand for these elements increases with building height due to flexural compression.

7.8.8. Longitudinal reinforcement ratios, ρ_b/ρ_w

The present study examines the relationship between the edge reinforcement ratio and the web reinforcement ratio as an indicator of the ratio of reinforcement concentrated at the wall ends. Designers

often adjust the reinforcement configuration to increase the wall's flexural-compression capacity. However, a significant concentration of reinforcement at the wall ends, without adequate control of the reinforcement ratio in the web could result in the propagation of cracks along the wall once stress levels cause high deformations in the fibers adjacent to the heavily reinforced areas. The distribution of this parameter across the buildings in the database is illustrated in the Figure 34. The Table 9 presents the percentages of each group of longitudinal reinforcement ratio (ρb/ρw) grouped by building height categories.

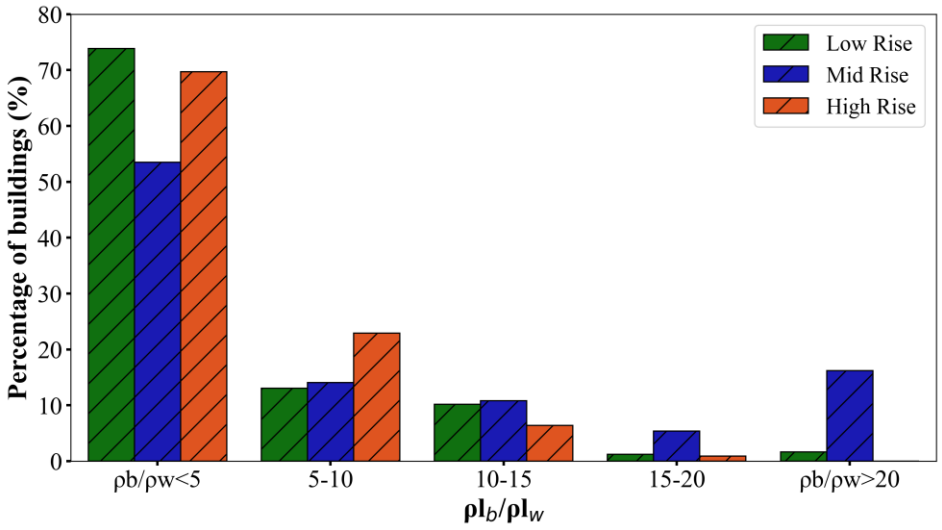

Figure 34. Distribution of Longitudinal Reinforcement Ratio.

Table 9. Percentage of high-rise buildings in each category by Longitudinal Reinforcement Ratio, ρb/ρw.

Group of Buildings	<5	5-10	10-15	15-20	>20
Low-rise	73.9%	13.1%	10.2%	1.2%	1.6%
Mid-rise	53.5%	14.1%	10.8%	5.4%	16.2%
High-rise	69.8%	22.9%	6.4%	0.9%	0.0%

The results reveal distinct patterns in the ratio of boundary reinforcement to web reinforcement across different groups of buildings. For low-rise buildings, the majority (73.9%) have a ratio below 5, indicating that the boundary reinforcement is not significantly higher than the web reinforcement. In contrast, mid-rise buildings display a more varied distribution, with a notable proportion (16.2%) having a ratio greater than 20, suggesting a higher concentration of reinforcement at the wall ends. High-rise buildings show a similar trend to low-rise buildings, with the majority (69.8%) having a ratio below 5, but they have a smaller presence in higher ratio categories. These results suggest that mid-rise buildings are more likely to have a greater concentration of boundary reinforcement relative to the web, while low-rise and high-rise buildings maintain a more balanced reinforcement distribution. This may be due to the fact that high-rise buildings experience greater shear forces than mid-rise buildings, making it impossible to reduce the reinforcement

quantity in these elements, as seen in Figure 33, where the majority of high-rise buildings exhibit web reinforcement ratios equal to or greater than 0.25%.

8. NUMERICAL MODELING

This section outlines the approach and methodology employed to model RCW buildings. It begins with a description of the approach used for representing the walls, followed by the definition of the elements and their dynamic properties. Subsequently, the process, results, and analysis of the buildings' nonlinear response are presented.

For each building in the database, a representative archetype was modeled in both longitudinal and transverse directions. The representative walls for each direction were selected based on their percentage contribution to the building's seismic base shear. The materials were modeled using constitutive laws available in OpenSees, and their properties were calculated based on information found in the literature. For all archetypes, both pushover and nonlinear time-history analyses were conducted. In the former, the analyses were performed considering a loading pattern proportional to the structure's first mode. With the results of these analyses, performance points of the structures were compared, and damage states were calculated, serving as a benchmark for dynamic analyses. In the latter, time-history analyses were conducted using seismic records representative of the country's hazard. Finally, fragility curves were constructed.

8.1. TYPE OF MODELING

In this study, the analytical modeling of RCWB was conducted using macroscopic models, which are practical and computationally efficient compared to microscopic models based on the Finite Element Method (FEM). A practical modeling approach should be straightforward to implement, computationally efficient, numerically stable, and provide adequate accuracy in inelastic prediction. In this regard, macro-models allow for a reduction in the number of degrees of freedom compared to FEM models, resulting in a smaller stiffness matrix and a faster, more efficient analysis (Rezapour & Ghassemieh, 2018). Various approaches are available in the literature for macroscopic modeling of walls. The software PERFORM3D (Computers and Structures Ink, 2005) is commonly used to model walls as "Shell" type, using force wall elements, nonlinear truss models, or elements based on multiple vertical mechanisms like MVLEM and SFI-MVLEM (Esmaeiltabar et al., 2019; Haghi et al., 2020; Kolozvari et al., 2018). As highlighted in Section 2, OpenSees (Open System for Earthquake Engineering Simulation) (McKenna et al., 2010) is one of the most widely used software for seismic analysis of RC buildings due to its extensive library of elements and materials to represent different structural systems. It also allows for the use of MVLEM and SFI-MVLEM modeling approaches.

8.2. MODELING ELEMENT

Based on the distribution of aspect ratios outlined in Chapter 7.8.1 of this document, it can be concluded that the primary structural walls in these buildings, which have aspect ratios (Ar) greater than 2.0, are predominantly influenced by flexural behavior. This suggests that the design and performance of these walls are primarily governed by bending moments rather than shear forces, which is consistent with the observed geometric proportions. This finding aligns with the conclusions presented by Pozo, Hube, and Kurama (2020), who emphasize the significance of flexural response in the behavior of planar reinforced concrete walls.

In this report, RCWB were modeled using the OpenSeesPy tool, employing 2D representations of the structures. The walls were represented using MVLEM elements, which, among the previously mentioned approaches, have demonstrated a good balance between simplicity, numerical stability, and accuracy (Haghi et al., 2020), along with efficient computational times (Pozo et al., 2020). It is important to highlight that the SFI-MVLEM element type could not be used due to numerical convergence issues, which would have posed significant challenges in obtaining reliable results from the models. This limitation underscored the need for opting for the MVLEM elements, ensuring that the modeling process remained robust and that the resulting analyses provided meaningful insights into the structural performance of the buildings (Portwood, 2024).

In the MVLEM elements, the approach divides the walls into horizontal sections (see Figure 35b), defined as macrofibers, modeled with a series of uniaxial vertical elements that capture the axial/flexural response of the element. These series of vertical elements are connected to a rigid beam at the top and bottom levels of the wall, as shown in Figure 35a. The relative rotation between the top and bottom of the element is concentrated at a rotation center defined at a height “ch” from the bottom of the element, assuming a uniform distribution of wall curvature over the height of each element. Typically, this height is set to a value of “c” equal to 0.4, following the recommendations of Vulcano et al., (1988). Furthermore, the shear response of the element is simulated by a horizontal spring located at the rotation center “ch” (element k_H in Figure 35a), whose behavior is defined by a force-displacement relationship.

The stiffness properties k_i and the force-displacement or behavior of these uniaxial elements are defined based on stress-strain constitutive relationships of the materials that make up the walls, in this case, concrete and steel, and the area of the macrofiber assigned to each uniaxial element.

Figure 36 shows a section of a rectangular wall divided into 10 macrofibers (k1 to k10). To analyze the behavior of the wall in the x-direction, two variables defining the element's geometry are considered: the width of each macrofiber (w) and the wall thickness (t). These variables allow for the calculation of the area

of each macrofiber associated with the uniaxial elements. The constitutive relationships of the materials forming the wall are also considered; in this case, fibers k1 and k10 are edge elements with confinement, so the response of the uniaxial elements in these macrofibers is linked to the properties of confined concrete (Conf) and ductile reinforcement bars (RB). For the fibers k2 to k9, the response would be determined by the behavior of unconfined concrete (Unconf) and welded wire meshes (WWM).

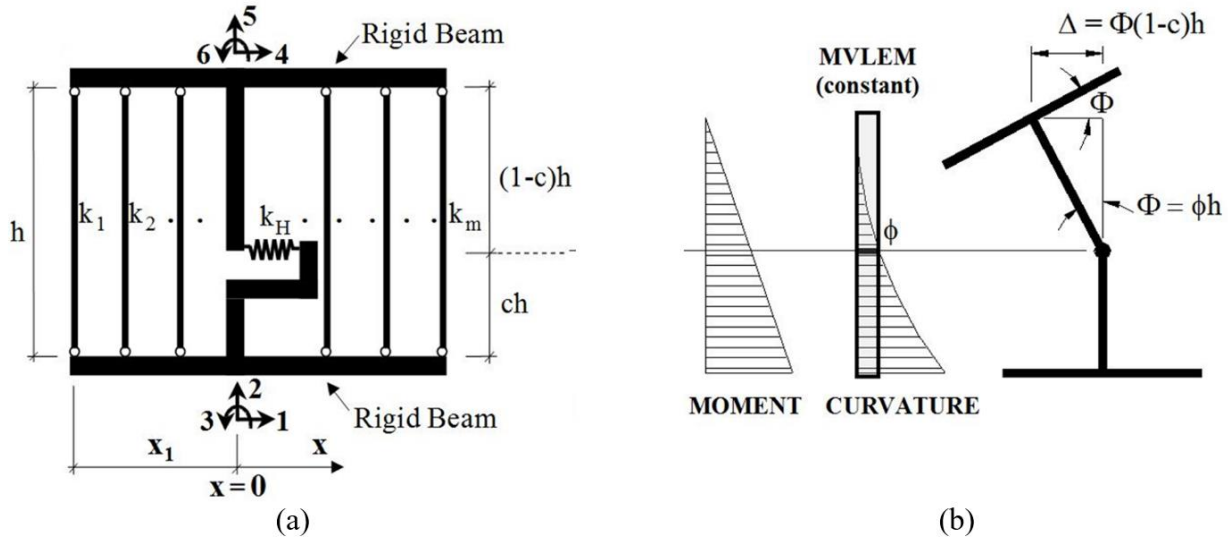

Figure 35. Representation of a) MVLEM Element and b) MVLEM Rotations and Displacements. Adapted from Kolozvari et al. (2015).

In addition to the above, the reinforcement ratios present in each macrofiber must also be considered, and the material representing the shear behavior of the wall must be defined. The information presented in the database drawings was useful in determining the reinforcement ratio in each macrofiber. Regarding the wall's shear behavior, it can be simulated using a linear-elastic relationship (Cando et al., 2020) with an effective shear modulus G_{eff} value dependent on the concrete's modulus of elasticity. Table 10 provides a summary of the input data required to define the walls as MVLEM elements in OpenSeesPy.

Table 10. Input Data for Defining the MVLEM Element in OpenSeesPy.

m	Number of macrofibers
c	Location of the rotation center (0.4)
Thick	Thickness vector of each macrofiber (direction perpendicular to the wall analysis axis)
Widths	Vector of widths of each macrofiber (direction parallel to the analysis axis of the wall)
Reinforcement ratio (*rho)*	Vector of reinforcement ratio for each macro-fiber

Material tag for the concrete (*matConcreteTags)*	Vector with the concrete constituent for each macrofiber
Material tag for the rebar steel (*matSteelTags)*	Vector with the reinforcement constitutive for each macrofiber
Material Tag for the Spring *(matShearTag)*	Vector with the material constitutive defined for the spring where the shear is concentrated (Geff = $1.5G_c$).

8.3. REPRESENTATION OF THE WALL IN THE NUMERICAL MODEL

The number of macrofibers for each wall varied depending on its length, ensuring that the width of each division remained between 30 cm and 50 cm. This was done to guarantee that the element adequately captures the unit deformations of the materials.

To represent these elements, a subdivision of the elements was made, identifying the different regions with their respective types of reinforced concrete and reinforcing steel, as well as their reinforcement ratios. This process ultimately idealized a section as shown in Figure 36. This figure illustrates the representation of material and reinforcement properties within each macrofiber. For each macrofiber, a thickness t_w is defined, consistent with the wall's geometry, as well as a width or K_i value that depends on the number of subdivisions of the main wall. Additionally, the longitudinal reinforcement ratio is specified, along with the definition of the concrete material type (confined or unconfined) and the steel type (RB or WWM) as applicable

Additionally, in the configuration of typical walls used in Colombia, special wall sections such as T-shaped, L-shaped, H-shaped, and C-shaped walls were identified. Considering this, it was necessary to create an approach for the representation of the walls that could capture the behavior of these shapes within the limits of the MVLEM, which was not developed to model irregular elements with out-of-plane boundary elements, such as the T-wall shown in Figure 37a. In some cases, elements where flanges coincided with the boundary element required a specific approach. Here, the macro-fiber was divided into two, and an equivalent thickness was used so that the total area of the element matched the area of the macro-fiber. The results of the study and the proposed approach are described by Feliciano et al. (2023). This approach was developed despite that Kolozvari introduced a 3D version of the MVLEM suitable for irregular walls. Due to its 3D formulation, the number of degrees of freedom increases, leading to higher computation times and reduced efficiency. Given that chronological analyses require intensive processes, it was necessary to propose a modeling approach based on the MVLEM to simulate the behavior of walls with out-of-plane boundary elements.

Figure 37a shows an example of a T-shaped element analyzed in the x-direction (parallel to the web axis). This wall has a flange of 3.0 m and a web of 4.0 m, with boundary elements of 0.45 m and 0.50 m and

reinforcement ratios of 1%. The rest of the wall is reinforced with welded wire mesh with a reinforcement ratio of 0.25%.

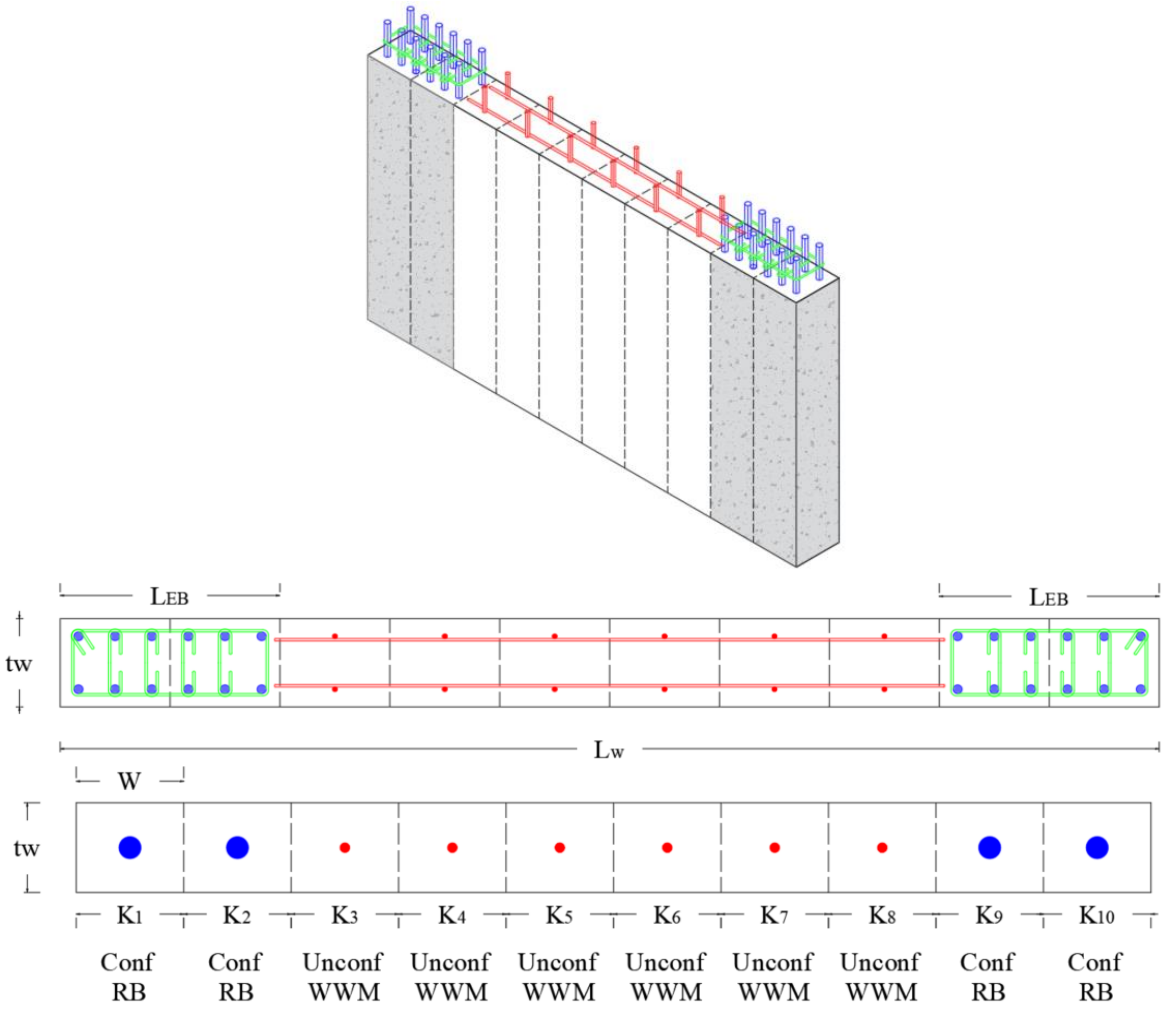

Figure 36. Idealization of reinforced concrete wall.

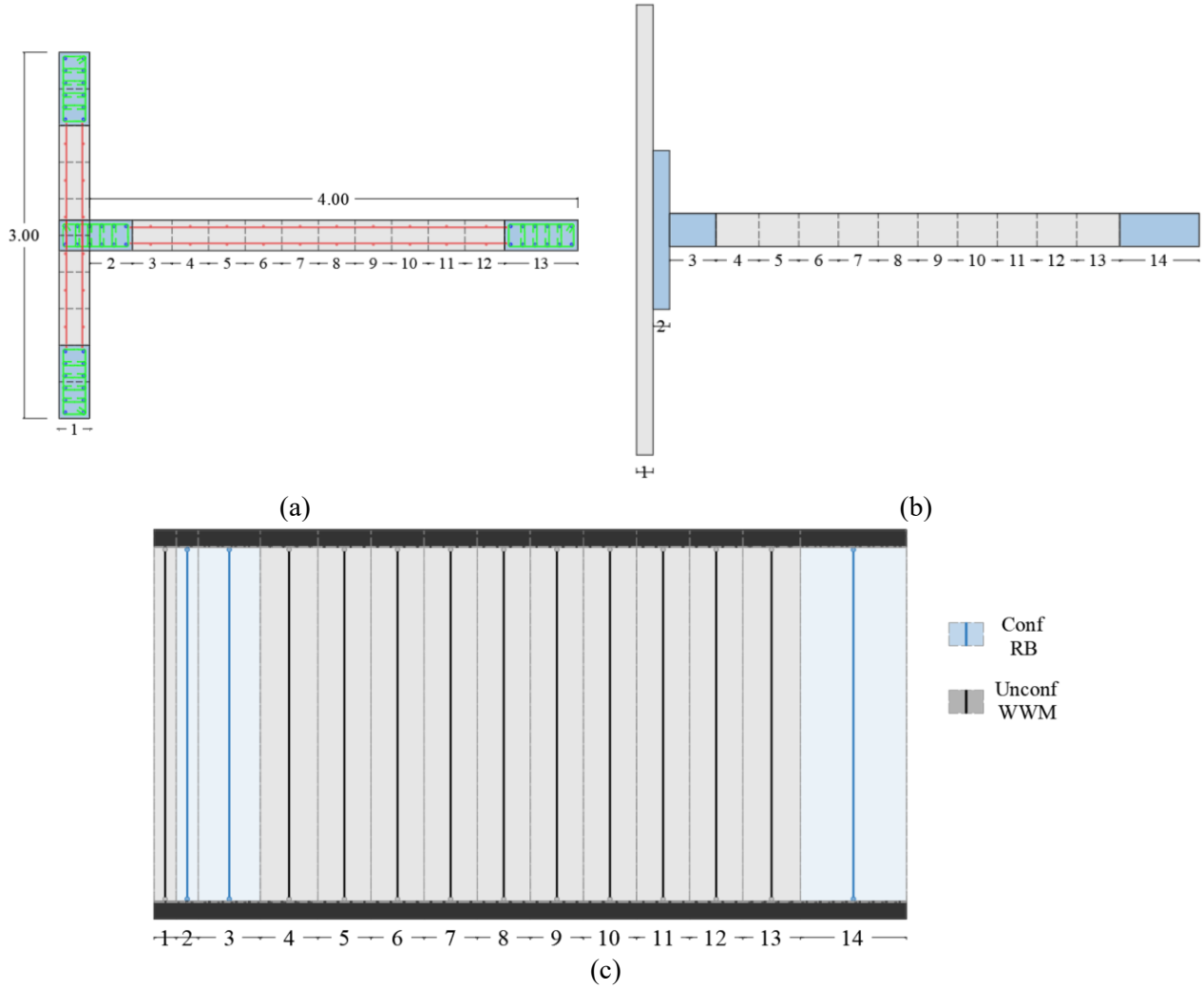

Figure 37. (a) Initial representation of the T-wall with the location of the boundary elements, (b) corresponding macrofibers after adapting the flange into two parts, and (c) vertical elements corresponding to each macrofiber.

8.4. MECHANICAL IDEALIZATION OF MATERIALS

Each macrofiber in the MVLEM element is associated with two types of materials: concrete, which can be either confined or unconfined, and reinforcing steel, which can consist of either welded wire mesh or ductile bars. OpenSees provides an extensive library of materials with their respective constitutive relationships that can be used in modeling. In this case, the materials Concrete01 and Hysteretic were used to represent concrete and reinforcement, respectively.

Concrete01 is characterized by nonlinear compressive strength and zero tensile strength. This material requires the definition of maximum and ultimate stress, as well as their corresponding strains, as shown in Figure 38a. The Hysteretic material is a uniaxial trilinear material that accounts for strength reduction, cyclic

deterioration due to strains and dissipated energy, and unloading stiffness degradation based on ductility. The input data for this material includes the definition of initial elastic stiffness, maximum compressive and tensile strength, yield strain, post-yield stiffness, and hardening and softening parameters (see Figure 38b).

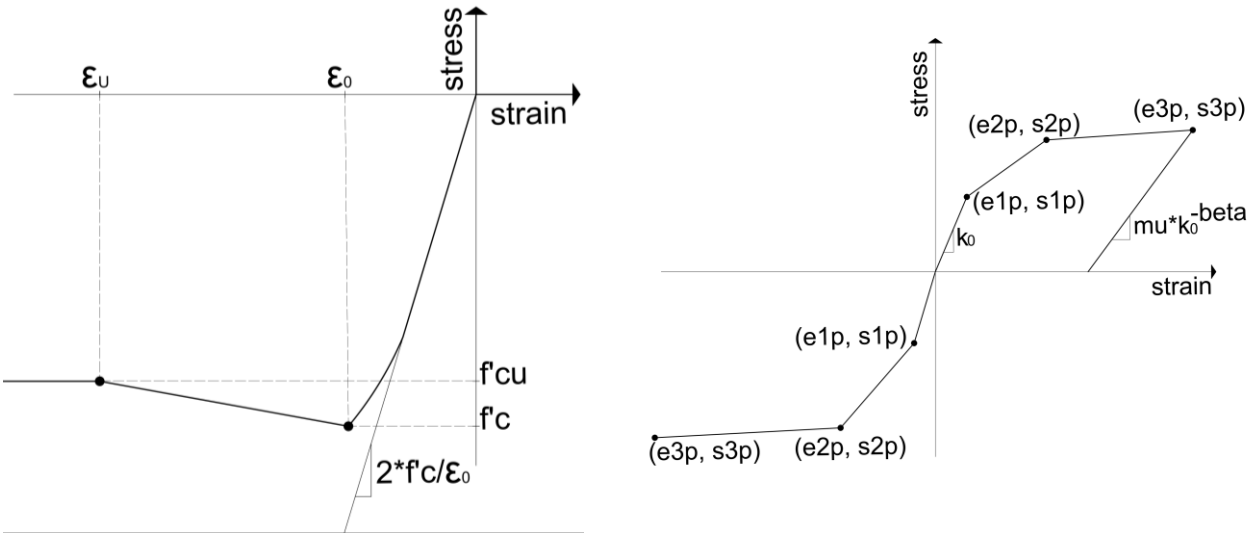

(a) (b)

Figure 38. Constitutive materials for: a) Concrete -Concrete01 and b) Reinforcement Hysteretic.

For the case of unconfined concrete, the first point $f'c$ was defined as the 28-day compressive strength of the concrete. This information was obtained from the plans and models in the database presented in Section 7.5. The ultimate strength points $f'c$u was calculated as 10% of the maximum strength value. The strain corresponding to the maximum strength ε0 was calculated based on the initial slope of the stress-strain curve using Eq. 7, and the ultimate strain εu was set to a fixed value of 0.006.

$$\varepsilon_0 = \frac{2 * f'c}{Ec} \qquad 7$$

The modulus of elasticity Ec was calculated based on the study reported in the CEER 001-2020 using Eq. **8**.

$$\mathrm{Ec} = 4300 * \sqrt{\mathrm{f'c}} \qquad 8$$

The constitutive curve for confined concrete was established based on the proposal by Mander et al. (1988), where the confined concrete strength $f'c$c is calculated as a factor k times $f'c$c. In this case, $f'cc$ was calculated as 1.3×$f'c$, representing an average value obtained for typical confined sections in this study. The strain corresponding to the maximum strength of confined concrete εcc was calculated using Eq. 7. The

ultimate strength of confined concrete was 20% of the maximum strength $f'ccu$, and its corresponding strain was set to a value of 0.02. Based on this, the constitutive relationships for concrete would have the response shown in Figure 39 for a 28 MPa concrete.

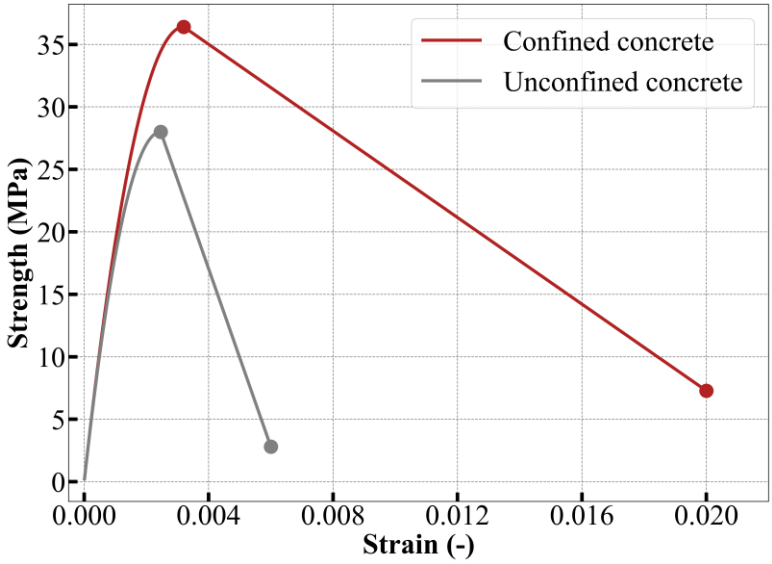

Figure 39. Constitutive model for concrete considering a f'c of 28 MPa.

Regarding reinforcement, three studies were considered: Carrillo et al. (2021) and Miranda-Giraldo et al. (2022). The latter study was supplemented and complemented with findings reported by Carrillo, Diaz, et al. (2019) for ductile reinforcement and welded wire mesh, respectively. In the first case, statistical analyses of tensile mechanical properties were conducted to characterize the stress-strain curve of steel bars commonly available in the central region of the country. In the second case, the hysteretic behavior of Colombian WWM was analyzed during cyclic testing, and constitutive models were calibrated for implementation in OpenSeesPy. Another consideration in modeling RC walls is that longitudinal reinforcement may exhibit buckling after concrete crushing, which can be simulated using the MinMax material available in OpenSeesPy (Marafi et al., 2019). With this approach, the steel loses tensile and compressive strength once the concrete reaches its ultimate strain (0.006). To simulate the failure of the reinforcement due to fatigue from multiple load cycles, the material was defined to lose strength once the strain exceeds its ultimate tensile strain value, taken as 0.05 for bars and 0.02 for mesh. Thus, the resulting constitutive relationships for the reinforcement follow the form shown in Figure 40.

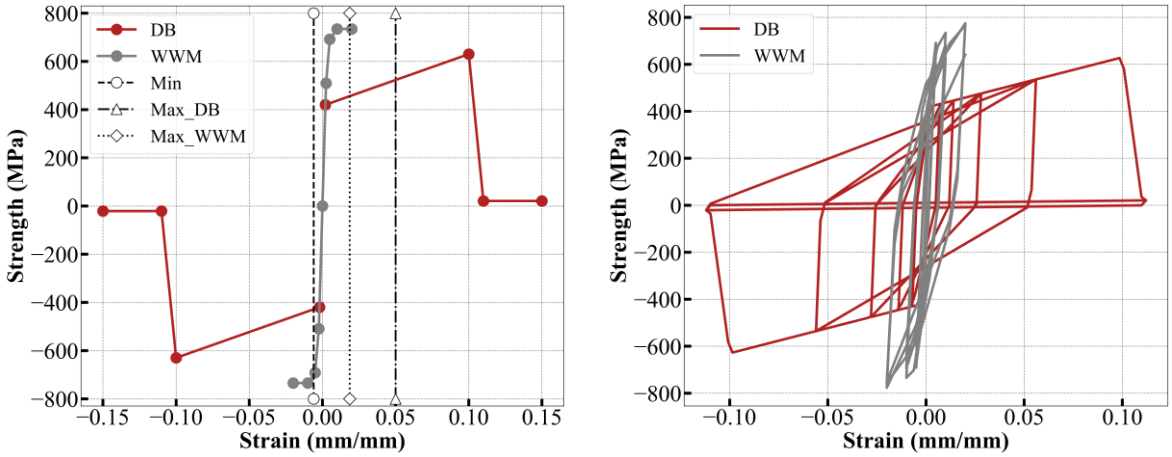

(a) (b)

Figure 40. a) Constitutive Models with Their Respective Limits for the Two Types of Reinforcement Present in CR Walls and b) Their respective hysteresis cycles.

Finally, to capture the shear behavior of the wall and assign a material to the spring, an elastic material was defined with a value of $G_{eff} = 1.5Gc$, where $Gc = 0.4Ec$.

9. ANALYSIS OF STRUCTURAL RESPONSE

This chapter presents a detailed analysis of the structural response of reinforced concrete wall buildings under the considered seismic demands. The analyses were carried out using two main approaches: the capacity curve evaluation and the nonlinear time-history analysis. The capacity curve allows for the assessment of the overall behavior of the structures under lateral loads, identifying their ultimate capacity and potential failure mechanisms. On the other hand, the nonlinear time-history analysis provides a more accurate view of the dynamic behavior of the structures under real seismic loads, considering the inelastic nature of the materials and the cumulative effects of vibrations. The combination of these two approaches offers a comprehensive understanding of seismic performance, providing key insights into ductility, energy dissipation capacity, and potential modes of structural collapse.

9.1. CAPACITY CURVE (PUSHOVER ANALYSIS)

The capacity curve, commonly known as the Pushover curve, is a graphical representation of the structural capacity of a building against its deformation demand. It provides a holistic view of the building's global behavior under seismic loading, showcasing the distribution of ductility and strength demand throughout its height. In this study, the Pushover analysis was conducted for each building archetype using OpenSees software, allowing for a comprehensive understanding of the structural response under seismic events. The obtained curves serve as a pivotal tool for seismic assessment and design, aiding in the identification of potential weaknesses and the determination of the building's overall seismic performance.

To assess the structural behavior of the buildings included in the database, a nonlinear static analysis (Pushover) was conducted. Various factors within the capacity curve were identified, as detailed in the following sections. One key parameter used to evaluate structural performance is the roof drift ratio (RDR), defined as the ratio of the building’s roof displacement to its total height. This parameter provides insight into the global deformation capacity and helps assess the potential for structural damage under seismic loads.

Figure 41 shows a general schematic of the capacity curve for a 5-story RC wall building. In this figure, the spectral acceleration coefficient (Sa) and the seismic coefficient (Cs) are highlighted, which corresponds to the design shear force (Vd) normalized by the building's weight. The value of Vd is calculated as the elastic design shear force (Ve) divided by the force reduction factor (R), that is, Vd = Ve/R.

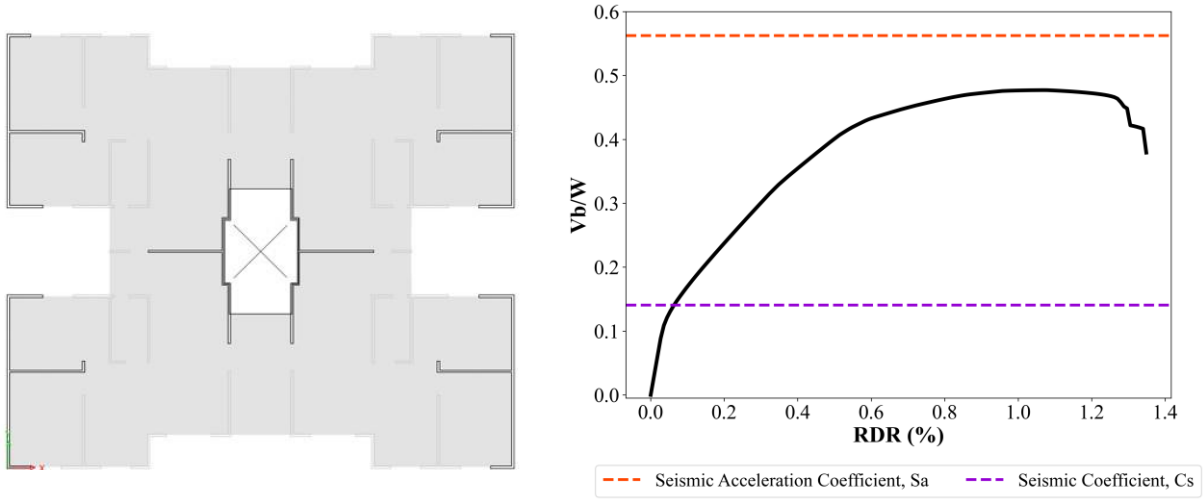

Figure 41. Capacity curve of 5-story RCW building and identification of the parameters used for seismic resistant design.

The results obtained for all study archetypes will be available in the repository: https://github.com/VidalesFrank/Seismic-Structural-Analysis-Platform.git.

9.1.1. Control points on the capacity curve

On the capacity curve, different limit states or control points can be identified to describe the damage progression of the structural elements within a building. For the specific case of Thin RCWB, the following points are distinguished on the curve: the onset of cracking, the initial yielding of reinforcement in the elements, the first rupture of the welded wire mesh (WWM), the point of maximum capacity or "peak" in the pushover analysis, and finally, the point of ultimate capacity or collapse. The definition of collapse can be based on various criteria, with one of the most common in literature being a 20% loss of the structure's maximum capacity.

Figure 42 illustrates the capacity curves and the dispersion of control points for buildings categorized by height. In Figure 42a, the capacity curve for a low-rise building is presented, along with the dispersion of control points for buildings in this category within the database. Similarly, Figure 42b displays the results for a mid-rise building, while Figure 42c presents the findings for high-rise buildings.

Additionally, in the final stages, there is significant dispersion in the results due to the high variability in both geometric and mechanical properties. It is important to note that in these advanced damage states, the type and amount of reinforcement plays a crucial role in the structural response. This variability in reinforcement can greatly influence the behavior, leading to more pronounced differences in the performance of the buildings as damage progresses.

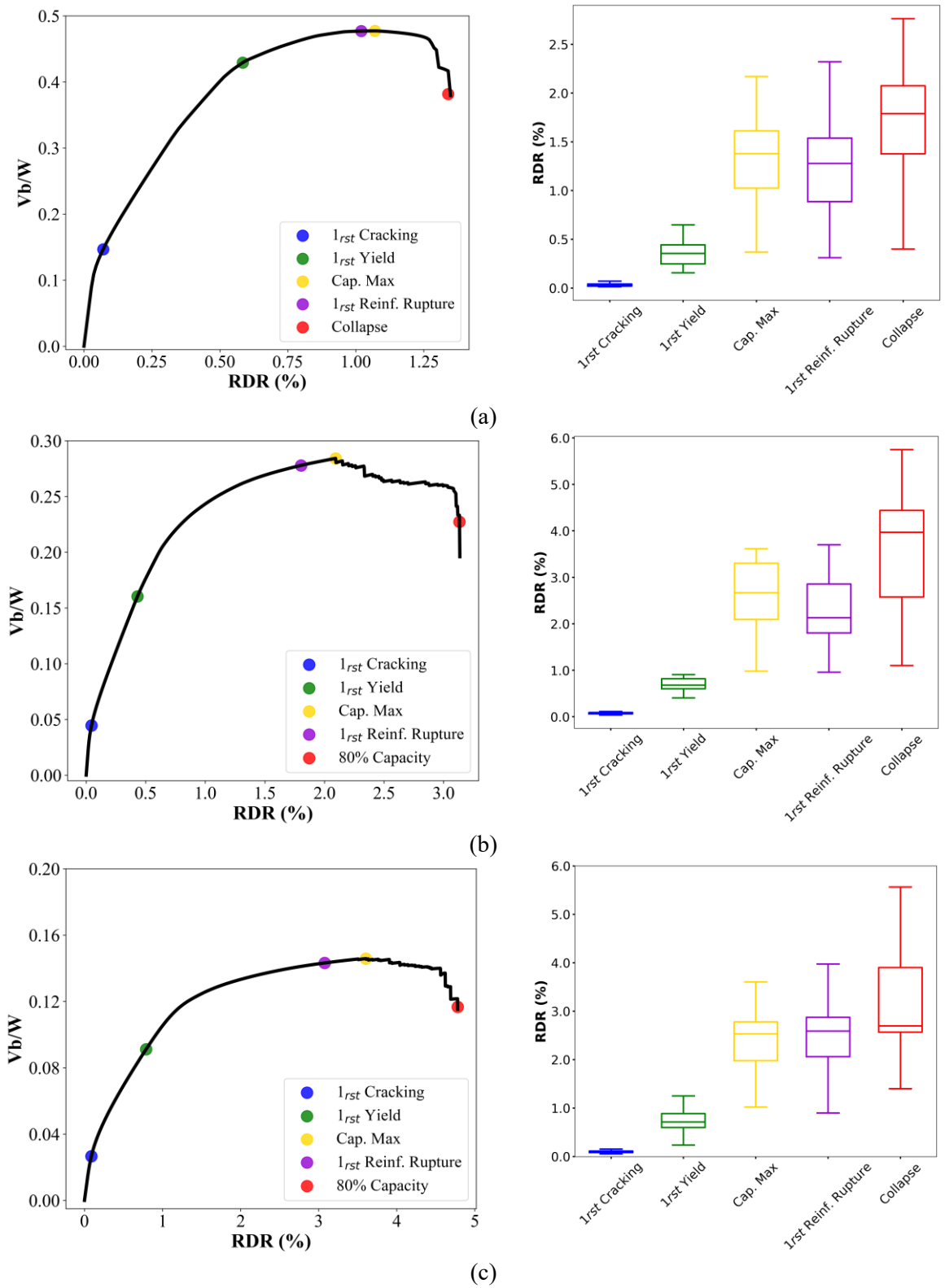

Figure 42. Control points in the capacity curve and building database in a) Low, b) Mid and c) High-rise buildings.

The values obtained from the control points are as follows:V_{Cr}, V_y, V_{Max}, V_{Rup}, and V_{ult} correspond to the shear values (VbV_bVb) at the control points for the first cracking, initial yielding, maximum capacity, first reinforcement rupture, and collapse, respectively. Additionally, the displacement values are denoted as . RDR_{Cr}, RDRy, RDR_{Max}, RDR_{Rup}, and RDR_{Ult}.

9.1.2. Idealization of the Pushover curve

Given that the structural system of Thin Reinforced Concrete Wall Buildings (TRCWs) experiences a significant loss of stiffness after cracking, the conventional bilinear curve idealization may overestimate the system's ductility. Therefore, this work proposes an idealization using a trilinear curve, formulated as follows:

- **Segment 1**: Identify the point on the curve at $0.6*V_{Cr}$ (first cracking) and draw a secant line from the origin to this point.
- **Segment 2**: Draw a tangent line passing through the midpoint between cracking and first yield, defined as $(0.5*(V_{Cr} +V_y))$.
- **Segment 3**: Determine the ultimate capacity point of the pushover, defined as the point at which there is a 20% reduction in the structure's maximum capacity. Draw a horizontal line to intersect the line plotted in Segment 2. Finally, adjust the height (shear) of this line to achieve an idealization that matches the area under the pushover curve by using an equal-area approach.

Figure 43 illustrates the procedure for obtaining the idealized trilinear curve from the pushover curve.

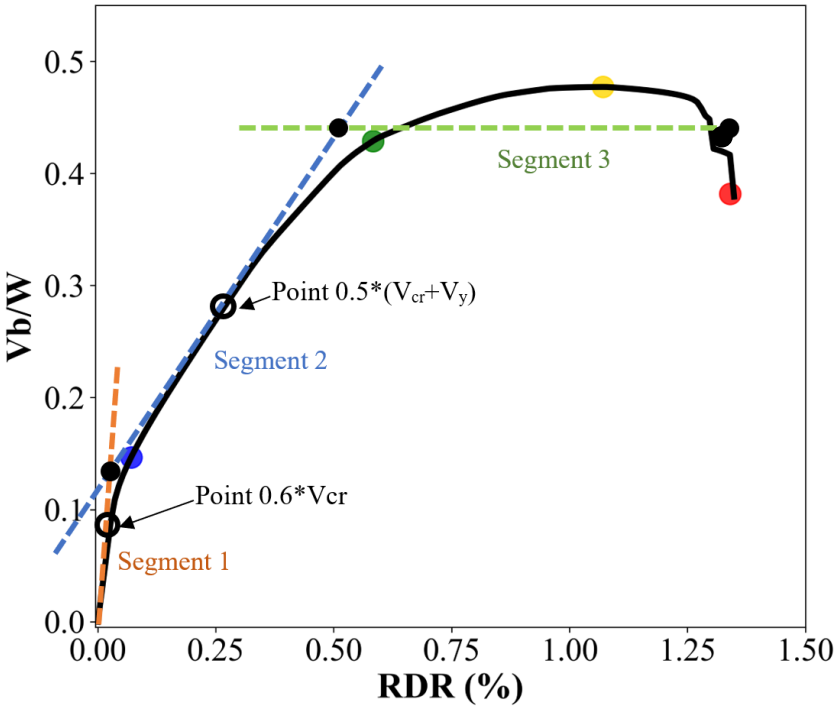

Figure 43. Procedure for obtaining the idealization using a trilinear curve.

Figure 44 the idealized capacity curve and the control points within it are presented.

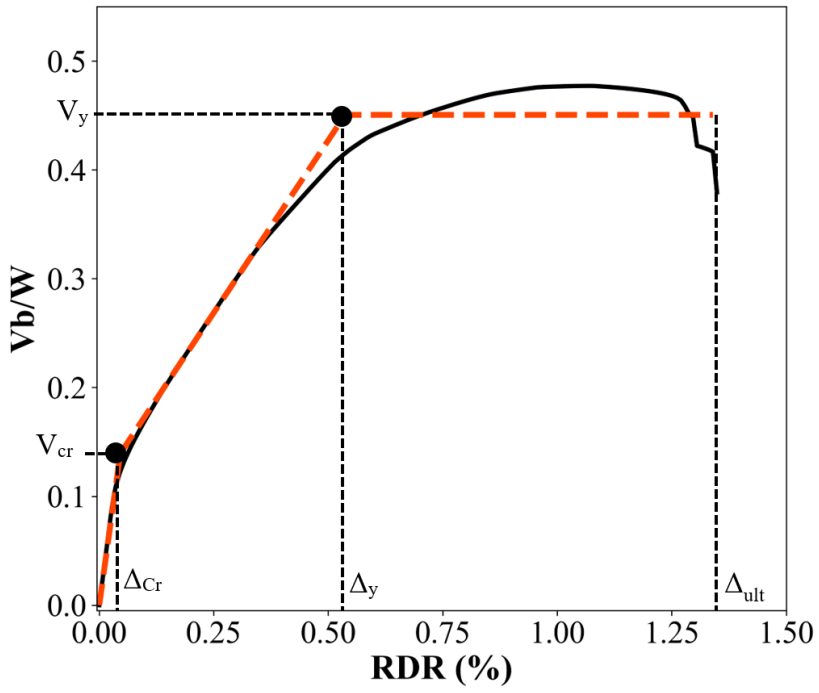

Figure 44. Points on the idealized pushover curve.

Additionally, as a proposal for the capacity curve idealization, the bilinear curve approach is considered. This approach involves idealizing an elastic zone of the response and defining a consistent maximum capacity for the post-yield segment of the response.

To determine this bilinear curve, the point of average yield is identified. Using the equivalent area approach described earlier, the ultimate capacity is then determined. The bilinear approximation was conducted following the methodology outlined in FEMA, which involves fitting an initial elastic slope and a post-yield slope to the pushover curve, ensuring that the areas under both the original and bilinear curves are equivalent. This approach captures the key elastic and inelastic properties of the structure's response. The representation of the bilinear curve is depicted in Figure 45.

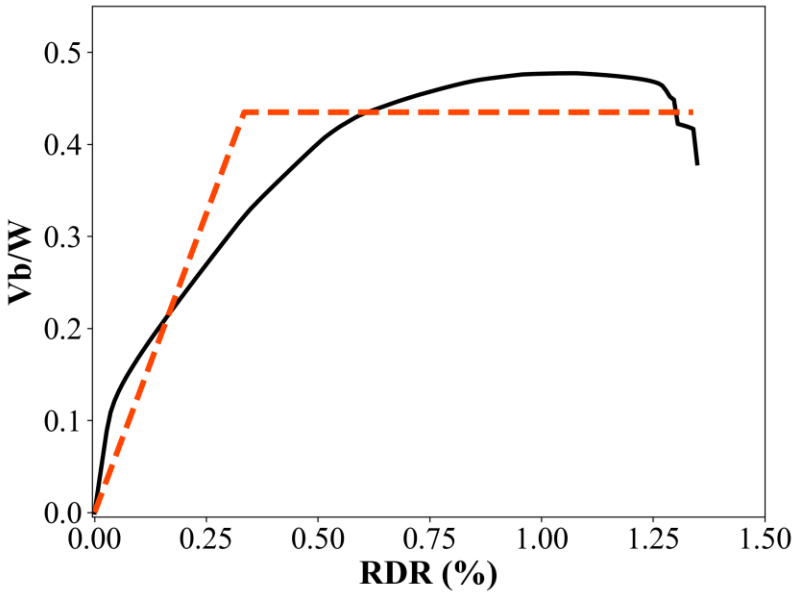

Figure 45. Idealization using a bilinear curve.

Figure 46 presents a comparison between two approaches for the pushover curve idealization. The results indicate that the bilinear curve overestimates the average yield of the building and fails to accurately represent the initial stiffness. This discrepancy arises from the fact that the bilinear method overlooks the significant loss in stiffness that occurs in TRCW buildings after the walls crack. In contrast, the trilinear curve effectively captures the variations in initial stiffness and the post-cracking behavior observed in these structures.

Moreover, the average yield point of the building aligns more closely with the actual trajectory of the pushover curve when using the trilinear approach. Specifically, the average yield is 0.33 with the bilinear method and 0.54 with the trilinear approach. This difference highlights the trilinear model's capacity to offer

a more accurate estimation by accounting for both the initial stiffness and the structural response after cracking.

In conclusion, the trilinear approach provides a more realistic representation of the structural response, addressing the limitations of the bilinear approach, which tends to overestimate yield and fails to capture the nuanced characteristics of the curve. This improvement is essential for accurately modeling the seismic behavior of reinforced concrete buildings, thereby enhancing the reliability of structural assessments and design decisions.

In light of these findings, subsequent chapters will utilize estimations based on the trilinear idealization, as it offers the most reliable approach for accurately predicting the structural response.

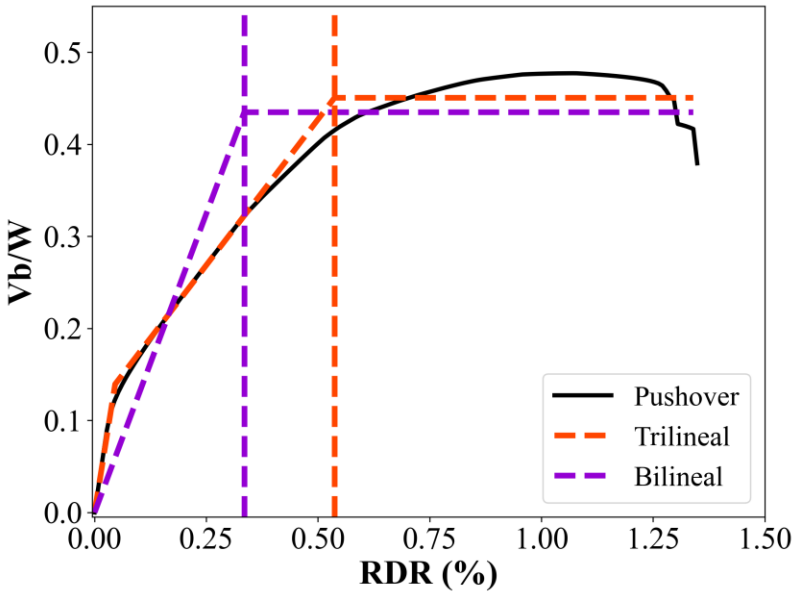

Figure 46. Comparison between pushover curve idealizations.

9.2. NONLINEAR TIME-HISTORY ANALYSIS

9.2.1. Seismic Hazard

The selection of seismic ground motions in this study was based on the Conditional Scenario Spectra (CSS) approach, which allows for an accurate representation of site-specific seismic hazard by ensuring consistency between the selected records and the corresponding hazard level. This methodology has been used in the Colombian National Seismic Risk Model (MNRS) to characterize seismic hazard across different regions of the country. To optimize the performance of the nonlinear response analyses, seismic records were selected across different return periods, covering seven hazard levels ranging from 75 to 9,975 years.

Additionally, three extra hazard levels were incorporated by applying scaling factors of 1.5, 2.0, and 2.5 to the highest hazard level (4,975 to 9,975 years), improving the characterization of regions with a high probability of structural collapse. The selection process considered the influence of various tectonic settings, including the subduction of the Nazca Plate, the Bucaramanga deep seismic nest, and active faults in the Andes, ensuring a comprehensive assessment of seismic demand in the analyzed archetypes.

The Nonlinear Time-History Analysis is a dynamic analysis method used to evaluate the seismic response of structures by considering the ground motion records as input. Unlike the Pushover analysis, which applies a static equivalent lateral force, this method simulates the actual time-dependent behavior of the structure subjected to the ground motion. In this study, the nonlinear time-history analysis was conducted for each building archetype using OpenSees software. This approach offers a detailed insight into the structural response, capturing the intricate behavior of the building under real seismic events. The obtained results are crucial for assessing the building's performance under different earthquake scenarios and for developing appropriate seismic retrofitting strategies.

To illustrate the seismic demand imposed on the buildings, acceleration and displacement response spectra were obtained for different levels of seismic intensity. These spectra provide insights into how the buildings respond under varying levels of seismic demand, helping to assess their performance and vulnerabilities. Figure 47 presents the acceleration and displacement spectra for a specific archetype.

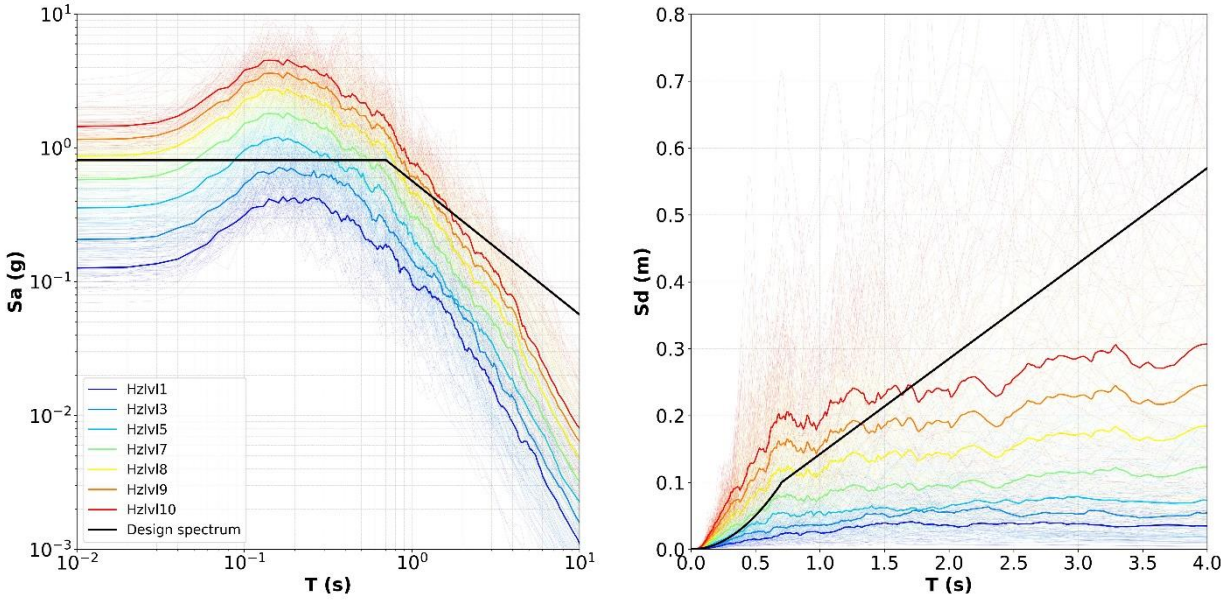

(a) (b)

Figure 47. a) Acceleration and b) Displacement Response Spectra for a Representative Building Archetype under Different Seismic Intensities.

Additionally, a key aspect of the analysis is the structural response in terms of spectral acceleration (Sa) versus maximum roof drift for each demand level. This relationship is crucial for understanding how the building behaves at different levels of seismic intensity, from minor to extreme events. The results provide a clear indication of when the structure reaches critical damage states, such as yielding or collapse. Figure 48 presents a representation of these results for a specific archetype from the database.

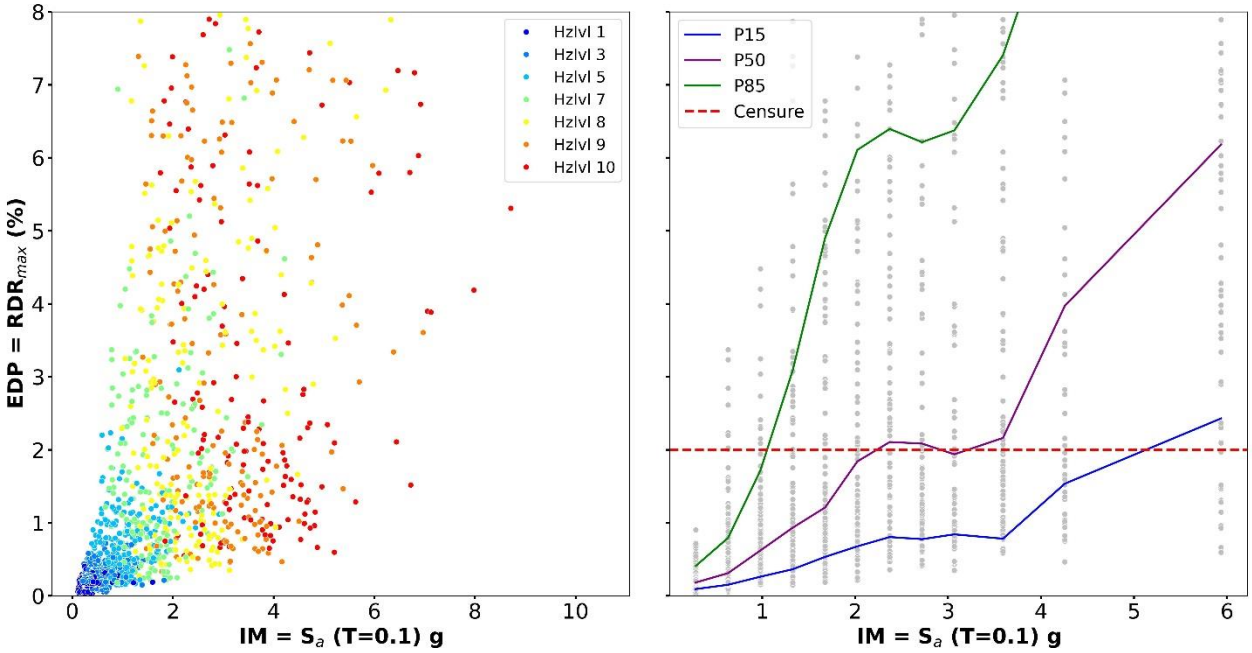

Figure 48. Spectral Acceleration (Sa) vs. Maximum Roof Drift for a Representative Building Archetype.

Finally, Figure 49 presents the dispersion of floor displacements for a 5-story building, illustrating the variation in displacements across the height of the structure for different seismic intensities. This graph highlights the distribution of seismic demand among the floors, which is important for identifying potential weak points in the structure that may require strengthening or retrofitting.

A key parameter for evaluating the relative displacement between consecutive floors is the story drift ratio (SDR), defined as the difference in lateral displacement between two adjacent floors divided by the story height. This parameter is crucial for assessing local deformation demands, as excessive SDR values can indicate potential structural damage or failure mechanisms, particularly in regions of high seismic demand.

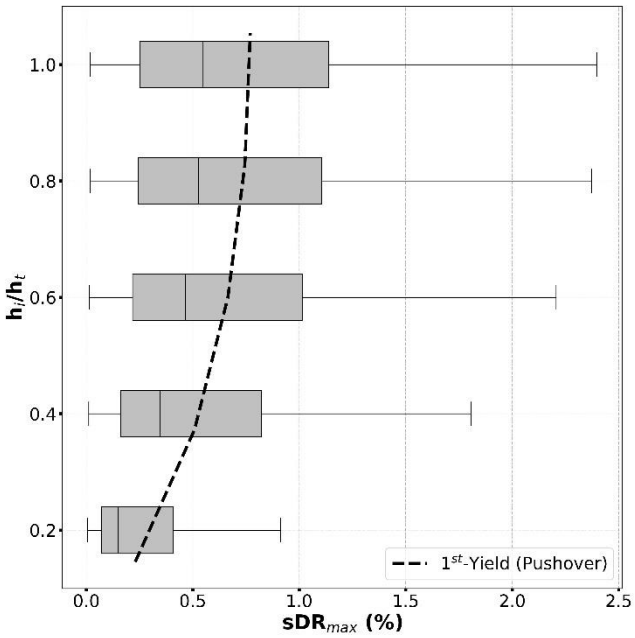

Figure 49. Dispersion of Floor Displacements for a 5-Story Building under Different Seismic Intensities.

These results provide a detailed understanding of the dynamic response of the reinforced concrete wall buildings analyzed and are essential for developing effective seismic retrofitting strategies. By capturing the time-dependent behavior under actual earthquake records, the analysis offers a more comprehensive approach to evaluating seismic resilience, allowing structural engineers to better predict how these buildings will perform in future seismic events.

It is essential to highlight that the results presented here are based on the methodology and findings described in the study titled "METHODOLOGY FOR THE GENERATION OF FRAGILITY CURVES: APPLICATION TO INDUSTRIALIZED WALL BUILDINGS" by Ocampo J. This reference serves as a foundational resource for understanding the analytical approach employed in this research and underlines the significance of the findings in the context of seismic performance evaluation.

10. ANALYSIS OF RESULTS AND SIMPLIFIED EXPRESSIONS

In this section, the outcomes derived from the structural analysis are comprehensively presented and interpreted. A key contribution to this thesis is the development of simplified expressions based on an extensive dataset and detailed analysis. These expressions provide a practical tool for the preliminary evaluation of a building's seismic performance, offering reliable insights without the need for complex nonlinear modeling. By leveraging fundamental principles and well-founded assumptions, these simplified expressions efficiently capture the essential aspects of structural behavior, enabling a more accessible yet robust assessment. The results are systematically examined and compared against expectations, demonstrating the effectiveness of these simplified expressions in accurately reflecting the structural response. This approach not only enhances the efficiency of preliminary assessments but also bridges the gap between detailed modeling and practical evaluation methods.

10.1. ANALYSIS OF PERIODS OF TRCW BUIDING SYSTEM

In this section, the vibration periods of the TRCWB are analyzed and discussed. The vibrational characteristics play a crucial role in determining the dynamic behavior and response of the structure under seismic actions. Computed periods offer valuable insights into the natural frequency and stiffness distribution of the system, aiding in the understanding of overall dynamic behavior and potential vulnerabilities under seismic loads.

Figure 50 shows the fundamental period of the analysis archetypes and their variation with height. It also shows the variation of the approximate period Ta estimated from numeral A.4.2.2 of the NSR-10, calculated as $0.049*Hw^{0.75}$. As can be seen, for low-rise buildings (less than 10 stories), the fundamental period of the archetype is generally lower than the estimated period recommended by the code, indicating that these buildings are somewhat more rigid than the normative estimation would suggest. On the other hand, as the height of the archetypes increases, the fundamental period is found to be higher than the period Ta suggesting that the structures are more flexible than what the approximate period would estimate.

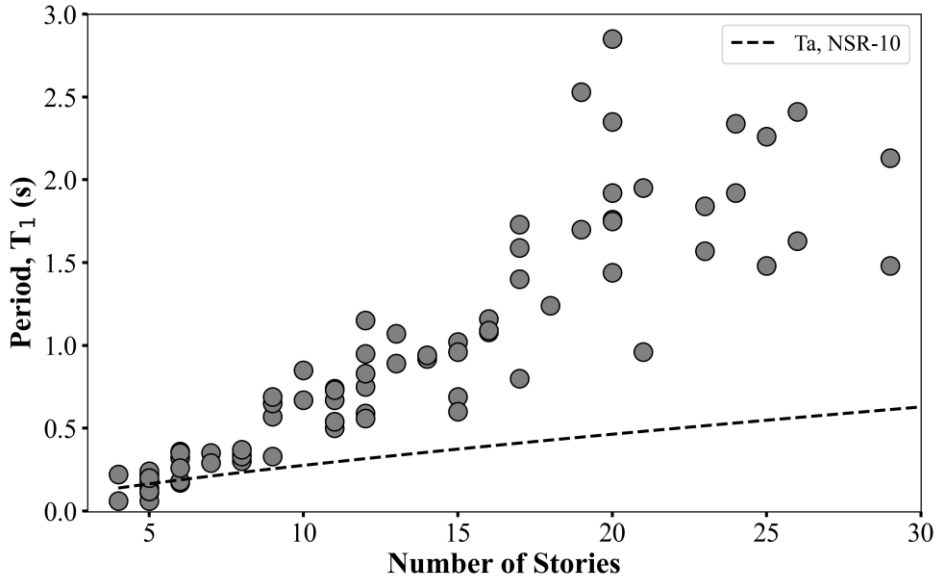

Figure 50. Variation of Period in Buildings from the Database vs Ta According to A.4.2-3 of the NSR-10 for Concrete Walls.

Figure 51 illustrates the relationship between the fundamental period of the database archetypes and the approximate period T_a calculated for one of them. It shows that for buildings up to 10 stories, T_1 values are lower than the calculated Ta. However, for taller buildings, the T_1/T_a ratio can reach up to 3, indicating a significant discrepancy when estimating an approximate period for the structural system under analysis.

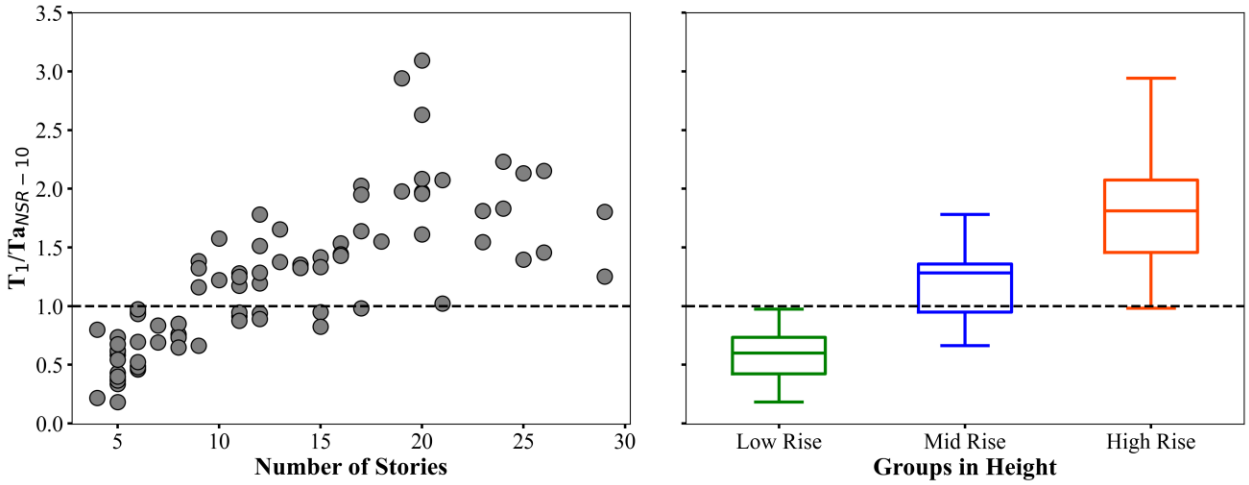

Figure 51. Relationship of Ta in NSR-10 vs. Periods in Database Buildings.

Figure 52 shows the relationship between the number of stories (NS) and the fundamental period calculated with cracked sections (denoted T_{cr}). A linear regression with the functional form T=N/Cn was performed to obtain a C_n value of 13. The dashed lines in Figure 52 also indicated that the lower and upper bounds of C_n

for cracked sections are 9 and 22, respectively. For low-rise buildings, a better correlation is observed with C_n close to 22, whereas for mid and high-rise buildings, a better fit is obtained with Cn close to 9.0 (Bonett et al, 2024).

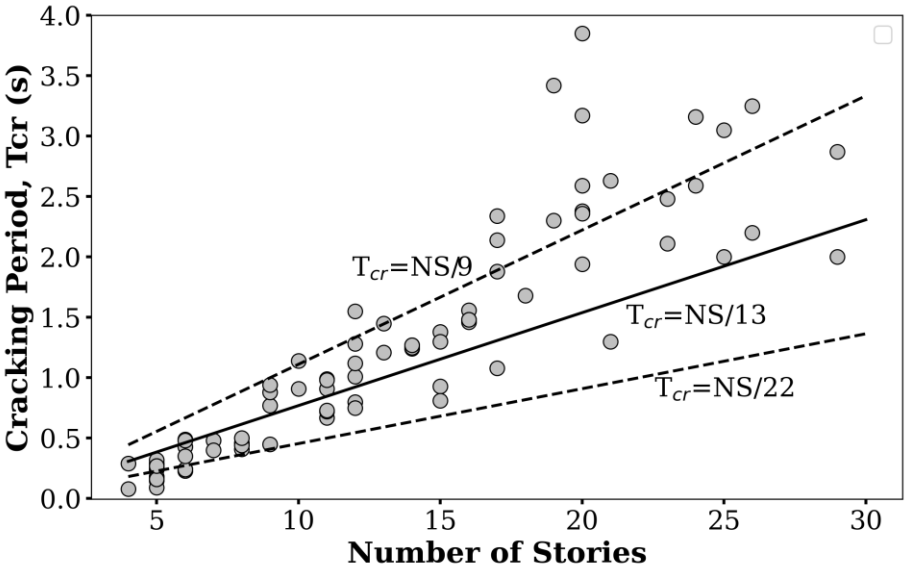

Figure 52. Fundamental period (cracked section, T_{cr}) versus number of stories (Bonett et al, 2024).

Bonett et al. (2024) proposed an approximation for estimating the cracked periods, T_{cr}, for the two main directions of buildings ("X" and "Y"), This approximation is defined by a geometric relationship given by $\sqrt{(H_w^3/B)}$, where H_w is the building height and B is the plan dimension in the direction of analysis. They determined that the coefficient b1of the linear regression for the estimation of Tcr is 0.0291 for the longitudinal direction and 0.0194 for the transverse direction. For the buildings in the database, this estimation was performed, revealing a slight variation in these coefficients, being 0.0362 for the longitudinal direction and 0.0233 for the transverse direction, as shown in Figure 53, and the Eq. **9** and Eq. **10**.

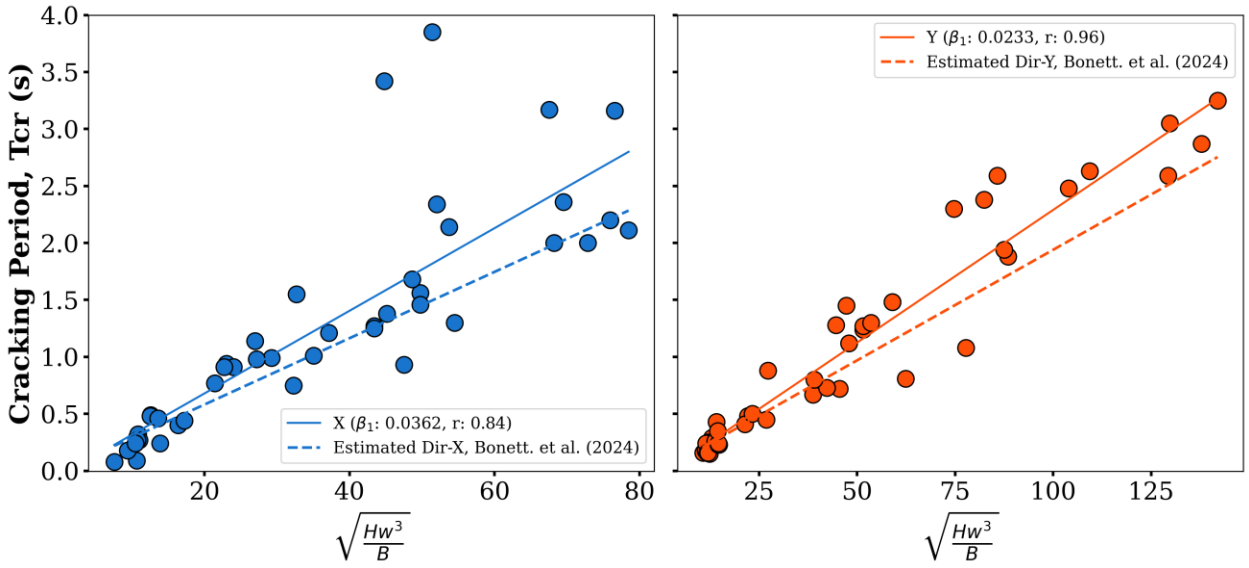

Figure 53. Estimated Cracked Period (T_{cr}) and Comparison According to Bonett et al. (2024).

$$T_{Cr_X} = 0.0362 \cdot \sqrt{\frac{Hw^3}{B}} \quad (9)$$

$$T_{Cr_Y} = 0.0233 \cdot \sqrt{\frac{Hw^3}{B}} \quad (10)$$

10.2. OVERSTRENGTH FACTOR

The overstrength factor was estimated from the capacity curve obtained through a nonlinear static analysis (pushover). These analyses were conducted considering a loading pattern proportional to the fundamental mode of the structure. During the pushover analysis, the point at which the archetypes reached their maximum capacity was selected and referred to as the maximum resistant shear (V_{max}), see in the Figure 41. The capacity curve displays on the ordinate axis the shear force value normalized by the seismic weight of the building. Based on the information contained in structural plans and design specifications, the design strength (V_d) was determined for each archetype and normalized with respect to weight to obtain the seismic coefficient (C_s). V_d is a function of building height and localization within a specific seismic hazard region, as well as the level of energy dissipation, represented by the elastic force (V_e) divided by the strength reduction factor (R), as $V_d=V_e/R$. This design strength is determined based on the elastic design spectrum, which incorporates a seismic event with a return period (T_r) of 475 years, in accordance with the precise design code applicable to each archetype's location. In this process, the highest spectral acceleration value obtained for the archetype's fundamental period or the maximum allowable period in accordance with the Colombian building code (C_u*T_a) is selected. Here, T_a is computed as 0.49 $H_w^{0.75}$, and C_u is determined as

1.75-1.2 A_v * F_v where A_v and F_v corresponds to effective peak velocity and site coefficient, respectively which vary depending on the project's geographical location and the specific soil type. Finally, overstrength Ω is defined as the ratio as Eq. 11.

$$\Omega = \frac{V_{Max}}{V_d} \qquad 11$$

Figure 54 shows the overstrength values for each archetype categorized by the number of stories. According to NSR-10, reinforced concrete wall buildings must have an overstrength value of 2.5 or higher.

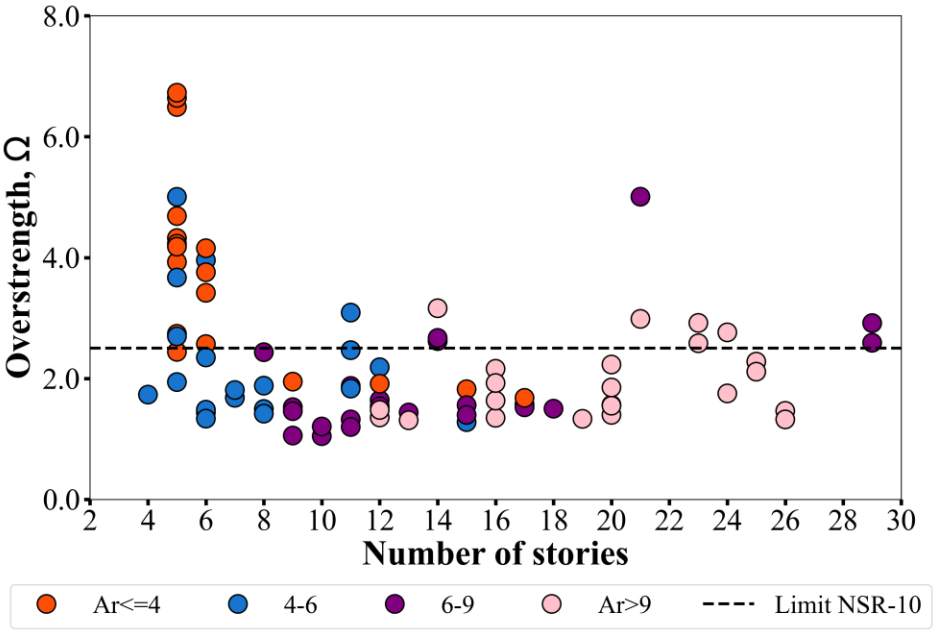

Figure 54. Variation of Overstrength Factor by number of stories.

10.3. SIMPLIFIED EXPRESSIONS FOR SEISMIC PERFORMANCE EVALUATION

In performance-based seismic design, curvatures corresponding to various limit states are employed to calculate the lateral displacements or drifts of structural elements. Estimating these curvatures typically requires calculating moment-curvature relationships for each cross-section of the analyzed walls. However, developing simplified expressions for these curvatures can provide quick and reliable estimates, allowing engineers to perform preliminary sizing of the project efficiently within a performance-based design framework.

Such simplification streamlines the design process, enabling engineers to effectively assess structural performance and make informed decisions that enhance the resilience of reinforced concrete buildings against seismic events. By reducing the reliance on detailed moment-curvature analyses during initial stages,

these simplified expressions offer a practical yet robust tool for achieving the desired performance targets in seismic design.

10.3.1. Estimation of Curvature in Damage States

In this section, the curvature of the RC walls in Colombia is examined and discussed. Understanding the curvature of these structures is essential, as it provides insights into their deformation patterns, ductility, and overall structural behavior under different loading conditions, particularly during seismic events. The curvature analysis offers valuable data on the structural performance and integrity of these buildings, aiding in the assessment of their seismic resilience and safety.

To estimate curvature at various damage states, several parameters were selected based on the displacements observed in the studied building. Figure 55 through Figure 57 respectively illustrate the relationship between the first-story drift (SDR1) and the curvature at the base of the wall for the states of initial yielding, maximum capacity, and ultimate capacity. It is important to note that these results were derived from the capacity curves of all archetypes available in the database.

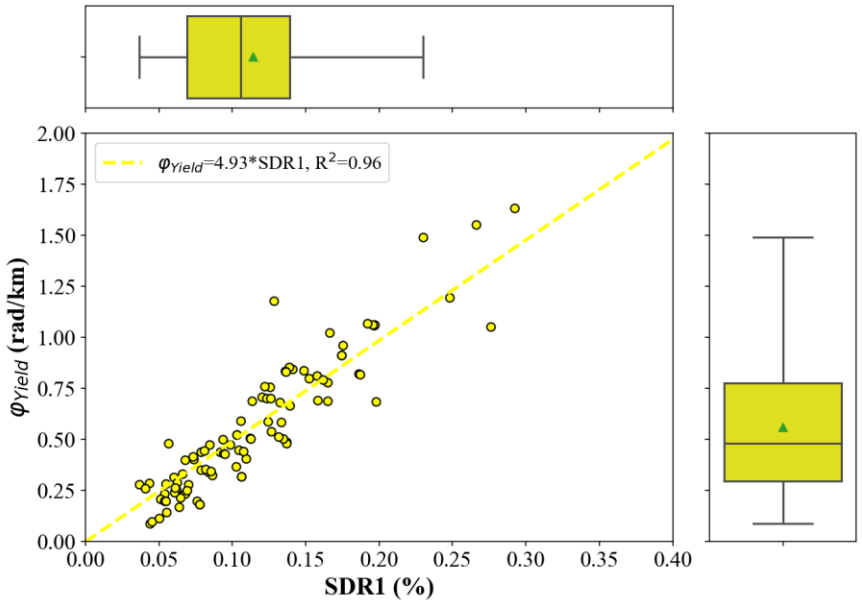

Figure 55. Relationship between SDR1 and Yield Curvature of Reinforcement in Reinforced Concrete Wall Buildings in Colombia.

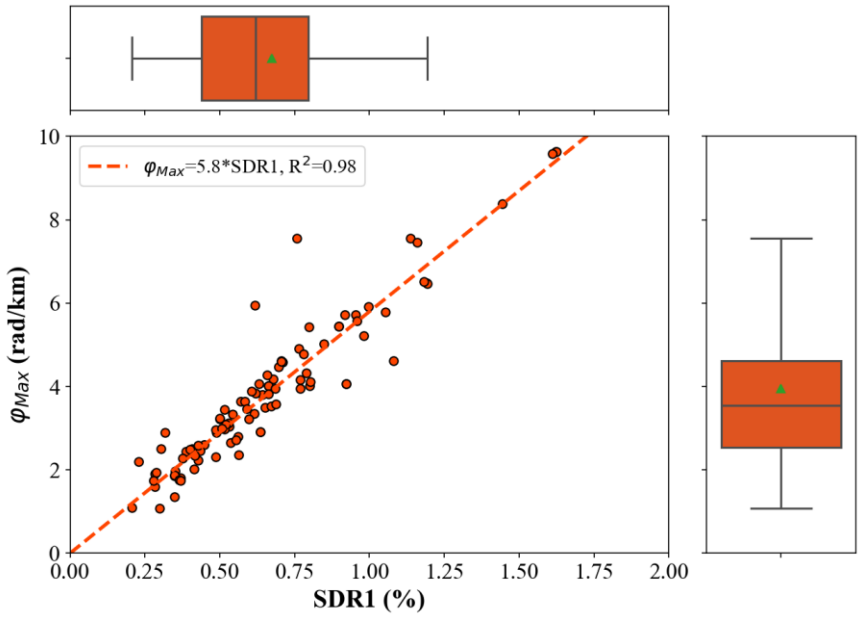

Figure 56. Relationship between SDR1 and Peak Point Curvature in Pushover Analysis for Reinforced Concrete Wall Buildings in Colombia.

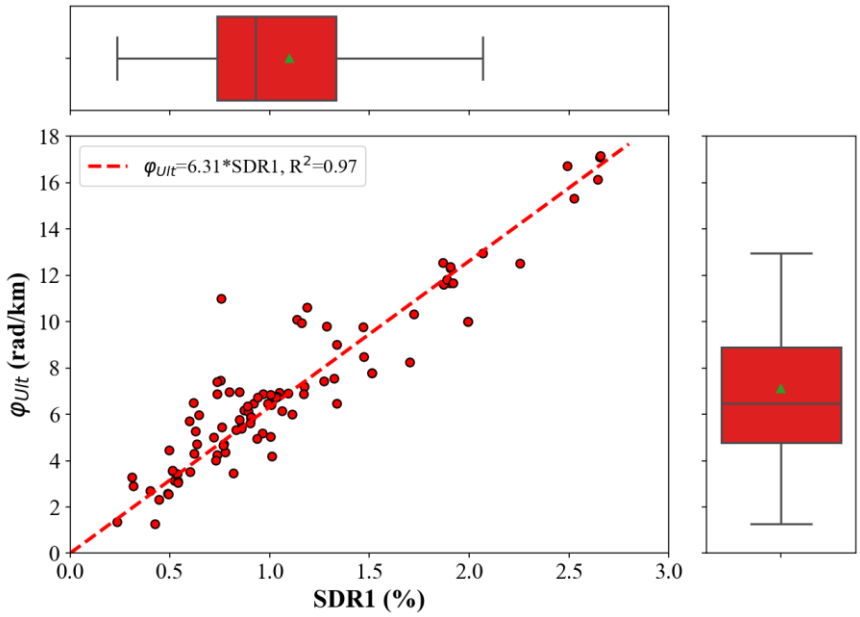

Figure 57. Relationship between SDR1 and Ultimate Curvature in Reinforced Concrete Wall Buildings in Colombia.

The following are the equations obtained from the linear regression analysis:

$$\varphi_{Yield} = 4.93 \cdot SDR_1 \quad (12)$$

$$\varphi_{Max} = 5.80 \cdot SDR_1 \quad (13)$$

$$\varphi_{Ult} = 6.31 \cdot SDR_1 \qquad 14$$

Additionally, the geometric relationship 1/Lw, which corresponds to the inverse of the length of the primary wall of the archetype, was determined. Figure 58 and Figure 59 show the relationship between the parameter 1/Lw and the respective curvature for the states of maximum capacity and reinforcement failure.

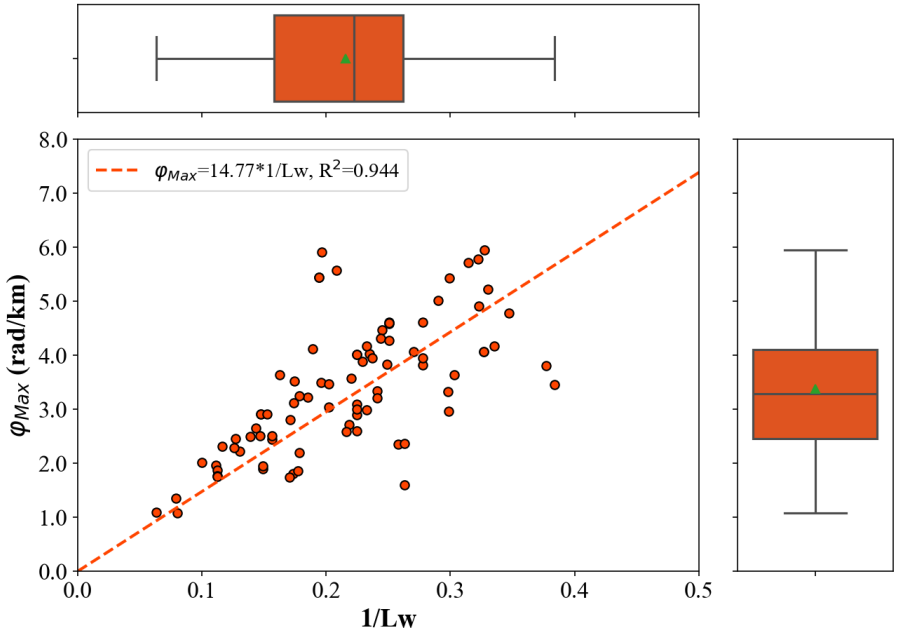

Figure 58. Relationship of 1/Lw to Curvature and Maximum Capacity in RCW Buildings.

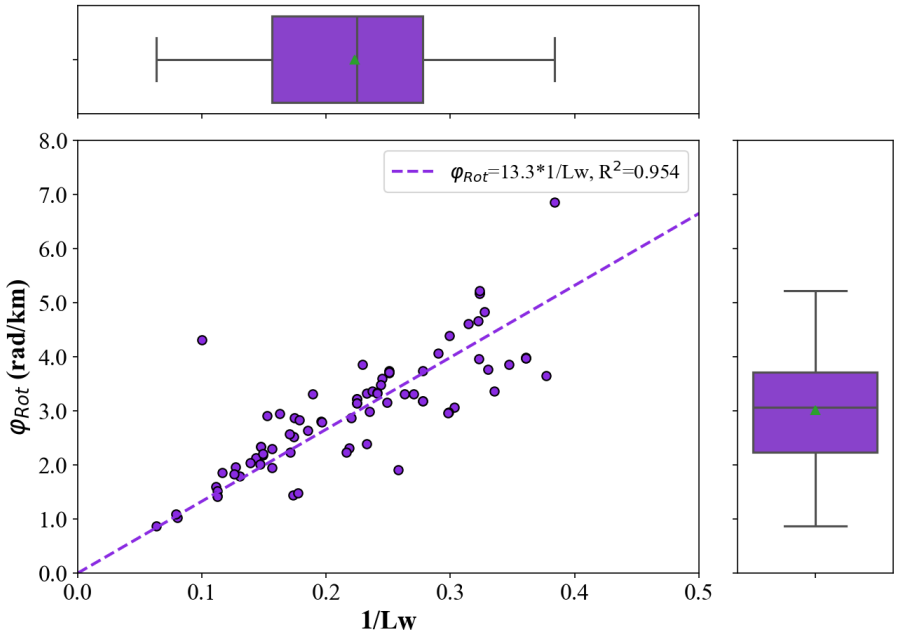

Figure 59. Relationship between 1/Lw and Reinforcement Fracture Curvature in RCW Buildings**.**

The following are the equations obtained from the linear regression analysis:

$$\varphi_{Max} = 14.77 \cdot {}^{1}/_{L_W} \quad 15$$

$$\varphi_{Rot} = 13.3 \cdot {}^{1}/_{L_W} \quad 16$$

10.3.2. Estimation of Roof Displacements for Different Damage States

This section focuses on the estimation of roof drift for reinforced concrete wall buildings at four critical states: cracking, first yield, maximum capacity, and collapse. Each of these states represents a key point in the structural behavior of buildings under seismic loads.

The cracking state refers to the moment when the concrete begins to crack, marking the onset of the nonlinear response of the structural system. Next, the yielding state occurs when the reinforcing steel in the walls reaches its elastic limit, indicating the initiation of permanent deformations in the material. The analysis also considers the maximum capacity, which defines the point at which the structure reaches its peak strength before experiencing significant stiffness and load-bearing capacity loss. Finally, the roof drift is estimated at the collapse state, identified as the point where the structure loses approximately 20% of its maximum capacity, indicating that it can no longer support itself and is at risk of catastrophic failure.

Estimating roof drifts at these four states is crucial for evaluating the seismic performance of buildings and their ability to withstand earthquakes. These values help establish safety thresholds and inform structural retrofitting strategies, ensuring that buildings can endure seismic events without endangering occupants or sustaining irreparable damage.

Figure 60 visually represents the estimated roof drift values for these states, highlighting critical points in the structural response. These values serve as a quick estimation tool to understand the limits at these damage states, allowing engineers to make informed decisions during the structural design process of such systems. By defining approximate thresholds, designers can more effectively assess the performance of reinforced concrete wall buildings under seismic conditions and implement necessary measures to enhance their resilience.

The estimation of roof drift ratios (RDR) at different damage states is influenced by the average aspect ratio of the walls, which has been identified as a key parameter in this study. The analysis revealed that this geometric property serves as a reliable predictor of structural response, directly affecting the displacement capacity of reinforced concrete wall buildings. By considering the average aspect ratio, the proposed

estimations provide a more accurate representation of the expected seismic performance, enhancing their applicability in structural design and assessment

The estimations are presented from Eq. **17** to **20**, providing a clear framework for understanding these critical parameters and supporting the development of robust and reliable structural designs.

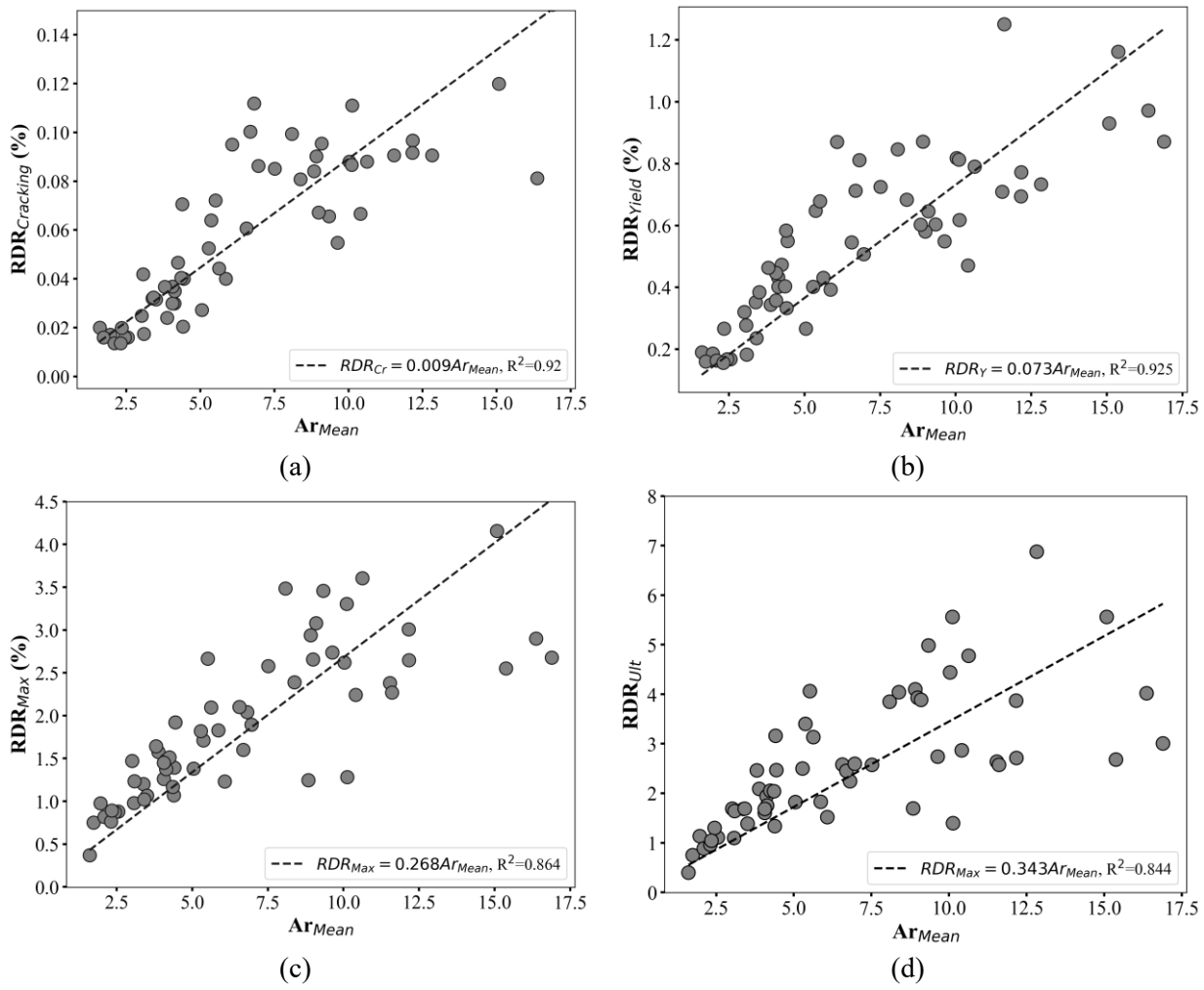

Figure 60. Roof Drift Estimation at a) Cracking State, b) the Elastic Limit State, c) Maximum Capacity State and d) the Collapse State.

$$RDR_{Cracking} = 0.009 \cdot Ar_{mean} \quad 17$$

$$RDR_{Yield} = 0.073 \cdot Ar_{mean} \quad 18$$

$$RDR_{Max} = 0.268 \cdot Ar_{mean} \quad 19$$

$$RDR_{Ult} = 0.343 \cdot Ar_{mean} \quad 20$$

10.3.3. Estimation of the Idealized Pushover Curve Points

This section presents the estimated points for the idealization of the capacity curve, incorporating both the roof displacement and the capacity normalized by the structure's weight for each key point outlined in the idealization approach described in Chapter 7.1.2. incorporating both the roof displacement and the capacity normalized by the structure's weight for each key point outlined in the idealization approach described in Chapter 7.1.2.

The control points associated with the cracking point (Cr), elastic limit (Yield), and ultimate capacity (Ult) of the capacity curve for the analyzed buildings are approximated, as shown in Figure 61, Figure 62 and Figure 63 respectively.

By establishing the relationship between these variables, a linear regression analysis was performed, resulting in Eq. 21 through 25. These equations provide a simplified method for estimating both the roof drifts ratios (RDR) and the normalized seismic shear (Vb/W) for each of these critical states in reinforced concrete wall building.

The combination of these metrics enables the construction of a trilinear representation of the capacity curve, which facilitates the identification of key load states, and the magnitudes of performance parameters related to the seismic behavior of the structure. By applying these equations, structural engineers can derive a simplified representation of the capacity curve, allowing for the estimation of displacement capacity levels and resistance in the analyzed building. This streamlined approach supports efficient performance evaluations and informed design decisions

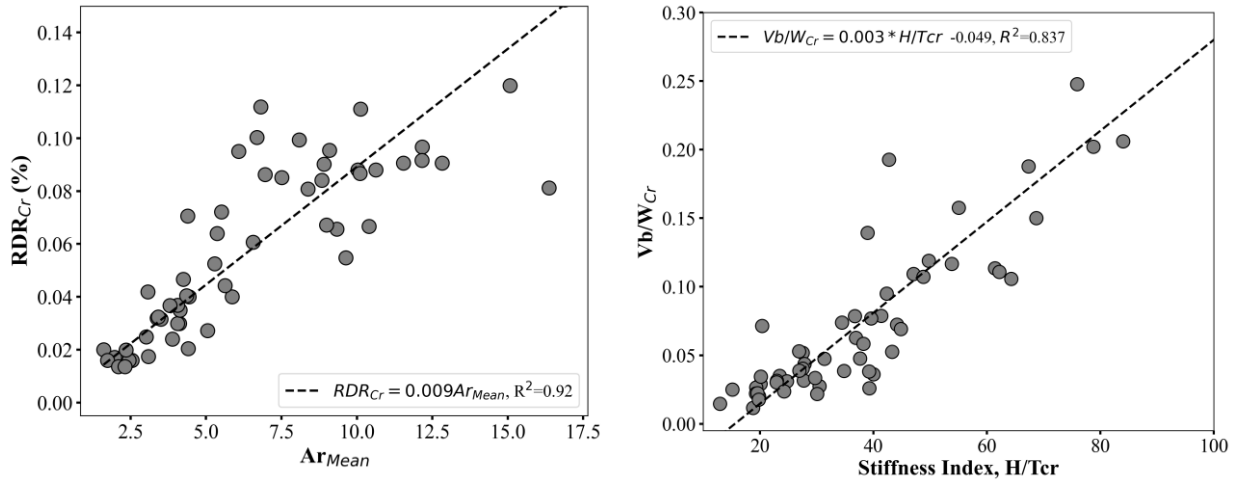

Figure 61. Roof Drift Estimation at the Cracking State.

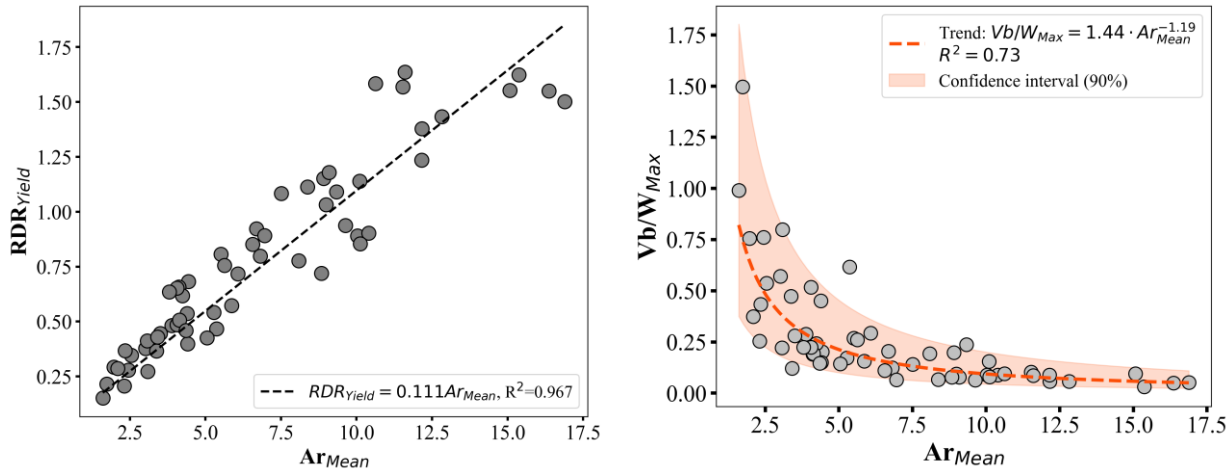

Figure 62. Roof Drift Estimation at the Elastic Limit State.

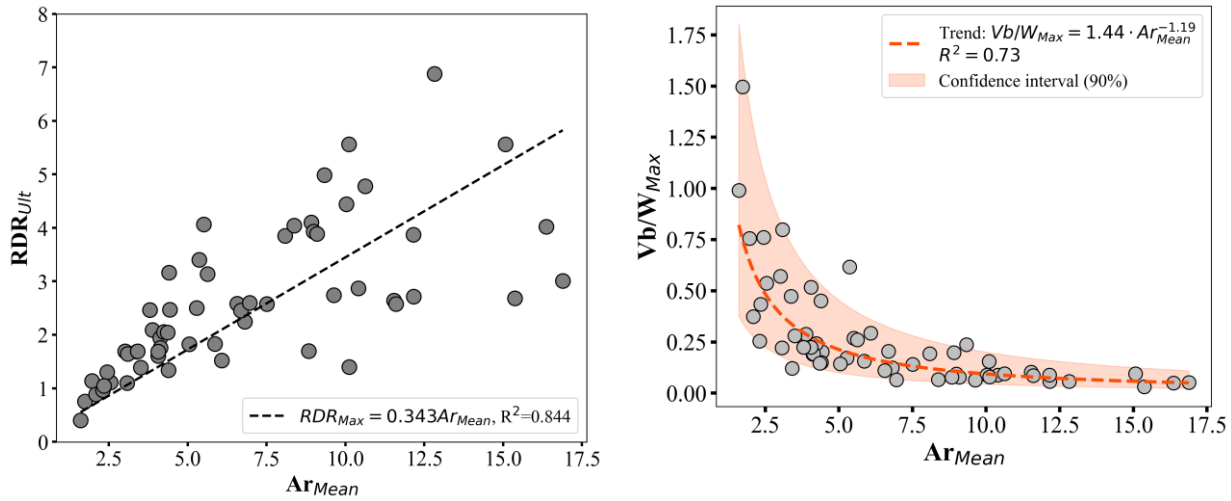

Figure 63. Roof Drift Estimation at the Collapse State.

$$RDR_{Cr} = 0.009 \cdot Ar_{mean} \quad 21$$

$$Vb/W_{Cr} = 0.003 \cdot H/T_{Cr} \quad 22$$

$$RDR_{Yield} = 0.111 \cdot Ar_{mean} \quad 23$$

$$Vb/W_{Max} = 1.44\ Ar_{mean}^{-1.19} \quad 24$$

$$RDR_{Ult} = 0.343 \cdot Ar_{mean} \quad 25$$

10.3.4. Relationship between damage estimator parameters (EDP)

This section explores the relationships among key damage estimator parameters, with a specific focus on the correlations between the maximum story drift ratio (SDR), roof drift ratio (RDR), and first-story drift ratio (SDR1), as well as the interactions among various interstory drift parameters. Figure 64 through Figure 66 present graphical representations that visualize these relationships, providing a clear understanding of how different drift ratios interact in reinforced concrete buildings. Additionally, Equations 18 through 20 summarize the estimations for each relationship, establishing a concise mathematical framework for evaluating these interactions. These estimations enable structural engineers to translate results obtained from various damage estimator parameters (EDPs) and assess seismic behavior at multiple levels of interest.

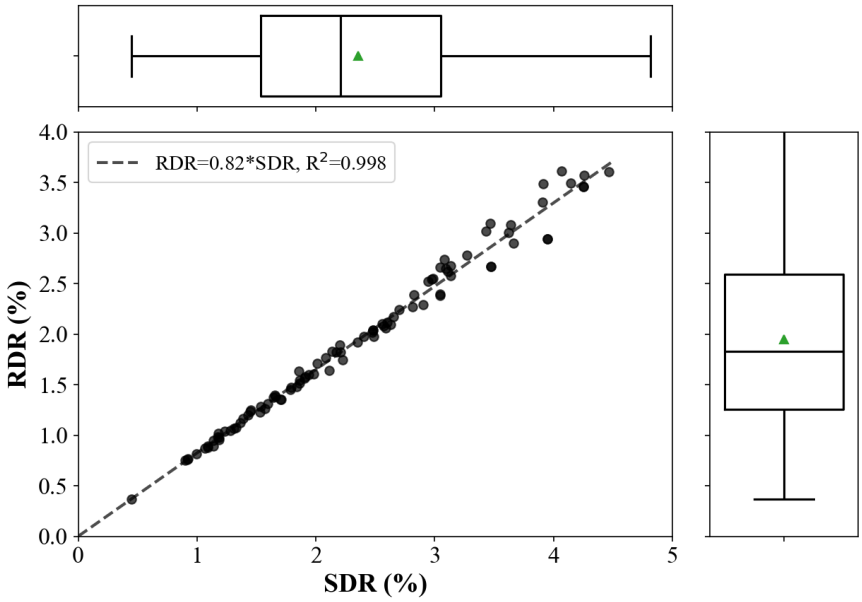

Figure 64. Relationship Between SDR and RDR in TRCW Buildings.

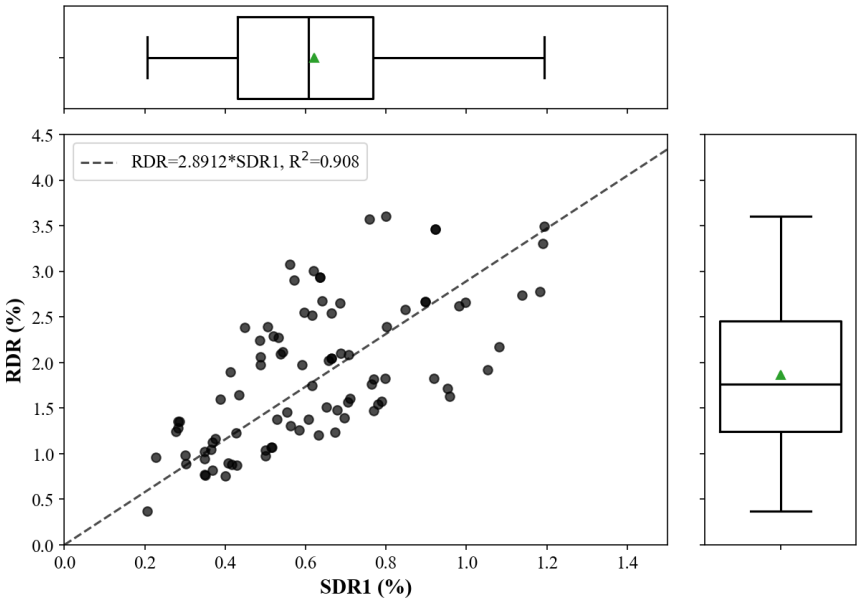

Figure 65. Relationship Between SDR1 and RDR in TRCW Buildings.

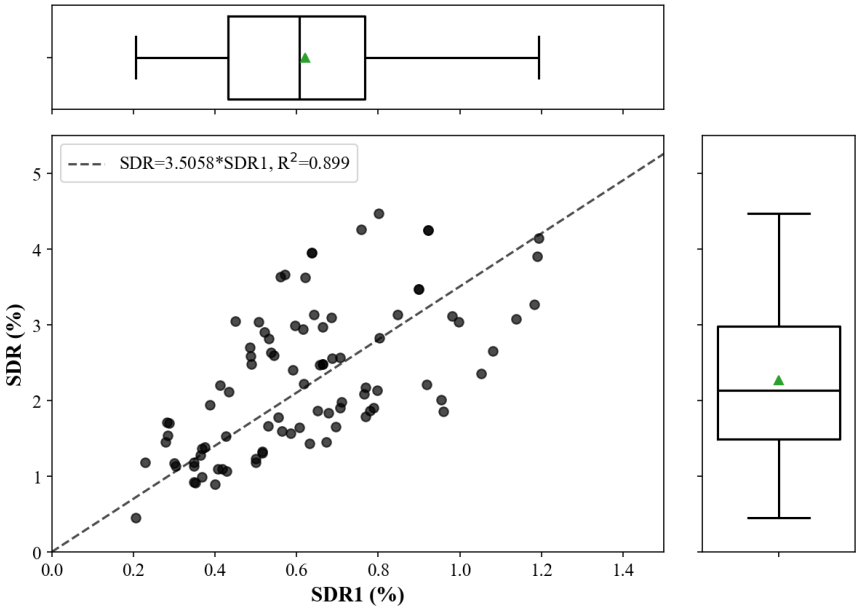

Figure 66. Relationship Between SDR1 and SDR in TRCW Buildings.

$$RDR = 0.82 \cdot SDR \quad (26)$$

$$RDR = 2.89 \cdot SDR1 \quad (27)$$

$$SDR = 3.51 \cdot SDR1 \quad (28)$$

11. SEISMIC FRAGILITY OF BUILDINGS

This chapter describes the methodology used to develop fragility curves for thin reinforced concrete wall buildings. This methodology was created by the vulnerability group of the National Seismic Risk Model, with further details available in Ocampo et al. (2024).

The methodology employed in this study to generate the fragility curves is organized into several key steps:

1. Building Characterization: the characteristics of the buildings, such as the number of stories, dimensions, occupancy type, and intended use, are analyzed. This process was detailed in the characterization section of this thesis.
2. Analysis Archetype Definition: Key walls in each building are identified to define the archetype for analysis, as outlined by Arroyo et al. (2024). These archetypes form the basis for developing numerical models using OpenSeesPy (Zhu et al. 2018). Each archetype is represented by a two-dimensional (2D) model, with walls simulated as multi-vertical-line-element models (MVLEM), with balances simplicity, stability, and accuracy for computational efficiency (Haghi et al., 2020; Pozo et al., 2020). A detailed description of the numerical modeling approach is provided in Chapter 8.3.
3. Hazard-Consistent Ground Motion Selection: A set of ground motions consistent with the seismic hazard for each building's location is selected, based on the Conditional Scenario Spectra (Arteta & Abrahamson, 2019).
4. Dynamic Analysis Execution: Dynamic analyses are performed for each archetype, recording roof and inter-story drifts to evaluate the structural response under seismic loading. Detailed results of the study are described in Chapter 9.2.
5. Collapse Threshold Definition and Fragility Function Calculation: A collapse threshold is established for each archetype, enabling the computation of the collapse fragility function which provides insights into the probability of collapse under varying seismic demands.

The fragility functions derived from this analysis are essential for assessing the seismic performance of low- and mid-rise TLRCW buildings, offering a framework to understand how various structural configurations and detailing levels influence the probability of collapse during seismic events.

Additionally, these fragility functions will support the development of performance-based design methodologies aimed at improving both safety and economic efficiency in seismic design practices. By focusing on the TRCW structures common in the Colombian construction industry, this study contributes

valuable insights into the seismic resilience of urban structures in the region, there by informing future design and retrofitting efforts.

11.1. GROUND MOTION SELECTION AND SCALING

The selection of ground motions for nonlinear analysis has advanced significantly over the past decade, particularly with methodologies such as the Conditional Scenario Spectra (CSS) (Arteta & Abrahamson, 2019). This approach enables the reproduction of seismic hazard at a given site across varying hazard levels by assigning occurrence rates to seismic records based on their intensity and spectral shape. The CSS methodology was utilized to create a set of hazard-consistent ground motions for Colombia (Pájaro & Arteta, 2022) as part of the National Seismic Risk Model (MNRS, by its acronym in Spanish).

For this analysis, seven hazard levels were selected (see Table 11), comprising ground motions with different return periods across five cities—Barranquilla, Bogotá, Medellín, Cali, and Armenia—representing three seismic hazard zones: Low, Intermediate, and High. To further assess the response of TLRCW system buildings under various seismic scenarios, three additional hazard levels were introduced by scaling the ground motions from hazard level 7 by factors of 1.5, 2.0, and 2.5.

To enhance computational efficiency, records corresponding to specific hazard levels were selectively excluded from the analysis. A critical parameter in this process was the conditional period, denoted as T*, which was carefully determined for each building height group within each city. Each ground motions set includes between 1500 and 1650 signals extracted from the National Seismic Risk Model database, offering a comprehensive representation across building types and hazard levels. Table 11 summarizes the hazard levels and return periods of the ground motions used in this study.

Table 11. Characterization of the ground motion records used for nonlinear dynamic analyses.

Return Period, TR (years)	[75, 150, 225, 475, 975, 2475, 4975, 9975]
Hazard Level	[low; intermediate; high]
Soil Types	[soil] = [360 m/s ≥ Vs30 ≥ 180 m/s]
Conditional Periods, T* (s)	[0.1, 0.3, 0.6, 0.7, 1.0, 1.5, 2.0, 3.0]

11.2. NONLINEAR DYNAMIC ANALYSIS

Nonlinear dynamic analysis of TLRCW system buildings was conducted to accurately capture the structural response to seismic activity. Each archetype was subjected to between 1500 to 1650 hazard-consistent seismic records, yielding data on inter-story drifts, roof drifts, floor accelerations, and velocities.

Figure 67 presents the dynamic results for a 5-story archetype located in Pereira, Colombia (0220-MCR-PER-05P-L). Roof drifts for each seismic record (Figure 67a) are plotted against the corresponding intensity

measure (IM), which, in this case, is the spectral acceleration at 0.3 seconds. The nonlinear analysis results (Figure 67a) were grouped to form "stripes" that represent ground motions of equal intensity (Figure 67b). In this figure, individual gray points indicate unique records, while continuous lines denote the median (50th percentile) drift for each intensity bin. This approach facilitates the fitting of a probability distribution function of seismic demand at each bin, enabling the calculation of fragility functions.

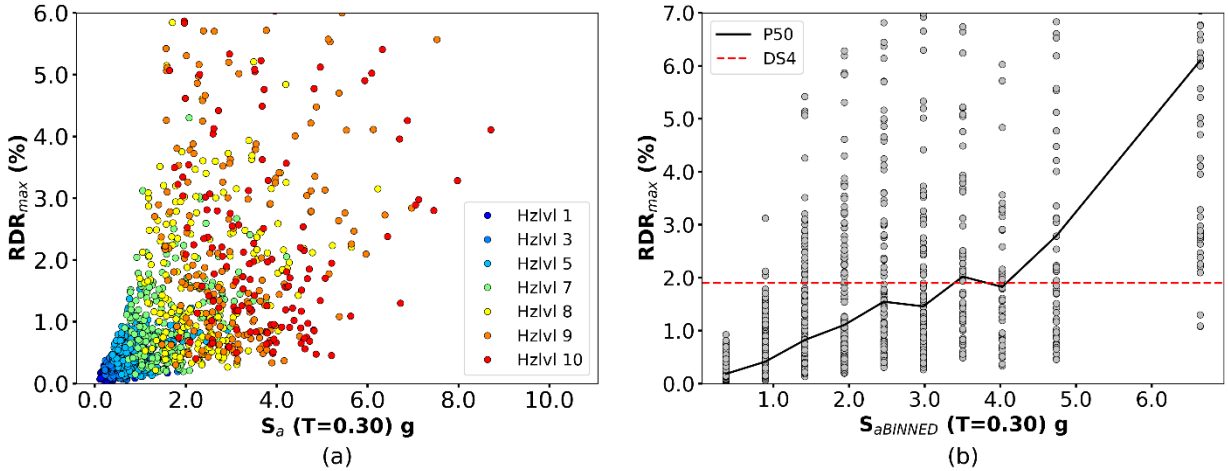

Figure 67. Example of the a) Dispersion of spectral acceleration Sa (T = 0.3s) and the maximum roof drift ratio, b) binned data for fragility function fitting for the archetype 0220-MCR-PER-05P-L.

11.3. COLLAPSE THRESHOLDS

The binning process was used to establish a threshold for significant wall damage in the archetype during a seismic event. This threshold was determined by examining the binned results (Figure 67b). Given that the TLRCW system is unlikely to experience abrupt vertical load-bearing capacity failures, the collapse threshold was defined by analyzing the slopes of the median roof drift ratio-spectral acceleration (RDR – Sa) curves.

Here, "collapse" is defined as a sudden increase in the roof drift ratio (RDR) along the RDR-Sa curve, indicated by a horizontal dashed line in Figure 67b. Further analysis of the demand-to-capacity ratios for the walls confirmed that at least one wall in the archetype had reached three times its strength capacity. The decision to use a global parameter such as the RDR, is supported by studies showing that the variability of such global parameters is significantly lower than that of the local wall response (Pozo et al., 2023).

11.4. COLLAPSE FRAGILITY CURVE

The following procedure was employed to calculate the fragility curves for each archetype:

1. Data binning: The output from the nonlinear dynamic analysis was processed and binned, resulting in the data shown in Figure 67.
2. Collapse probability calculation: The probability of reaching the collapse threshold (DS4) was calculated for each bin, based on the criteria defined in the Chapter 11.3 of this document.
3. Fragility function fitting: Collapse fragility functions were fitted to a lognormal distribution following the methodology described by Baker (2015).

Figure 68a illustrates the collapse fragility curve for a sample archetype. Spectral acceleration values for the Maximum Considered Earthquake (MCE) and the median of the distribution (representing a 50% probability of collapse) are shown with blue and gray dashed lines, respectively. Figure 68b displays the median values (Θ_{DS4}) for each archetype, categorized by building height (number of stories). The results reveal significant variations in median values among archetypes with the same number of stories, highlighting the need for further examination.

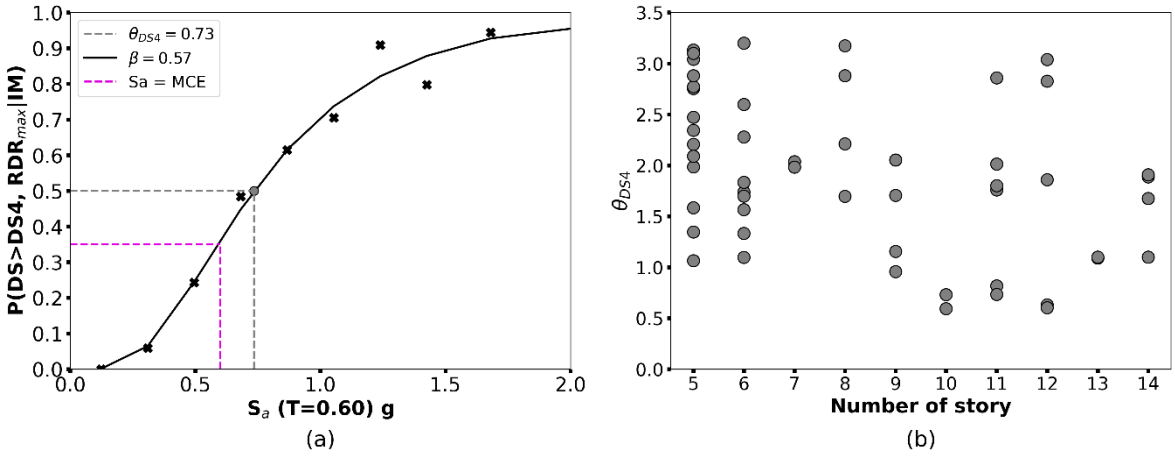

Figure 68. a) Scheme of Fragility curve with Sa in MCE and Θ_{DS4}, and b) Variation of Θ_{DS4} of the fragility function by Number of stories.

12. SEISMIC PERFORMANCE ASSESSMENT OF REINFORCED CONCRETE SHEAR WALL BUILDINGS

This chapter presents the results of a seismic performance assessment of reinforced concrete wall (RCW) buildings in Colombia, focusing on their collapse potential under the Maximum Considered Earthquake (MCE) scenario. The study specifically examines buildings with TRCW buildings, commonly used in low- and mid-rise buildings, up to 14 stories. Beyond this threshold, taller buildings typically require shear walls thicker than 0.15 m to accommodate the increased structural demands from higher seismic forces, which falls outside the scope of this study.

The emphasis on TRCW buildings was selected due to their prevalence in the Colombian construction industry and their critical role in reducing seismic risk. These buildings represent a key component in evaluating the seismic resilience of urban structures in the country. While the current focus is on buildings up to 14 stories, further research will be needed for taller structures with thicker walls, which will be addressed in future investigations.

The seismic performance evaluation employed advanced modeling techniques, with seismic input based on the MCE—the most severe earthquake anticipated during the building's design life. The analysis centers on key performance metrics such as inter-story drift ratios (SDR), roof drift ratios (RDR), and base shear (Vb). These metrics provide a comprehensive understanding of the structural response under extreme seismic events. Additionally, the assessment identifies critical damage states, including cracking, yielding, ultimate capacity, and potential collapse. Recognizing these states is essential to ensure that buildings can meet life safety requirements and minimize the risk of catastrophic failure during seismic events.

By focusing on these TRCW structures, the study provides significant insights for developing simplified design methodologies that enhance both safety and economic efficiency in seismic design. The findings contribute to a deeper understanding of how low- and mid-rise TRCW buildings perform under extreme seismic conditions, offering guidance for future design and retrofitting efforts, particularly in seismically active regions like Colombia.

The seismic performance assessment includes two main aspects: building categorization and fragility analysis. Buildings are categorized based on their stiffness index and the detailing level, which is directly related to the seismic hazard levels defined in the Colombian seismic code—low, intermediate, and high hazard. For buildings up to 14 stories, this assessment categorizes the structures into three stiffness-based groups: very stiff ($H/Tcr > 50$), stiff ($30 \leq H/Tcr < 50$), and flexible ($H/Tcr < 30$).

Furthermore, three detailing levels are applied: DMI (low hazard), DMO (intermediate hazard), and DES (high hazard). The influence of various structural parameters, including longitudinal reinforcement distributed along the web, vertical reinforcement at wall edges, wall thickness, the use of confinement in boundary elements, and reinforcement type in the web, is evaluated for each category. This detailed analysis is key to understanding how different design and reinforcement strategies affect seismic performance.

The fragility functions derived for each building are used to estimate seismic performance under the MCE scenario. Two performance levels have been defined based on the probability of collapse under MCE conditions. These levels provide a benchmark for assessing whether the building meets performance requirements, with a 20% probability of collapse set as the acceptable limit. Buildings with a probability of collapse exceeding this threshold are classified as non-compliant. This evaluation allows designers to make informed decisions regarding structural resilience and safety.

Figure 69 provides a schematic representation of the methodology used in this study to assess the seismic performance of TRCW buildings. This framework integrates building categorization, consideration of detailing levels according to seismic hazard zones, and fragility analysis under MCE conditions. By following this structured approach, it is possible to estimate the probability of collapse and classify buildings based on their compliance with seismic performance requirements.

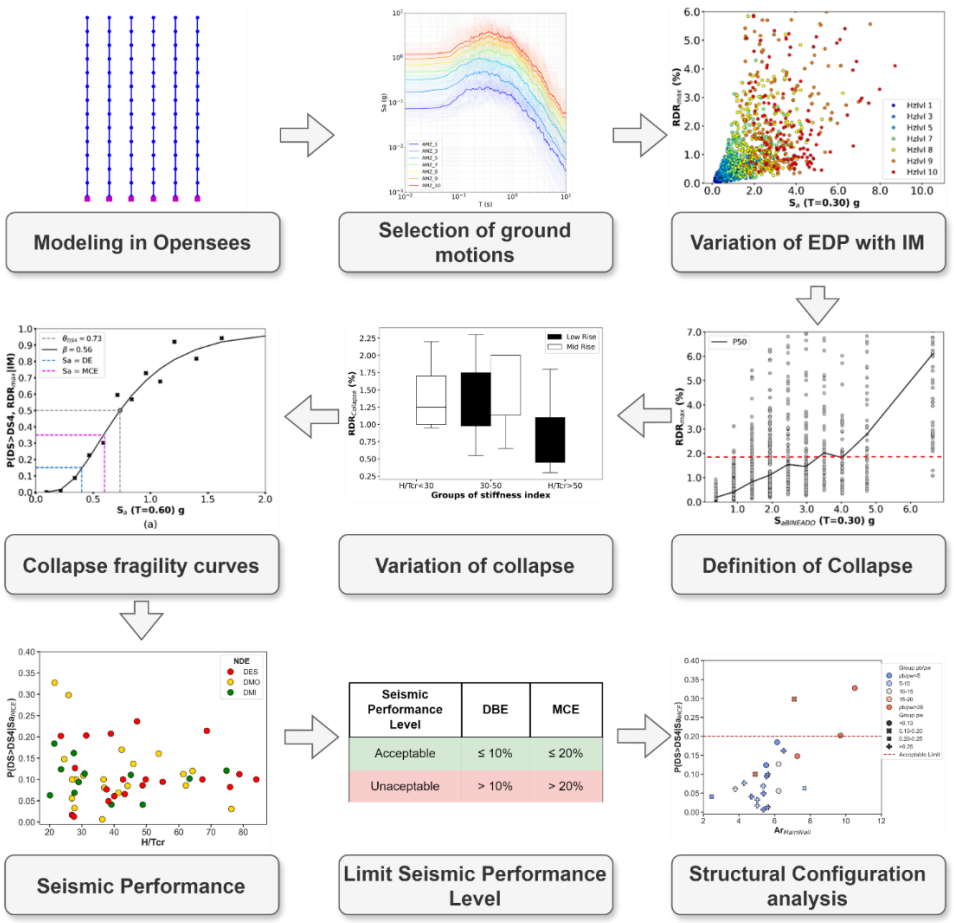

Figure 69. Scheme of the developed framework for evaluating seismic performance of TRCW buildings.

Figure 70a shows the inverse correlation between the probability of collapse under MCE and H/Tcr, demonstrating a decrease in the probability of collapse as the stiffness index increases. Additionally, these figures show the variability range of Ar_{Mean} for the three groups defined by H/Tcr, highlighting the correlation between H/Tcr and Ar_{Mean}. For the 'very stiff' category, Ar_{Mean} values remain lower, around 4.0, while 'flexible' buildings exhibit Ar_{Mean} values greater than 6. For the 'stiff' category, Ar_{Mean} values range from 4 to 6. These findings emphasize the critical role of Ar_{Mean} in determining the structural response of buildings to seismic forces, effectively categorizing them into different stiffness and flexibility levels.

The previously defined threshold for evaluating the probability of collapse is indicated by dashed lines in this figure. This figure also illustrates the design detailing requirements for each building category (DMI, DMO, and DES), enhancing the analysis of how seismic hazard levels and reinforcement detailing influence the probability of collapse.

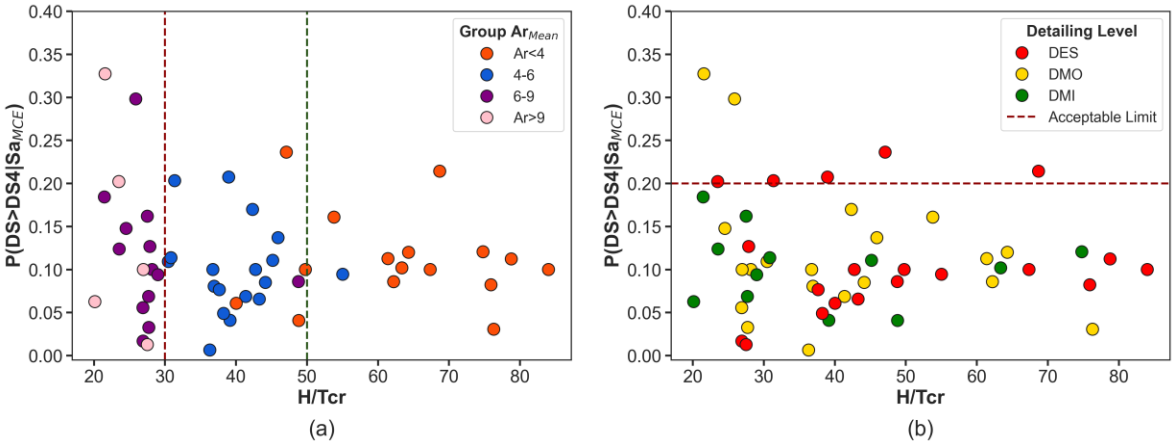

Figure 70. Variation in the Probability of collapse for the MCE (Maximum Considered Earthquake) with H/Tcr: a) Ar_{mean} and b) Detailing level.

12.1. SEISMIC PERFORMANCE OF LOW-RISE BUILDINGS

From the analyzed database, most low-rise buildings show a favorable structural configuration from the perspective of seismic performance. However, the result highlights the characteristics of TLRCW buildings that cause the probability of collapse to increase beyond the acceptable limits associated with acceptable seismic performance. Figure 71 shows the distribution of the probability of collapse for MCE based on the stiffness index and the detailing- or seismic hazard level. A color scale is used to represent buildings with acceptable seismic performance (green) and unacceptable seismic performance (red).

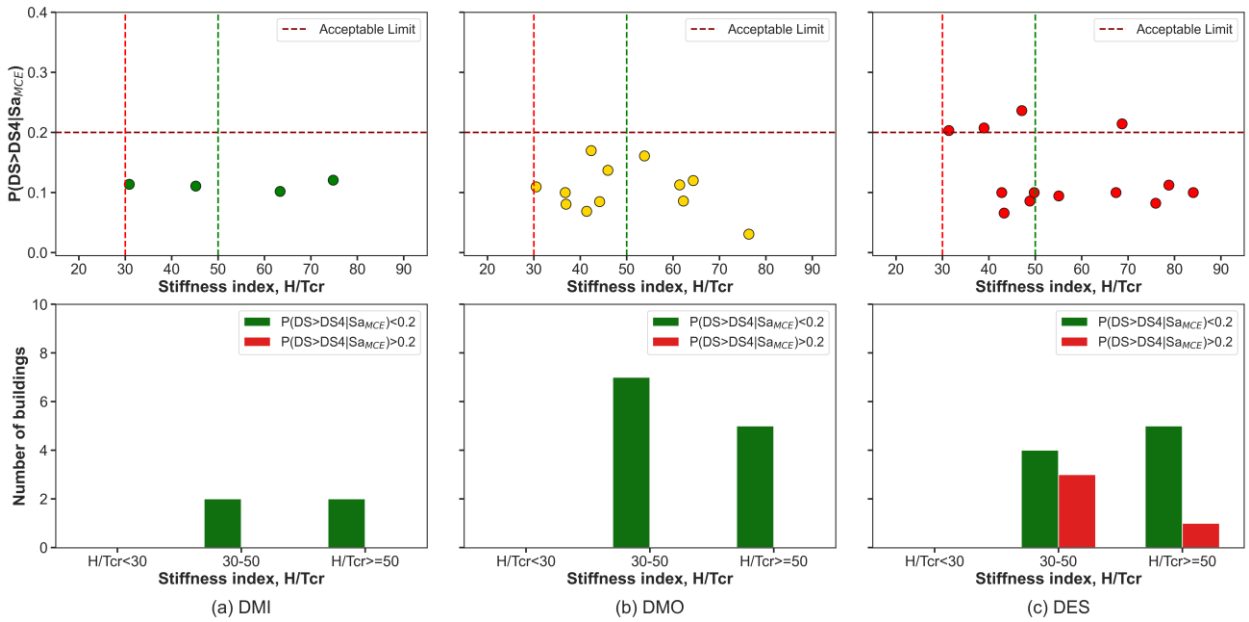

Figure 71. Distribution of seismic performance vs. Stiffness index and Detailing level – Low-rise buildings.

12.1.1. Unacceptable Performance

The analysis of the compiled database revealed that 4 low-rise of buildings demonstrated an unacceptable seismic performance when subjected to the Maximum Considered Earthquake (MCE) and Design Basis Earthquake (DBE) scenarios as shown in Figure 71c. All of them correspond to DES detailing with wall thickness ranging of 80 mm to 100 mm. They were found to have a web reinforcement ratio lower than 0.25% and use steel bars at the wall edge but with a reinforcement ratio lower than 0.50% (see Figure 72a and Figure 726b). The low reinforcement ratio at the edge promotes cracks to concentrate at the base and not extend along the height, reducing the plastic hinge length as reported by Blandon and Bonett (2020) and the probability of collapse is increased.

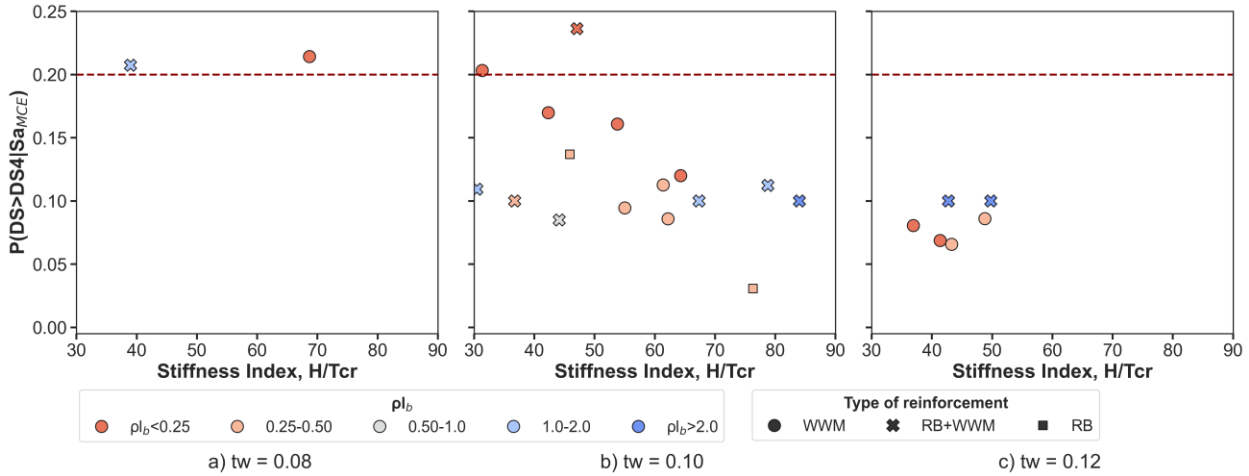

Figure 72. Effect of wall thickness, type of reinforcement and web reinforcement ratio over the probability of collapse.

12.1.2. Acceptable seismic performance

Within the database of the study, 25 low-rise buildings exhibited an acceptable seismic performance under DBE and MCE scenarios as shown in Figure 71. The results show that 13 stiff low-rise buildings and 12 very stiff low-rise buildings comply with the acceptable seismic performance criteria outlined in Table 5. These buildings have a Wall Index (WI) exceeding 0.25, featuring wall thicknesses of 100- and 120-mm. Wall lengths and reinforcement detailing vary, with very stiff buildings having longer walls, reflected in an Ar_{Mean} smaller than 6.0. The reinforcement detailing in the walls comprising these buildings vary according to the hazard seismic level and the detailing level but typically, all of them use WWM as longitudinal reinforcement distributed in the web and steel bars concentrated at the wall edges, with reinforcement ratios between 0.5% and 2% as shown in Figure 72b-c. Most walls do not have confinement at the ends; only some walls in buildings located in high seismic hazard zones have confinement. These confined walls have thicknesses of 150 mm or 200 mm. Low-rise buildings in the database with DMI detailing show acceptable seismic performance, despite having low reinforcement ratios in the web and at the ends. The reason is that these buildings combine good stiffness with low displacement demands, and therefore, the reinforcement detailing does not have a significant impact on seismic performance. The response is controlled by the lateral stiffness of the building. In general, in low-rise buildings, increasing both the wall thickness and the web reinforcement ratio decreases the probability of collapse, as shown in Figure 72. The use of WWM with steel bars distributed along the web also reduces the probability of collapse, except when there is a low web reinforcement ratio (<0.25%).

12.2. SEISMIC PERFORMANCE OF MID-RISE BUILDINGS

Figure 73. shows the distribution of the probability of collapse based on the stiffness index and the detailing or seismic hazard level. Most mid-rise buildings present an acceptable seismic performance (green) like to low-rise buildings, except two DMO buildings and one DES building which exhibit unacceptable seismic performance (red). In both cases, the stiffness index is lower than 30, corresponding to flexible buildings. However, the increase in the probability of collapse is not associated with flexibility, as most buildings with acceptable seismic performance are also flexible.

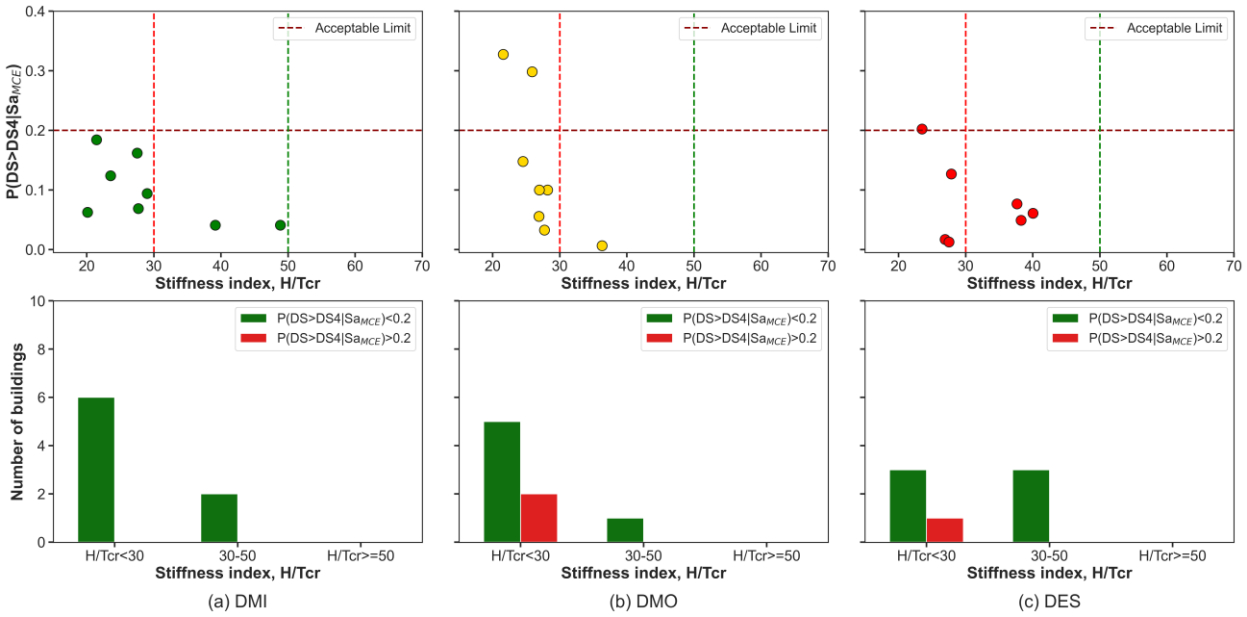

Figure 73. Distribution of seismic performance vs. Stiffness index and Detailing level – Mid-rise buildings.

12.2.1. Unacceptable Performance

Mid-rise buildings exhibiting unacceptable seismic performance are characterized by having longitudinal reinforcement ratios along the web (ρ_w) lower than 0.20% and vertical reinforcement concentrated at the wall edges (ρ_b) greater than 2%, using deformed steel bars. Figure 74a shows that as the web reinforcement ratio decreases, the probability of collapse increases. Additionally, Figure 74b illustrates that as the ratio between reinforcement concentrated at the wall edges and reinforcement distributed through the web (ρ_w/ρ_b) increases, the probability of collapse grows.

For special structural walls, ACI 318 and the Colombian seismic code NSR-10 (DMO and DES detailing) require a minimum reinforcement content of 0.25% regardless of concrete or reinforcement strength. This requirement can be reduced to 0.12–0.15% when the ultimate shear remains below a specific limit. Eurocode

8 specifies a minimum vertical reinforcement of 0.25% across cold joints to minimize shear sliding at crack interfaces and 0.5% in boundary elements of seismic walls (Sritharan, et al. 2014).

Previous studies by Beyer et al. (2008), Aeleti, et al (2013) and Lu & Henry (2018), highlighted potential failure modes and risks associated with over-concentration of vertical reinforcement at the wall edges and insufficient longitudinal reinforcement in the web regions. This imbalance can leave the web vulnerable to developing discrete wide cracks, leading to concrete crushing in the web, premature reinforcement fracture, large shear deformations, and potential shear sliding due to the formation of wider cracks. Additionally, buckling of the wall edges may occur as the web experiences significant damage.

Lu and Henry (2018) recommend limiting the ratio of reinforcement concentrated at the wall edges to distributed reinforcement in the web to ensure effective crack control. They also suggest using smaller diameter bars with reduced spacing in the wall web region to promote the propagation of secondary cracks and improve overall structural resilience.

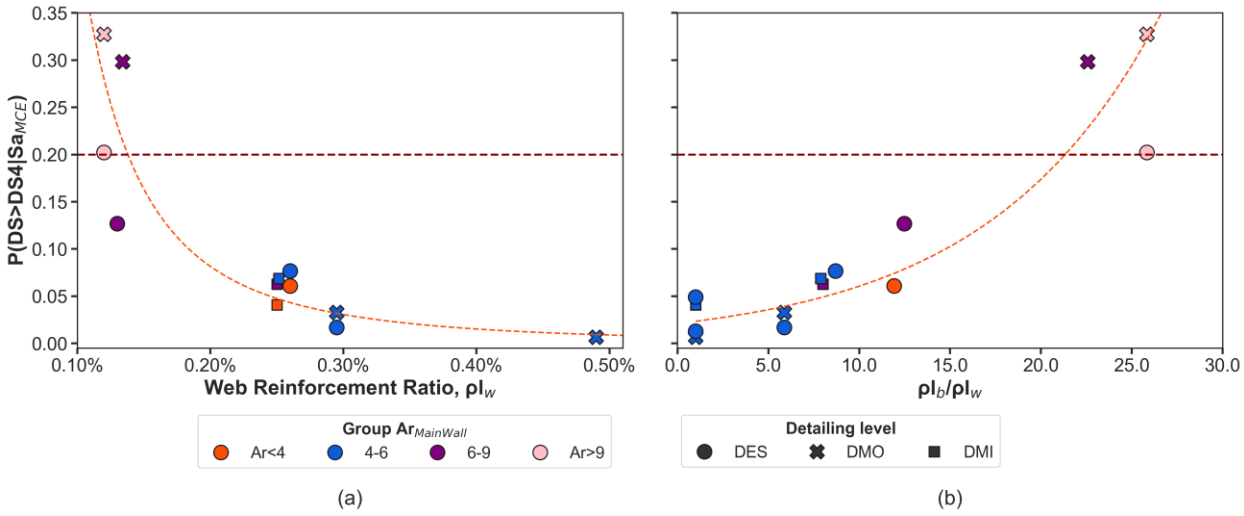

Figure 74. Relationship between the probability of collapse for MCE vs. (a) vertical web reinforcement ratio, (b) the ratio between reinforcement concentrated at the wall edges and along the web (ρ_b/ρ_w).

12.2.2. Acceptable seismic performance

In the category of mid-rise buildings, the study identified six stiff buildings and fourteen flexible buildings. Overall, the majority of this group of buildings is characterized by having a vertical reinforcement distributed in the web region of at least 0.25%, longitudinal reinforcement concentrated at the wall edges do not exceed to 2.0% and the ratio between reinforcement concentrated at the end of the walls and distributed reinforcement through the web is limited to 15 (see Figure 75). A few buildings located in areas of low to intermediate seismic hazard have reinforcement ratios along the web of 0.13% but with low

reinforcement at the wall edge such as $\rho_b<5\rho_w$ (see Figure 75). The reduced probability of collapse for both DBE and MCE scenarios can be attributed to an increase in the longitudinal reinforcement ratio along the web and the use of confinement at the edges, especially when high steel edge ratios are employed. Figure 75 shows that as the aspect ratio of the main wall ($Ar_{MainWall}$) increases, the probability of collapse also increases. For TLRC wall mid-rise buildings, $Ar_{MainWall}$ values less than 9.0 indicate acceptable seismic performance.

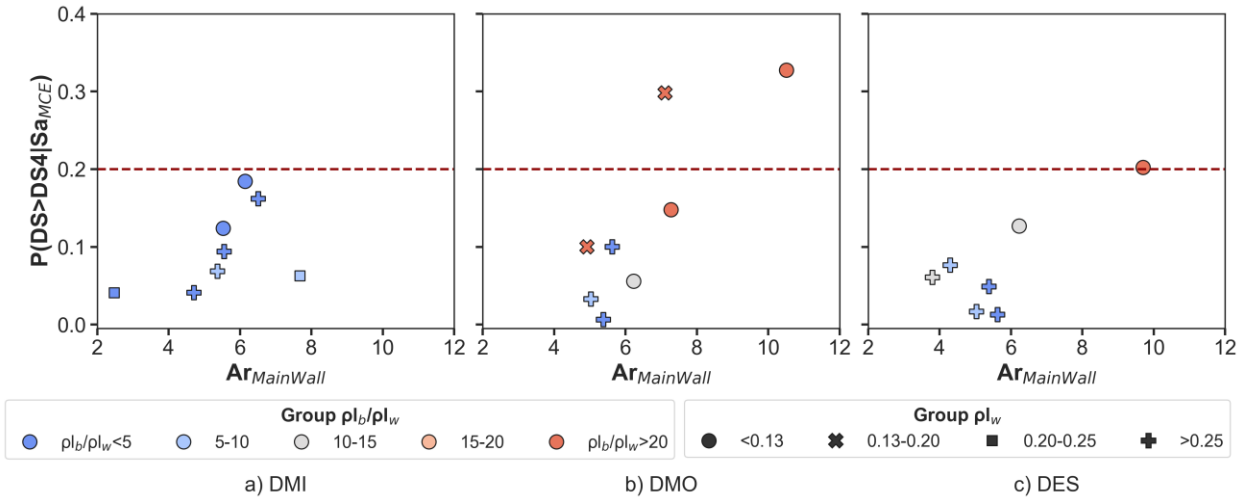

Figure 75. Relationship between the probability of collapse for MCE vs ArMainWall, the ratio between reinforcement concentrated at the end of the walls and distributed reinforcement through the web ($\rho l_b/\rho l_w$) and longitudinal reinforcement along the web.

13. DESCRIPTION OF THE STRUCTURAL CONFIGURATION ANALYSIS PLATFORM

This chapter presents an overview of the structural configuration analysis platform developed in this study. The platform comprises a set of algorithms and tools designed to facilitate the nonlinear modeling, analysis, and interpretation of the behavior of reinforced concrete wall buildings under seismic loading. The chapter is organized into two parts: the first describes the Python-based algorithms for modeling and analysis, and the second introduces the C#-based platform for visualization and in-depth study of key variables.

13.1. ALGORITHMS FOR NONLINEAR MODELING AND ANALYSIS

The first part of this platform consists of several algorithms that manage the creation and execution of nonlinear planar models for buildings with reinforced concrete walls. Each algorithm is designed to perform a specific task within the analysis workflow:

1. Nonlinear Planar Model Generation: This algorithm automates the development of two-dimensional nonlinear models for reinforced concrete walls. It facilitates the creation of models with appropriate material properties, boundary conditions, and loading scenarios, ensuring consistency with the structural characteristics of the buildings under study. This functionality is implemented in the file "00_XXXX-MCR-XXX-XXP-L", as shown in Figure 76. Table 12 provides a description of the taxonomy generation, along with the corresponding file names.

Table 12. Description of Project Taxonomy Generation.

Id	Specification	Description
1	Id	Corresponds to a unique four-digit numerical ID used to identify the building in the database
2	MCR: Muros de concreto reforzado (Reinforced concrete walls).	MCR corresponds to the abbreviation for reinforced concrete walls in Spanish, written as MCR in the database.
3	City	The three-letter abbreviation represents the city where the project is located.
4	Number of stories	The number of floors in the project.
5	Direction	Since planar archetypes will be used, it is necessary to indicate the orientation of the project corresponding to the archetype. Therefore, 'L' is used for longitudinal orientation and 'T' for transverse orientation

2. Pushover Analysis Algorithm: This script conducts the pushover analysis to capture the building's lateral load-displacement behavior. It automates the application of incremental lateral loads and records the structural response up to failure. This functionality is implemented in the file "01_PUSHOVER", as shown in Figure 76.
3. Nonlinear Time-History Analysis Algorithm: This algorithm carries out a dynamic time-history analysis by subjecting the model to recorded ground motions. It monitors various structural response parameters including interstory drifts, floor accelerations, and velocities during seismic events. This functionality is implemented in the file "02_CNL", as shown in Figure 76.
4. Post-processing for Pushover Analysis: This code processes the results of the pushover analysis, generating detailed response curves and extracting key performance metrics, including maximum roof displacement and base shear capacity. This functionality is implemented in the file "04_POST-PUSHOVER", as shown in Figure 76.
5. Post-processing for Time-History Analysis: Similarly, this script processes the results of the nonlinear time-history analyses, compiling data on roof drifts, interstory drifts, and other dynamic responses for each seismic record. The outputs support further statistical analysis and the development of fragility curves. This functionality is implemented in the file "05_POST_CNL_FULL", as shown in Figure 76.

Figure 76 provides a screenshot of the folder containing these Python scripts, along, with a brief description of each file's functionality. These scripts form the computational backbone of the modeling process, automating time-intensive tasks while ensuring accuracy and consistency across analyses.

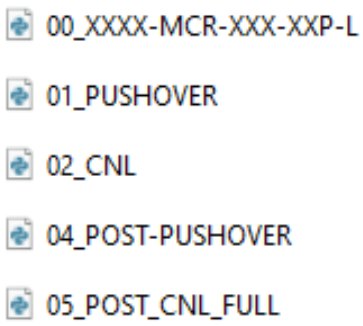

Figure 76. Main source code files for nonlinear modeling and structural analysis.

In addition to the codes shown in Figure 76, a series of libraries were developed to include essential functions for data processing, material generation, and analysis procedures. Figure 77 provides an overview of these files.

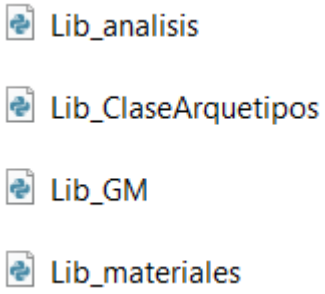

Figure 77. Complementary libraries for data processing, material generation, and analysis procedures.

The codes developed for this study are available in the following repository: https://github.com/VidalesFrank/Seismic-Structural-Analysis-Platform.git.

13.2. PLATFORM FOR VARIABLE ANALYSIS AND VISUALIZATION

The second part of this chapter details the development of a dedicated platform, implemented in C#, for visualizing and examining the structural variables of interest. This platform is designed to provide a user-friendly interface for navigating the extensive data generated by the nonlinear analyses, offering clear visualizations and insightful metrics to facilitate understanding of the building behavior under various seismic scenarios. The platform was initially developed in Spanish to serve primary regions where the thin reinforced concrete wall system remains in use. Work is currently underway on a second version, which will be available in English and adaptable to various structural systems.

- Data Visualization Module: This module enables users to visualize key structural response metrics, including base shear versus roof drift, interstory drifts, and fragility curves. Interactive plots allows users to zoom in on specific data points and explore various aspects of the structural response in detail.
- Variable Study Module: This module focuses on examining relationships between different design parameters (e.g., wall thickness, reinforcement ratios) and the resulting structural performance. Users can filter and compare data across various buildings and seismic intensities, facilitating the identification of trends and key performance indicators.

Figure 78 provides an overview of the platform´s main page, which general information about the buildings included in the database. For further details, please refer to Chapter 6 of this document.

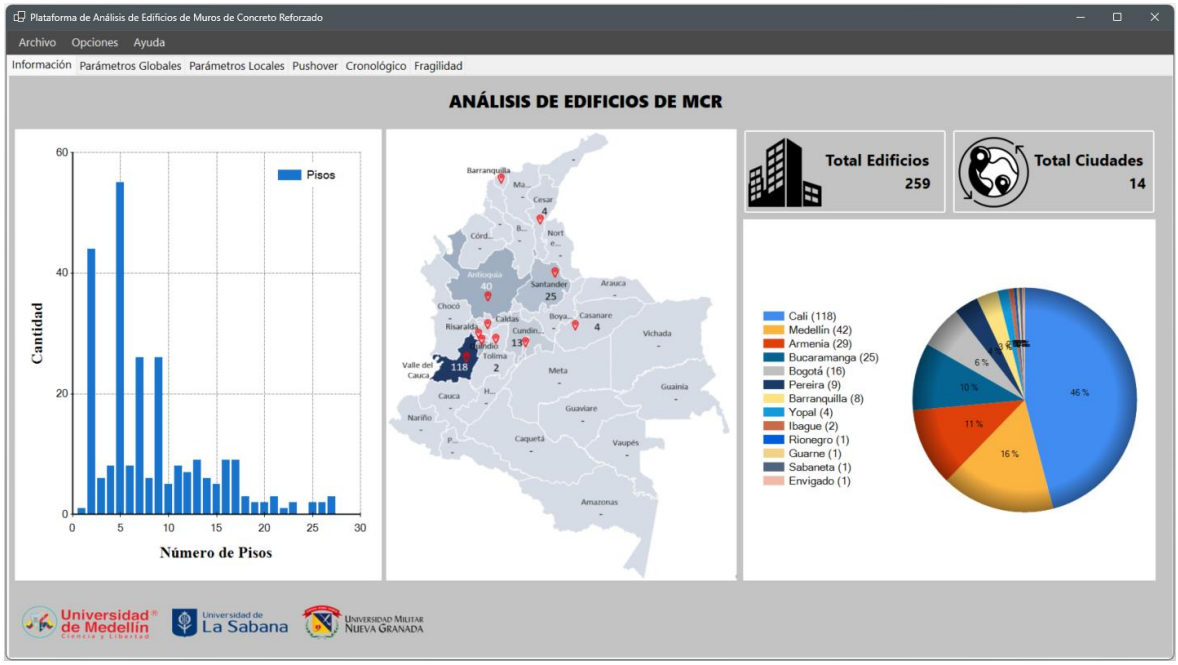

Figure 78. Main Page Overview and Summary of Buildings in the Database (in Spanish).

Figure 79 illustrates the visualization of global attributes of the buildings in the database. A detailed description of these global attributes is provided in Chapter 7.7 of this document.

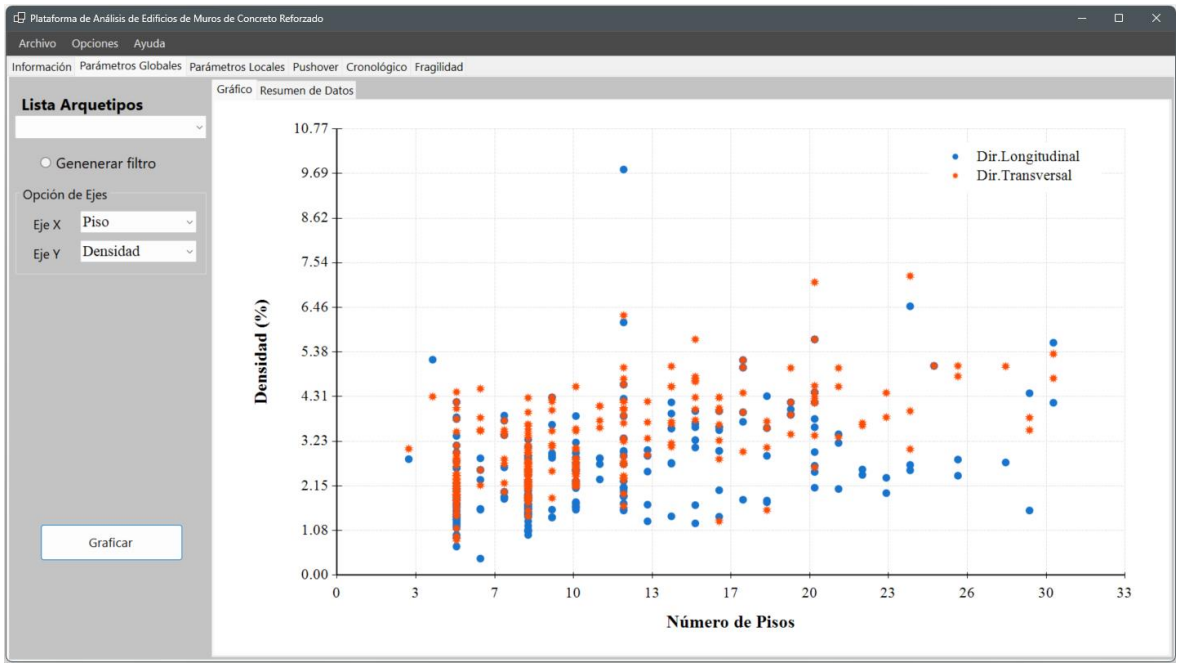

Figure 79. Visualization of Global Attributes of Buildings in the Database (in Spanish).

Figure 80 presents the visualization of local attributes of the buildings in the database. Detailed descriptions of these local attributes is provided in Chapter 7.8 of this document.

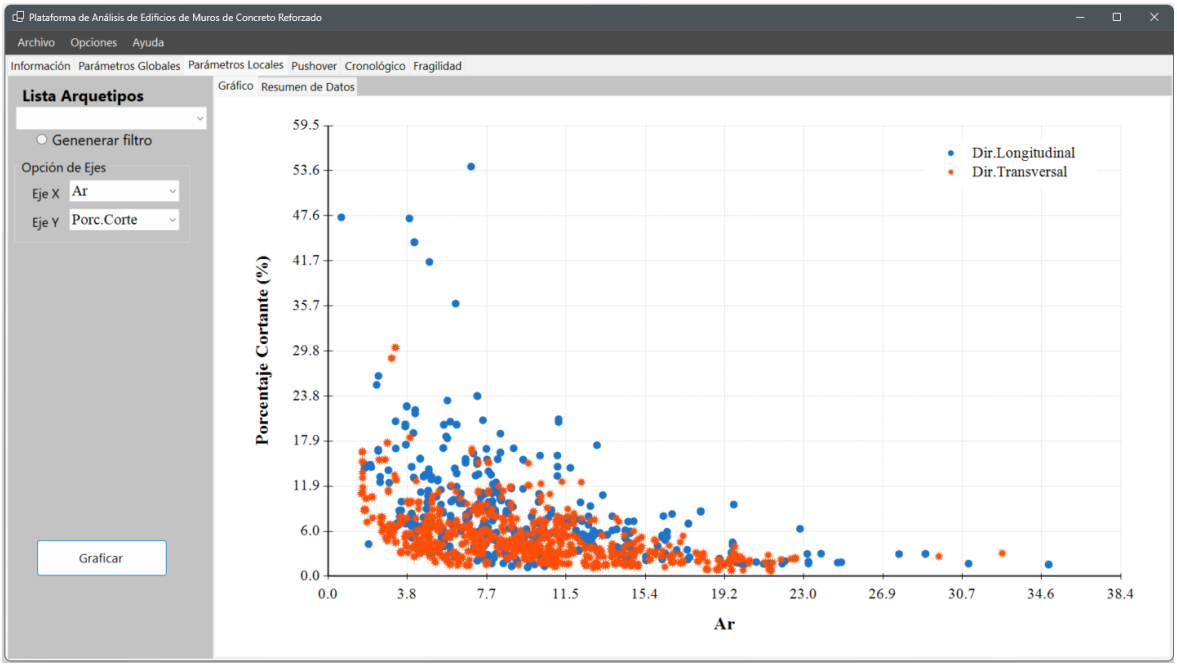

Figure 80. Visualization of Local Attributes of Buildings in the Database (in Spanish).

Figure 81 illustrates the visualization of pushover curves for the buildings in the database. This figure displays key metrics, including maximum inter-story drift (SDR), first-floor drift (SDR1), and maximum roof drift (RDR), along with the corresponding displacements at each of these points.

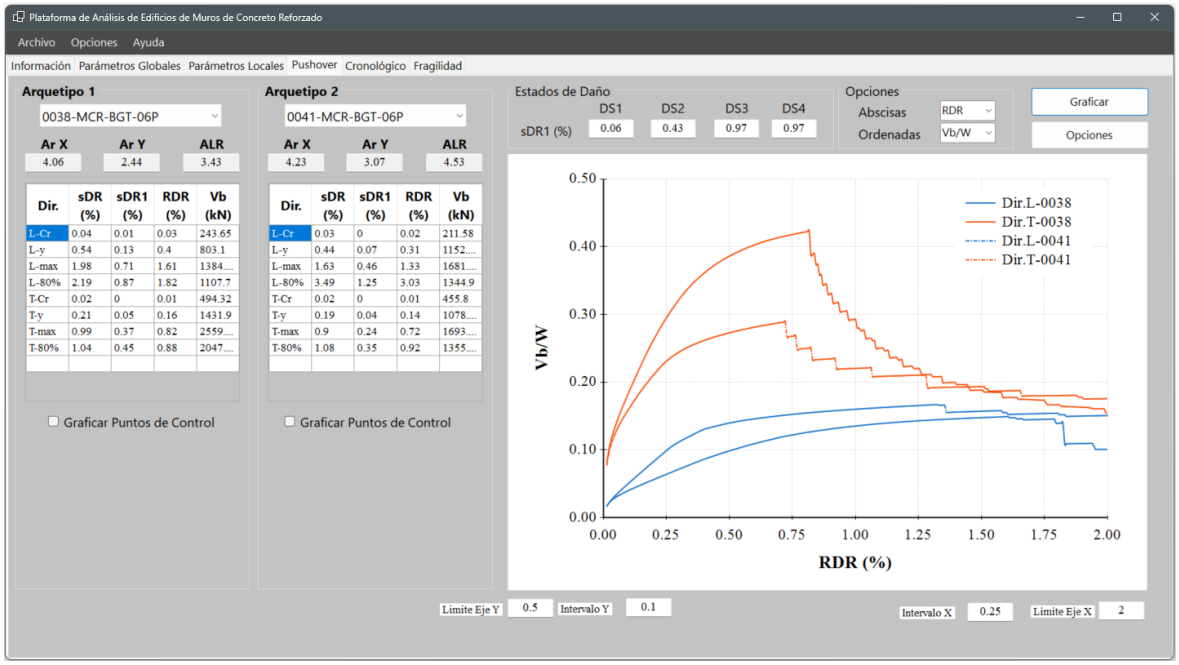

Figure 81. Visualization of Pushover Curves for Buildings in the Database (in Spanish).

Figure 82 presents the visualization of nonlinear time-history results for the buildings in the database. This figure illustrates the time-dependent behavior of the structures under various loading scenarios, enabling detailed analysis of their dynamic performance over time. Different engineering demand parameters (EDP's), such as maximum inter-story drift (SDR), the first-story drift (SDR1), and the maximum roof drift (RDR) can be visualized to assess this behavior comprehensively.

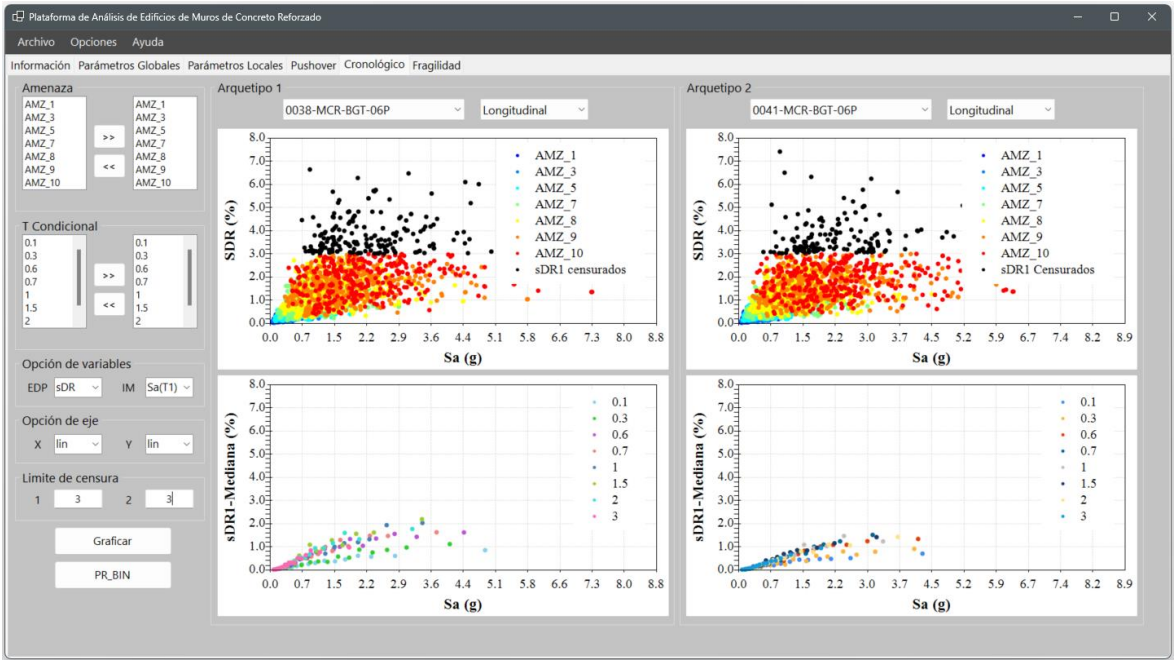

Figure 82. Visualization of Nonlinear Chronological Results for Buildings in the Database (in Spanish).

Figure 83 presents a summary of the pushover analysis results for the buildings in the database. This visualization encapsulates key performance indicators, including the maximum lateral load capacity and corresponding displacements, providing a clear understanding of structural responses during seismic events. The summarized results offer essential insights for assessing the seismic resilience of the buildings.

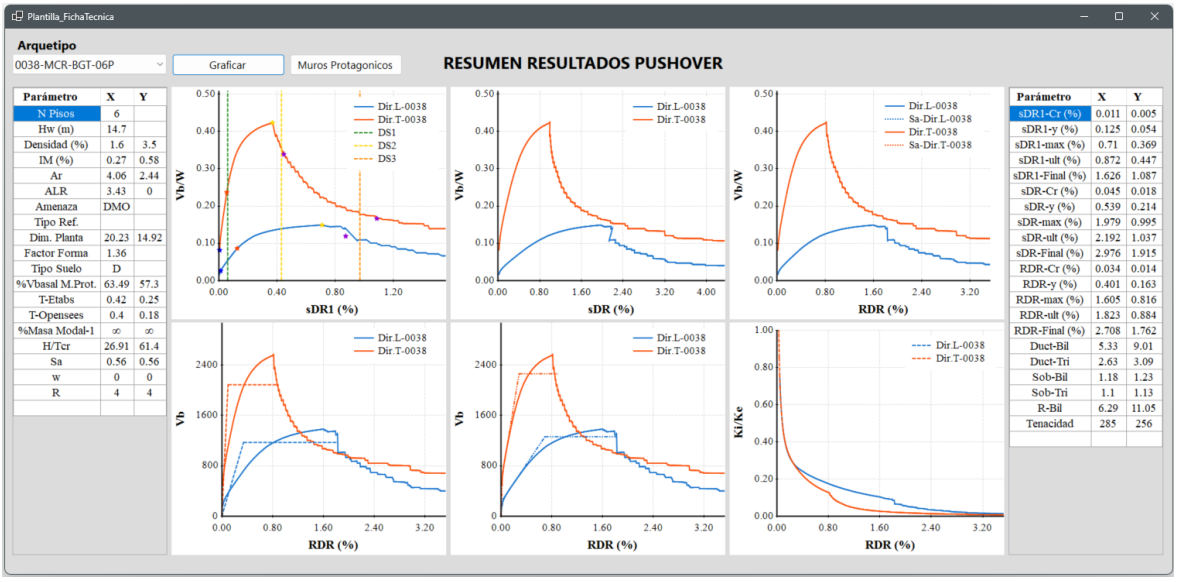

Figure 83. Visualization of Pushover Analysis Results Summary for Buildings in the Database.

Finally, Figure 84 provides a comprehensive overview of the pushover analysis results for the buildings in the database. This visualization highlights essential metrics, such as capacity curves and associated displacements, allowing for thorough assessment of the structural performance under lateral loading. Notably, this module facilitates the visualization of all results obtained from the analyses, enabling correlations between geometric and mechanical variables of the archetypes and the outcomes from pushover, time-history analyses, and seismic fragility calculations. This summarized data is crucial for understanding the seismic behavior of the buildings and supports informed decision-making in design and retrofitting processes.

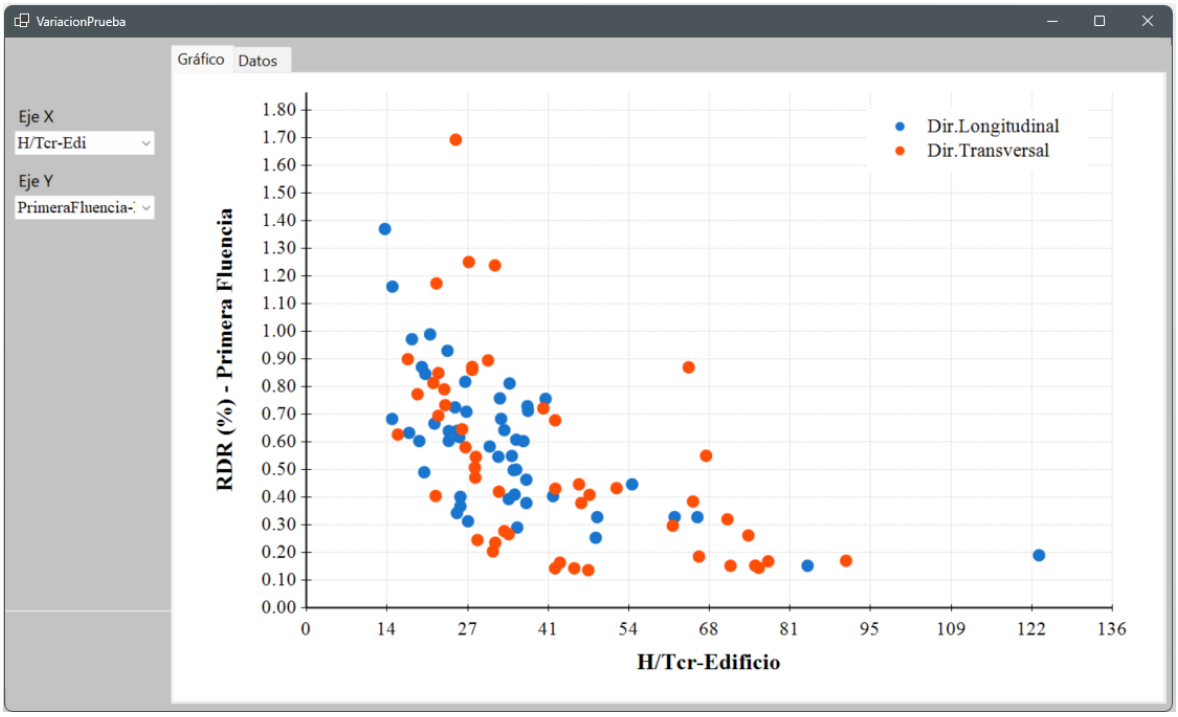

Figure 84. Comparison of Global Parameters and Response Variables in Analysis.

Figure 78 to Figure 84 showcase various visualizations generated by the platform, illustrating its capacity to handle complex data and deliver intuitive, insightful results. These visualizations are integral for interpreting the outcomes of nonlinear dynamic analysis and support the conclusions discussed in later chapters.

By integrating Python for the computationally demanding modeling tasks with C# for the visualization and analysis of results, the platform serves as an efficient and comprehensive tool for investigating the seismic performance of reinforced concrete wall systems.

In conclusion, this chapter has detailed the functionalities and visualizations offered by the developed analysis platform, specifically designed for studying thin reinforced concrete wall buildings. All results, along with a user manual and platform installer, will be available in the repository provided (https://github.com/VidalesFrank/Seismic-Structural-Analysis-Platform.git). This research has sought to understand the behavior of these structures while developing algorithms and routines that optimize both the time and computational costs of generating and visualizing results. The findings and methodologies presented in this thesis set a foundation for future research, allowing deeper exploration of the seismic performance of thin reinforced concrete buildings and contributing to the advancement of structural engineering knowledge.

14. CONCLUSIONS AND FUTURE WORK

This research accomplished several objectives related to the seismic performance assessment of reinforced concrete (RC) wall buildings. First, an analysis of a 256-building Colombian database was conducted to identify critical structural parameters. Subsequently, an efficient analysis platform was developed within the OpenSees framework, featuring a user-friendly interface through Excel spreadsheets to facilitate nonlinear pushover and dynamic analyses. Using this platform, sixty archetypes of low- and mid-rise RC buildings were analyzed to generate e pushover curves and derive seismic fragility functions. A correlation analysis then identified significant relationships between structural parameters and seismic performance indicators. These results lead to the following conclusions:

- The stiffness index, defined as the ratio of total building height to cracked period (H/Tcr), is shown to be inversely correlated with collapse probability. Higher stiffness index values correspond to reduced collapse risk, underscoring its importance in structural design and seismic resilience assessment.

- Low-rise TLRCW (Thin Lightly Reinforced Concrete Walls) buildings are often categorized as either rigid ($30 < H/Tcr < 50$) or very rigid ($H/Tcr > 50$), with generally favorable seismic performance. However, low-rise buildings in high seismic hazard areas, particularly those with DES detailing and walls as thin as 80 mm with low reinforcement ratios along the web (< 0.25%) and wall edges (< 0.50%), display higher fragility. This configuration limits the inelastic rotation capacity and directs damage to the wall's base, which restricts crack distribution along the wall height. Research indicates that this setup can result in abrupt failure due to concrete crushing and web reinforcement rupture.

- Increasing reinforcement at the wall edges, with ratios between 0.5% and 2.0%, has been observed to decrease collapse probability in low-rise buildings in areas with intermediate to high seismic hazard. For buildings in low seismic hazard regions, lower longitudinal web reinforcement ratios (below 0.25%) and vertical edge reinforcement (below 0.5%) do not notably elevate collapse risk, likely due to the inherent rigidity or extreme rigidity of these structures.

- Elevated reinforcement ratios along the wall edge, combined with lower ratios of electro-welded wire mesh (WWM) reinforcement in the web, can increase collapse probability and lead to insufficient seismic performance. This research suggests that in TLRCW walls (with thicknesses less than 150 mm), the longitudinal reinforcement at the wall edges should ideally not exceed 15 times the web's longitudinal reinforcement ratio to avoid excessive stiffness concentration and risk of collapse.

- Mid-rise TLRCW buildings meeting the minimum longitudinal reinforcement ratio (0.12%) defined per the NSR-10—based on ultimate shear resistance—may still result in subpar seismic performance. To

address this, it is recommended to re-evaluate and potentially increase the minimum vertical reinforcement requirements for TLRCW buildings. Specifically, a minimum longitudinal web reinforcement ratio of 0.25% is suggested for structures designed with intermediate (DMO) and special (DES) detailing to ensure enhanced seismic resilience.

- A notable contribution of this work is the formulation of simplified expressions for calculating seismic performance indicators tailored to the Colombian context. These expressions, derived from numerical regressions based on the nonlinear static analyses of 100 archetypes of reinforced concrete wall buildings, provide a rapid and approximate evaluation tool for assessing seismic performance. They focus on key engineering parameters, including elastic and inelastic displacements, elastic shear, and rigidity index, while also facilitating the determination of over-strength and displacement ductility. The primary advantage of these simplified expressions lies in their reliance solely on geometric parameters, which significantly expedites the evaluation process. They serve as an initial exploration phase that prioritizes assessments when evaluating numerous structures or when analyzing the impact of structural configuration on seismic performance. However, it is essential to acknowledge that these expressions do not substitute the need for detailed vulnerability analyses; instead, they offer critical insights that inform discussions prior to more comprehensive evaluations.

- The algorithms embedded within the developed platform automate the generation of nonlinear models and enable the execution of both pushover and nonlinear time-history analyses. This automation significantly reduces the computational time required for complex analyses.

- Moreover, the platform's visualization capabilities facilitate clearer interpretation of results, assisting in the communication of vital performance metrics and enabling informed decision-making regarding structural design and retrofitting.

By bridging the gap between computational analysis and practical application, this research contributes significantly to advancing knowledge in structural engineering, particularly in seismic performance evaluation of reinforced concrete wall systems.

This research paves the way for multiple research avenues regarding reinforced concrete walls in Colombia, particularly in advancing seismic performance assessments and structural design practices. The analysis platform developed here demonstrates significant efficiency and adaptability, making it a promising tool for developing seismic performance factors per the FEMA P-695 framework. Furthermore, the platform enables in-depth investigations into the impact of diverse structural configurations, such as alternative reinforcement strategies and the integration of materials like glass fiber-reinforced polymers (GFRP), as well as other innovative approaches. Its open-source design enhances its potential for adaptation, allowing researchers to expand its capabilities to include advanced modeling considerations, such as seismic isolation and soil-

structure interaction effects. This flexibility makes it a valuable resource for further studies aimed at refining seismic resilience and structural safety in reinforced concrete wall systems.

15. REFERENCES AND BIBLIOGRAPHY

Acevedo, A.B., Reyes, J.C., Arteta, C., Valcárcel, J., Mora, M., Pérez, H., Abuchar, V., Gómez, D., Clavijo, A., Daza, J., Echeverry, J. (2021). Acuerdos de Línea Base y Metodológica – Fragilidad y Vulnerabilidad: Reporte MNRS No. 0.002-2021

Alarcón, C., Hube, M.A. and De la Llera, J.C (2014). Effect of axial loads in the seismic behavior of reinforced concrete walls with unconfined wall boundaries. Journal Elsevier Engineering Structures.

Alfaro Montoya, L. Massone (2013). Estimación del desplazamiento lateral elástico e inelástico de muros esbeltos mediante un modelo de rotula plástica basado en un modelo de fibras. Universidad de Chile.

Arteta, C. (2017). Simple mechanics of reinforced concrete thinwall, design considerations for Colombia – Ceer. VII Congreso Nacional de Ingeniería Sísmica. http://ceer.co/mecanica-simple-de-muros-delgados-con-aleta-aspectos-a-considerar-para-su-diseno-en-colombia-2/?login=success&lang=en.

Arteta, C. A., Sanchez, J., Daza, R., Blandón, C. A., Bonett, R. L., Carrillo, J., & Velez, J. C. (2017). Global and local demand limits of thin reinforced concrete structural wall building systems. Paper presented at the 16th World Conference on Earthquake Engineering, Santiago de Chile.

Blandon C., Arteta C., Bonett R., Carrillo J., Beyer K. and Almeida J. (2018) Response of thin lightly reinforced concrete walls under cycling loading. Engineering structures, 176:175-187, DOI: 10.1016/j.engstruct.2018.08.089.

Blandón, C., & Bonett, R. (2020). Thin slender concrete rectangular walls in moderate seismic regions with a single reinforcement layer. Journal of Building Engineering, 28, 101035. https://doi.org/10.1016/J.JOBE.2019.101035.

Bohl, A. and Adebar, P. (2011) Plastic Hinge Lengths in High-Rise Concrete Shear Walls. ACI Structural Journal 108(2):148-157.

Bonett, R., Arroyo, O., Zapata, A., Feliciano, D., Ocampo, J., Vidales, F. (2022). Funciones de fragilidad y vulnerabilidad sísmica para la tipología constructiva de muros en concreto reforzado: Reporte MNRS No. 005-2022. Bogotá: Preparado por la Asociación Colombiana de Facultades de Ingeniería (ACOFI) para el Servicio Geológico Colombiano (SGC).

Bonett, R. (2003). Vulnerabilidad y riesgos sísmicos de edificios. Aplicación a entornos urbanos en zonas de amenaza alta y moderada. Tesis doctoral. Universidad Politécnica de Cataluña. Barcelona – España.

Bonett, R., y Blandón, C. (2014). Informe final del proyecto de investigación titulado: Verificación del comportamiento de muros esbeltos de concreto reforzado ante desplazamientos laterales. Universidad de Medellín, Escuela de ingeniería de Antioquia, CAMACOL, Doing estudios de ingeniería, Conconcreto e Industrias del Hierro.

Bonett, R. Carrillo, J. Blandón, C. Arteta, C. Restrepo, J.F. Rosales, J.L. "Evaluación del Factor R para edificios de muros delgados y esbeltos en sistemas industrializados". IX Congreso Nacional de Ingeniería Sísmica. Santiago de Cali. Colombia. Mayo 29 al 31. 2019.

Bonett, R., Carrillo, J., Blandón, C., & Arteta, C. (2024). Understanding the behavior of the Thin Lightly-Reinforced Concrete Wall (TLRCW) building system. Journal of Structural Integrity and Maintenance, 9(1). https://doi.org/10.1080/24705314.2024.2337449.

Bonnet, R., Vidales, F., Arroyo, O., Ocampo, J., Feliciano, D., Carrillo, J. (2024).

Cando, M. A., Hube, M. A., Parra, P. F., & Arteta, C. A. (2020). Effect of stiffness on the seismic performance of code-conforming reinforced concrete shear wall buildings. https://doi.org/10.1016/j.engstruct.2020.110724.

Carrillo J, Alcocer SM. Acceptance limits for performance-based seismic design of RC walls for low-rise housing. Earthq Eng Struct Dyn 2012:n/a-n/a.. https://doi.org/10.1002/eqe.2186.

Carrillo, J., Diaz, C., & Arteta, C. A. (2019). Tensile mechanical properties of the electro-welded wire meshes available in Bogotá, Colombia. Construction and Building Materials, 195, 352–362. https://doi.org/10.1016/J.CONBUILDMAT.2018.11.096.

Carrillo, J., Oyarzo-Vera, C., & Blandón, C. (2019). Damage assessment of squat, thin and lightly-reinforced concrete walls by the Park & Ang damage index. Journal of Building Engineering, 26, 100921. https://doi.org/10.1016/J.JOBE.2019.100921.

Dazio, A., Beyer, K. and Bachmann, H. (2008). Quasi – static cyclic tests and plastic hinge analysis of RC structural walls. Journal Elsevier Engineering Structures.

Feliciano, D., Arroyo, O., Bonett, R., Carrillo, J., Arteta, C, Vidales, F. and Ocampo, J. (2023). The 2D-MVLEM formulation as a tool for assessing RC wall buildings with non-planar walls: case study in Colombia. Proceedings of the 18th World Conference on Earthquake Engineering.

FEMA. (2018). Seismic Evaluation of Older Concrete Buildings for Collapse Potential, FEMA P-2018, prepared by the Applied Technology Council for the Federal Emergency Management Agency (Vol. 1). Washington, D.C.: nehrp.

F. McKenna, M. H. Scott, and G. L. Fenves, "Nonlinear Finite-Element Analysis Software Architecture Using Object Composition," Journal of Computing in Civil Engineering, vol. 24, no. 1, pp. 95–107, 2010, DOI: 10.1061/(asce)cp.1943-5487.0000002.

Miao, Liyue & Jin, Liu & Li, Dong & Du, Xiuli & Zhang, Binlin. (2022). Effect of shear-span ratio and vertical reinforcement ratio on the failure of geometrical-similar RC shear walls. Engineering Failure Analysis. 139. 106407. 10.1016/j.engfailanal.2022.106407.

Ocampo, J., Vidales, F., Feliciano, D., Arroyo, O., Carrillo, J., Arteta, C., Bonett, R. (2023). Impacto de la configuración estructural sobre la fragilidad sísmica de edificios de muros de concreto reforzado en Colombia. XI Congreso Nacional de Ingeniería Sísmica. Armenia. Colombia. Octubre 5 al 8. 2024.

Park, R. and Paulay, T. (1994). Estructuras de concreto reforzado. Mexico D.F. Limusa.

Paulay, T. and Priestley, N. (1993). Stability of Ductile Structural Walls. ACI Structural Journal Vol.90 No.4.

Portwood, A. (2024). Murum cura te ipsum. Retrieved from https://portwooddigital.com/2024/09/02/murum-cura-te-ipsum/

Pozo, J. D., Hube, M. A., & Kurama, Y. C. (2020). Quantitative assessment of nonlinear macro-models for global behavior and design of planar RC walls. Engineering Structures, 224, 111190. https://doi.org/10.1016/J.ENGSTRUCT.2020.111190.

Reporte CEER No. 002-2018. Estudio del Comportamiento Sísmico de Edificios de Muros Delgados de Concreto Reforzado. Universidad del Norte, Universidad EIA, Universidad de Medellín, Universidad Militar Nueva Granada. Noviembre 2018.

Reporte CEER No. 001-2021. Propuestas de adiciones a la Norma AIS-100-2X Respecto al Diseño del Sistema de muros Industrializados de concreto reforzado colombiano. Febrero de 2021.

Riva, A. Franchi (2001). Behavior of Reinforced Concrete Walls with Welded Wire Mesh Subjected to Cyclic Loading. ACI Structural Journal Vol.98 No.3.

Rosso, A., Jiménez-Roa, L. A., De Almeida, J. P., Zuniga, A. P. G., Blandón, C. A., Bonett, R. L., & Beyer, K. (2018). Cyclic tensile-compressive tests on thin concrete boundary elements with a single layer of reinforcement prone to out-of-plane instability. Bulletin of Earthquake Engineering, 16(2), 859–887. https://doi.org/10.1007/S10518-017-0228-1/TABLES/4.

Rosso A., Jimenez L., Almeida J. and Beyer K. (2020) Instability of thin concrete walls with a single layer under cycling loading: numerical simulation and improved equivalent boundary element model for assessment. Earthquake Engineering. DOI: 10.1080/13632469.2019.1691679.

Rosso, A., Jiménez-Roa, L. A., Almeida, J. P. De, & Beyer, K. (2022). Instability of Thin Concrete Walls with a Single Layer of Reinforcement under Cyclic Loading: Numerical Simulation and Improved Equivalent Boundary Element Model for Assessment. Journal Of Earthquake Engineering, 26(1), 493–524. https://doi.org/10.1080/13632469.2019.1691679.

Su, R. and Wong, S.M (2006). Seismic behaviour of slender reinforced concrete shear walls under high axial load ratio. Journal Elsevier Engineering Structures.

Tjhin, T.N., Aschheim, M.A. and Wallace, J. (2006). Yield displacement – based seismic design of RC Wall buildings. Journal Elsevier Engineering Structures.

Thomsen, J.H and Wallace, J.W (2004). Displacement – Based Design of Slender Reinforced Concrete Structural Walls – Experimental Verification. Journal of Structural Engineering © ASCE.

Ugalde, D., Parra, P.F. & Lopez-Garcia, D. Assessment of the seismic capacity of tall wall buildings using nonlinear finite element modeling. Bull Earthquake Eng 17, 6565–6589 (2019). DOI: https://doi.org/10.1007/s10518-019-00644-x.

Universidad de Los Andes (2019). Vulnerabilidad Sísmica. (Capítulo 4). En Estudio del riesgo sísmico del Valle de Aburrá. Bogotá: Preparado por la Universidad de los Andes, para el Área Metropolitana del Valle de Aburrá.

Vidales, F., Ocampo, J., Feliciano, D., Arroyo, O., Carrillo, J., Arteta, C., Bonett, R. (2023). Overstrenght factor of thin, Lightly Reinforced Concrete Shear Wall Buildings. Proceedings of the 18th World Conference on Earthquake Engineering.

Vidales, F., Ocampo, J., Feliciano, D., Arroyo, O., Carrillo, J., Arteta, C., Bonett, R. (2023 Expresiones Simplificadas Para La Estimación De Parámetros De Desempeño Sísmico De Edificios De Muros Delgados De Concreto Reforzado. XI Congreso Nacional de Ingeniería Sísmica. Armenia. Colombia. Octubre 5 al 8. 2024.

Vidales, F. (2024). *Seismic-Structural Analysis Platform for Concrete Wall Buildings* [Source code]. GitHub. https://github.com/VidalesFrank/Seismic-Structural-Analysis-Platform.git

Yepes-Estrada C, Silva V, Valcárcel J, Acevedo AB, Tarque N, Hube MA, Coronel G, Santa Maria H (2017) Modeling the residential building inventory in South America for seismic risk assessment. EarthqSpectra 33(1):299–322. https://doi.org/10.1193/101915eqs155dp

Zhu, M., McKenna, F., & Scott, M. H. (2018). OpenSeesPy: Python library for the OpenSees finite element framework. SoftwareX, 7, 6-11.